

NASA Contractor Report 3528

NASA
CR
3528
c.1

Subsonic Panel Method for the Efficient Analysis of Multiple Geometry Perturbations

0062212



AFWL LIBRARY KAFB, NM

LOAN COPY AVAILABLE
AFWL TECHNICAL LIBRARY
KIRTLAND AFB, TEXAS

D. R. Bristow and J. D. Hawk

CONTRACT NAS1-16156
MARCH 1982

NASA



NASA Contractor Report 3528

Subsonic Panel Method for the Efficient Analysis of Multiple Geometry Perturbations

D. R. Bristow and J. D. Hawk
McDonnell Douglas Corporation
St. Louis, Missouri

Prepared for
Langley Research Center
under Contract NAS1-16156

NASA

National Aeronautics
and Space Administration

**Scientific and Technical
Information Branch**

1982

TABLE OF CONTENTS

<u>Section</u>	<u>Page</u>
SUMMARY	1
INTRODUCTION	2
DEFINITION OF THE ANALYSIS FLOW PROBLEM AND ANALYTICAL RESTRICTIONS	5
MATHEMATICAL FORMULATION	9
Division of a Body Into Segments	9
Division of a Segment Into Panels	13
Panel Properties	15
Boundary Condition Control Points	23
Doublet Interpolation Between Neighboring Control Points	27
Singularity Distributions on a Panel	36
Potential Influence Functions	38
Boundary Condition Satisfaction	39
Velocity and Pressure Calculation	41
GUIDELINES FOR USING THE THREE COMPUTER PROGRAMS	42
MCAIR 3-D Subsonic Potential Flow Program (Version 2)	42
MCAIR 3-D Geometry Influence Coefficient Program (Version 1)	42
MCAIR 3-D Perturbation Analysis Program (Version 1) . . .	43
EXAMPLE SOLUTIONS	46
Conventional Analysis of a Wing - Fuselage	46
Perturbation Analysis Method for an Isolated Wing . . .	47
CONCLUSIONS	74
APPENDIX A QUADRATIC SURFACE FIT THROUGH TWO SETS OF THREE COLINEAR POINTS	75
APPENDIX B DIVISION OF A PANEL INTO SUBPANELS	81
REFERENCES	91

LIST OF ILLUSTRATIONS AND TABLES

<u>Figure</u>	<u>Title</u>	<u>Page</u>
1	The Three Computer Programs for the Perturbation Analysis Method	3
2	Bodies Immersed in a Flow Field	5
3	Illustration of Isolated Points and Ridges	6
4	Illustration of Wake Segments	8
5	Division of a Body Into Segments	10
6	Ordering of Corners and Edges on a Segment	11
7	Body Segment Edges on a Ridge	12
8	Schematic of a Segment Divided Into Panels	13
9	Definition of Point Index "k" for a Panel	16
10	Definition of Point Index "l" for a Panel	17
11	Local (ξ, η, ζ) - Coordinate System for a Panel	18
12	Pair of Wake Control Points k_{CP} and k_{CP+1}	26
13	Doublet Spline Control Points on a Segment	28
14	Local Indexing at a Panel Corner Point	29
15	Local Indexing at a Panel Edge Point	29
16	Doublet Discontinuity at Wake - Fuselage Intersection	30
17	Four Panels Along a Ridge	34
18	Two Panelled Representations of a Wing - Fuselage	46
19	Calculated Pressures Near Wing Root (4° Angle of Attack)	48
20	Baseline Wing Panelling for Demonstration of Perturbation Analysis Method	49
21	Test Cases for the Perturbation Analysis Method	50

LIST OF ILLUSTRATIONS AND TABLES (Continued)

<u>Figure</u>	<u>Title</u>	<u>Page</u>
22	Baseline Pressure Distribution at 0° Angle of Attack (NACA 0012)	52
23	Baseline Force and Moment Distribution at 0° Angle of Attack (NACA 0012)	53
24	Baseline Pressure Distribution at 5° Angle of Attack (NACA 0012)	54
25	Baseline Force and Moment Distribution at 5° Angle of Attack (NACA 0012)	55
26	Pressure Distribution of Wing A at 0° Angle of Attack (NACA 0006)	56
27	Force and Moment Distribution of Wing A at 0° Angle of Attack (NACA 0006)	57
28	Pressure Distribution of Wing A at 5° Angle of Attack (NACA 0006)	58
29	Force and Moment Distribution of Wing A at 5° Angle of Attack (NACA 0006)	59
30	Pressure Distribution of Wing B at 0° Angle of Attack (10° Twist)	60
31	Force and Moment Distribution of Wing B at 0° Angle of Attack (10° Twist)	61
32	Pressure Distribution of Wing B at 5° Angle of Attack (10° Twist)	62
33	Force and Moment Distribution of Wing B at 5° Angle of Attack (10° Twist)	63
34	Pressure Distribution of Wing C at 0° Angle of Attack (Supercritical)	64
35	Force and Moment Distribution of Wing C at 0° Angle of Attack (Supercritical)	65
36	Pressure Distribution of Wing C at 5° Angle of Attack (Supercritical)	66
37	Force and Moment Distribution of Wing C at 5° Angle of Attack (Supercritical)	67

LIST OF ILLUSTRATIONS AND TABLES (Continued)

<u>Figure</u>	<u>Title</u>	<u>Page</u>
38	Pressure Distribution of Wing D at 0° Angle of Attack (Fighter)	68
39	Force and Moment Distribution of Wing D at 0° Angle of Attack (Fighter)	69
40	Pressure Distribution of Wing D at 5° Angle of Attack (Fighter)	70
41	Force and Moment Distribution of Wing D at 5° Angle of Attack (Fighter)	71
42	Pressure Distribution of Wing E at 0° Angle of Attack (20° Flaps)	72
43	Force and Moment Distribution of Wing E at 0° Angle of Attack (20° Flaps)	73
A-1	Nomenclature for Two Sets of Three Colinear Points	75
B-1	Division of a Panel Into Subpanels	81
B-2	Local Coordinate System for a Subpanel	82

LIST OF TABLES

<u>Table</u>	<u>Title</u>	<u>Page</u>
I	Geometric Quantities Subject to Perturbations	43
B-I	Conversion Between Index k and Indices (l, i_{gp})	83

LIST OF SYMBOLS

A_{ij}	Aerodynamic Influence Coefficient Matrix
a_{ij}	Rotation Matrix
$b_{i\ell}$	Coefficient Array for Quadratic Doublet Distribution on a Panel
C_L, C_D, C_M	Configuration Lift, Drag, and Pitching Moment Coefficients (moment reference at 25% mean aerodynamic chord)
CTYPE	Corner Type Indicator for a Segment (CTYPE is 1 if not isolated point, 2 otherwise)
c	Constant; Chord
c_i	Coefficients of equation (27)
c_{ℓ}, c_d, c_m	Section Lift, Drag, and Moment Coefficients (moment reference at section quarter chord)
c_p	Pressure Coefficient
DC_m	Coefficients of equation (B19)
$DPI_{\ell j}$	Panel Geometry Derivative Array [defined by equation (22)]
DXI_{kj}	Panel Geometry Derivative Array [defined by equation (20)]
dS_j	Magnitude of the j th Perturbation to the Baseline Geometry
E	Least Square Error Function
ETYPA	Edge Length Indicator for a Segment (ETYPA = 1 for finite length, 2 for zero length)
ETYPB	Indicator for Segment Edge on a Symmetry Plane [ETYPB = (0,1,2) if edge lies on (no symmetry plane, x-z symmetry plane, x-y symmetry plane)]
$\vec{e}_x, \vec{e}_y, \vec{e}_z$	Unit Vector in x, y, z -Direction, Respectively
$\vec{e}_\xi, \vec{e}_\eta, \vec{e}_\zeta$	Unit Vector in ξ, η, ζ -Direction, Respectively
i, j, k, ℓ, m	Indices

i_{CRN}	Index to Identify the Four Corners of a Segment (figure 6)
i_{EDG}	Index to Identify the Four Edges of a Segment (figure 6)
i_p, j_p	Index of a Panel Within a Segment (figure 8)
i_R	Index of a Ridge ($1 \leq i_R \leq n_R$)
i_S	Index of a Segment ($1 \leq i_S \leq n_S$)
i_{SIDE}	Index to Identify the Two Sides of a Ridge (figure 7)
i_{SP}	Subpanel Index (figure B-1)
i_μ, j_μ	Doublet Spline Control Point Indices Within a Segment (figure 13)
$k_O(i_S)$	Number of Defining Points on Segments 1 through i_S-1 [equation (1b)]
k_{CP}	Boundary Condition Control Point Index
$k_{CP_O}(i_S)$	Number of Boundary Condition Control Points on Segments 1 through i_S-1
k'_{CP}	Compressed Boundary Condition Control Point Index (one value k'_{CP} for each pair of wake control points)
k_p	Cumulative Panel Index [equation (2a)]
$k_{P_O}(i_S)$	Number of Panels on Segments 1 through i_S-1 [equation (2b)]
k_μ	Cumulative Index for Doublet Spline Control Points [equation (26)]
$k_{\mu_O}(i_S)$	Number of k_μ 's on Segments 1 through i_S-1
m, n	Number of Points i, j Used to Define the Panelling of a Segment (figure 8)
n_D	Number of Interpolation Points [equation (27)]
n_R	Number of Ridges
n_S	Number of Body and Wake Segments
n_W	Number of Wake Segment Corners in equation (36)
n_x, n_y, n_z	Components of Unit Normal Vector in (x, y, z) -Coordinate System
$\vec{P}_\ell, P_{i\ell}$	Geometry Displacement Vector

RHS_i	Right-Hand-Side Vector for a System of Linear Algebraic Equations
STYPE	Segment Type Indicator (STYPE = 1 for Body Segment, 2 for Wake Segment)
s, s'	Distance
u	Continuous Doublet Function (figure 16)
\vec{V}	Flow Velocity Vector
V_{NP}	Prescribed Normal Velocity at Panel Center
\vec{V}_∞	Free Stream Velocity Vector
v_m	Panel Corner Coordinates, Defined by equation (18)
W_i	Weighting Factor
\vec{W}_N	Unit Direction Vector for Wake Control Points (Kutta Condition: Velocity component = 0 in direction of \vec{W}_N)
X_{ik}	Difference Between Coordinates of Point "k" and First Corner of a Panel
(x, y, z)	Global Cartesian Coordinate System (figure 2)
α_i, β_i	Coefficients of Quadratic Doublet Distribution
$\epsilon(i_S)$	Retraction Factor for Boundary Condition Control Points at Segment Corners and Edges
η	Fraction Semi-span
θ	Half-Angle Between Two Line Segments
μ	Doublet Density
(ξ, η, ζ)	Local Cartesian Coordinate System
σ	Source Density
ϕ	Potential

SUBSCRIPTS:

CP	Control Point
CRN	Corner
D	Dependent
EDG	Edge
M	Edge Midpoint Between Interior and Exterior Subpanels
N	Normal
P	Panel; Prescribed
R	Ridge
S	Segment
SP	Subpanel
W	Wake

SUMMARY

An accurate and efficient method has been developed for the aerodynamic analysis of a series of arbitrary small geometry perturbations to a given baseline configuration. The method is appropriate for wings and wing-fuselage configurations in incompressible, potential flow. Mathematical formulations are presented for three computer programs that are employed.

The first computer program is a conventional panel method. The surface of an arbitrary baseline configuration is represented by an array of panels on which piecewise constant source and quadratic doublet singularity densities are distributed. Based on the classical third identity of Green, the source strength corresponding to prescribed normal velocity (Neumann) boundary conditions is calculated immediately from the local panel geometry. The doublet strength is determined from the theoretically equivalent boundary condition that the internal perturbation potential vanish. A matrix of aerodynamic influence coefficients is calculated in order to establish a linear, algebraic system of boundary condition equations. The solution to the system of equations provides the solution array of doublet strength at boundary condition control points.

The second program calculates a matrix of partial derivatives. Each element of the matrix is the rate of change of doublet strength at one boundary condition control point with respect to the change in a surface coordinate of the paneled baseline geometry. The matrix is generated by a first-order mathematical expansion to the equations of the conventional panel method. The mathematical expansion is based upon analytical differentiation, not numerical.

For each baseline configuration, the calculated quantities from the first two computer programs establish an input file for the third. The purpose of the third program is to calculate the surface pressure distribution and forces and moments for a series of perturbations to the baseline geometry. The third program is similar to the conventional panel method, with one major exception: the solution doublet strengths are generated by linear extrapolation using the partial derivative matrix. This eliminates the two expensive steps of a panel method: calculating the aerodynamic influence coefficient matrix and solving a large system of linear, algebraic equations. The accuracy and efficiency of the perturbation analysis method are demonstrated by example calculations for a low aspect ratio, swept wing.

INTRODUCTION

In the past decade, several surface singularity panel methods have been developed for calculating the incompressible, inviscid pressure distribution on arbitrary three-dimensional configurations (references 1-9). A characteristic of these methods is good prediction accuracy for complex configuration geometries. Compared to an exact potential flow solution, the accuracy is limited only by the number of panels used to represent the surface geometry. Nonetheless, surface panel methods are not widely used for the preliminary aerodynamic design of airplanes. The reason is computing cost. To analyze each change in geometry, it is necessary to compute a new, large matrix of aerodynamic influence coefficients and then solve a corresponding system of linear, algebraic equations for the solution singularity distribution.

This report presents a method recently developed at McDonnell Aircraft Company (MCAIR) for the efficient analysis of a series of arbitrary small geometry perturbations to a baseline configuration. Designated the perturbation analysis method, it was developed under contract to NASA, Langley Research Center. The approach is to first calculate a conventional panel method solution for an arbitrary baseline configuration and then calculate a matrix consisting of the partial derivatives of singularity strength with respect to geometry coordinates. The baseline solution and derivative matrix are calculated one time only and then stored for repetitive use. For each geometry perturbation, the solution singularity distribution is constructed by multiplying the derivative matrix by a new right-hand side. This bypasses the two computationally expensive steps of a conventional panel method: calculating the influence coefficients and solving the large system of linear algebraic equations.

The perturbation analysis method is especially appropriate for application to isolated wings and to wings on fuselages, because aerodynamic properties of wings tend to vary linearly with respect to thickness, camber, and twist. Unlike the existing small disturbance methods, however, the baseline wing is not limited to a zero thickness plate. Furthermore, the perturbation analysis method can accurately predict the change in peak pressure coefficient with respect to changes in leading edge camber and radius of curvature. Even small changes in wing planform and fuselage geometry can be analyzed.

To apply the perturbation analysis method, the following three computer programs are required (see figure 1):

- (a) MCAIR 3-D Subsonic Potential Flow Program (Version 2)
- (b) MCAIR 3-D Geometry Influence Coefficient Program (Version 1)

(c) MCAIR 3-D Perturbation Analysis Program (Version 1)

	MCAIR 3-D Subsonic Potential Flow Program (Version 2)	MCAIR 3-D Geometry Influence Coefficient Program (Version 1)	MCAIR 3-D Perturbation Analysis Program (Version 1)
Input	<ul style="list-style-type: none"> Baseline Geometry $(x, y, z)_j$ 	<ul style="list-style-type: none"> Baseline Geometry $(x, y, z)_j$ Baseline Singularity Distribution μ_i 	<ul style="list-style-type: none"> Baseline Properties $(x, y, z)_j, \mu_i$ Derivative Matrix $(\partial\mu_i/\partial x_j, \partial\mu_i/\partial y_j, \partial\mu_i/\partial z_j)$ Geometry Perturbation $(\Delta x, \Delta y, \Delta z)_j$
Approach	<ul style="list-style-type: none"> Conventional Panel Method 	<ul style="list-style-type: none"> First-Order Expansion to Panel Method Formulation 	<ul style="list-style-type: none"> Linear Extrapolation $\Delta\mu_i = \sum_j [(\partial\mu_i/\partial x_j) \Delta x_j + (\partial\mu_i/\partial y_j) \Delta y_j + (\partial\mu_i/\partial z_j) \Delta z_j]$
Output	<ul style="list-style-type: none"> Baseline Singularity Distribution μ_i Baseline Aerodynamic Properties 	<ul style="list-style-type: none"> Derivative Matrix $(\partial\mu_i/\partial x_j, \partial\mu_i/\partial y_j, \partial\mu_i/\partial z_j)$ 	<ul style="list-style-type: none"> Aerodynamic Properties of Perturbed Geometry

Figure 1. The Three Computer Programs for the Perturbation Analysis Method

The first program (a) is an improved version of the conventional surface panel method of reference 9. The improvements, developed as part of the 1980 MCAIR Independent Research and Development Program, include a subpanel formulation that enforces doublet continuity at panel edges. The mathematical formulation for the program is presented in this report. For the conventional calculation of pressures, forces, and moments on an arbitrary configuration, only the first program is used.

For the perturbation analysis method, the second program (b) employs an output solution file from the first program plus a differential mathematical formulation to calculate the partial derivative matrix. For each baseline configuration, the first two programs generate an input file for the third program (c). At any future date, the third program can be repeatedly executed at low computing cost in order to predict pressures, forces, and moments corresponding to arbitrary small geometry perturbations. Both the second and third programs were developed under NASA Contract NAS1-16156, and the mathematical formulation is presented in this report.

In addition to documenting the formulation of the three computer programs, the purpose of this report is to present example solutions that demonstrate prediction accuracy and computational efficiency. A review of classical surface singularity theory for Laplace's equation and the application to panel methods is available in reference 8 and is not repeated here.

Use of trade names or names of manufacturers in this report does not constitute an official endorsement of such products or manufacturers, either expressed or implied, by the National Aeronautics and Space Administration.

DEFINITION OF THE ANALYSIS FLOW PROBLEM AND
ANALYTICAL RESTRICTIONS

Consider any number of bodies immersed in an incompressible, potential flow field (figure 2). A body must have finite thickness, and no point on the surface of one body can contact the surface of another. The fluid velocity is measured with respect to an arbitrarily selected Cartesian coordinate system (x, y, z) . It is assumed that either (1) the fluid is unbounded and would have uniform velocity \vec{V}_∞ if the bodies were removed or (2) the entire field is bounded by (contained within) one additional body. Suppose that the component of flow velocity normal to the surface is known at every body surface point in the field. In the analysis or Neumann problem, the objective is to solve for the two tangential velocity components. For steady state flow, Bernoulli's equation can be used to convert velocity to surface pressure, and subsequent pressure integration can provide body forces and moments.

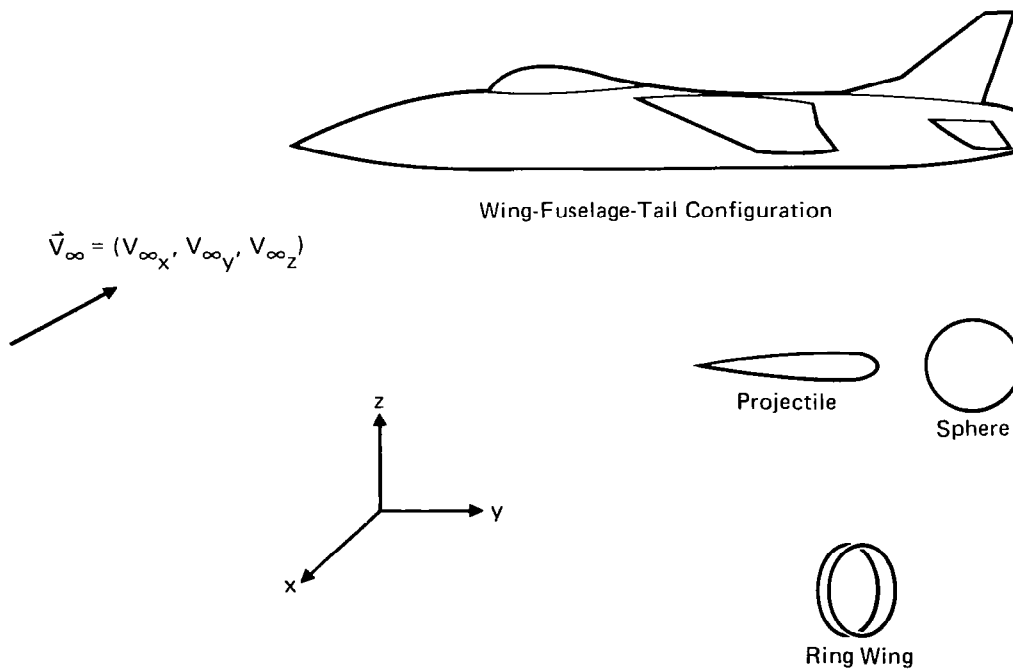


Figure 2. Bodies Immersed in a Flowfield

Sharp edges and points on a body are permissible and are designated "ridges" and "isolated points," respectively (figure 3). Formally, a ridge is a path on a body surface for which (1) the path is continuous, (2) the path direction is continuous, and (3) the body surface unit normal vector is generally discontinuous across the path. Examples of ridges are wing trailing edges and wing-fuselage intersections. An isolated point is a point where (1) every body surface path through the point has a discontinuity in direction and/or (2) three or more ridge endpoints coincide. Examples of isolated points are the vertex of a cone and trailing edge point of a wing tip. Typically, a ridge will begin and end at isolated points. However, a ridge can be a closed loop with no isolated points, in which case the selection of an endpoint is arbitrary.

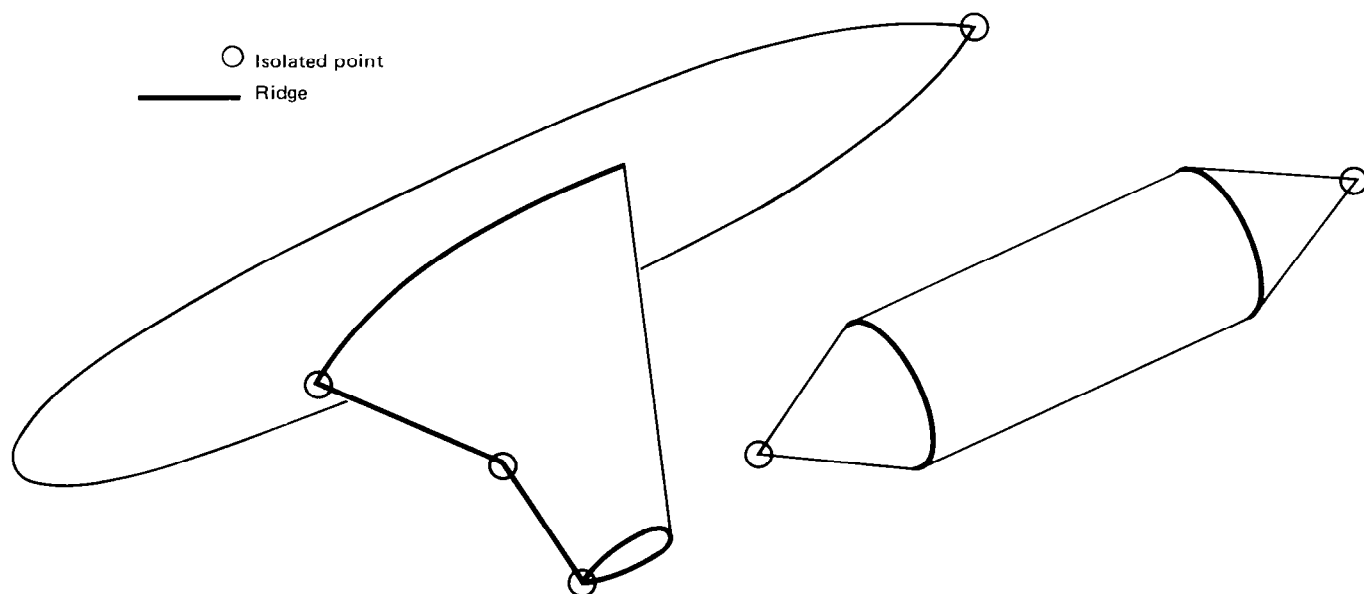


Figure 3. Illustration of Isolated Points and Ridges

In real flows, a thin viscous wake is convected from sharp edges by the fluid. In accordance with classical lifting surface theory, it is assumed that the effect of a wake on the flow field can be analytically simulated by introducing one or more trailing vortex sheets, herein designated "wake segments" (figure 4). It is also assumed that the geometry of each wake segment is known a priori. The four edges of a wake segment are designated the "forward edge," the "side edges," and the "rear edge." The side edges should be approximately aligned with the local flow direction. Restrictions on wake segments are presented below:

- (1) Every point on both surfaces of a wake segment must be wetted by the potential flow,
- (2) The length of each of the four edges of a wake segment must be finite (neither zero nor infinite),

- (3) The classical Kutta condition is imposed on the forward edge, which must entirely coincide with a ridge of a body. If the ridge is longer than the forward edge, one or more additional wake segments must be attached to the ridge. In general, either no portion of a ridge or else the entire length must coincide with wake forward edges,
- (4) A forward edge cannot coincide with any other wake segment edges,
- (5) It is permissible for any portion of a side edge to be exposed to the potential flow, to coincide with another side edge (of even the same wake segment), or to coincide with a body surface,
- (6) The rear edge, which corresponds to the starting vortex of classical lifting surface theory, must be fully exposed to the potential flow. The edge must not contact any part of any body or any wake segment.

The computer programs described in this report are dedicated to solving the analysis problem defined above. The mathematical solution formulation is presented in the next section.

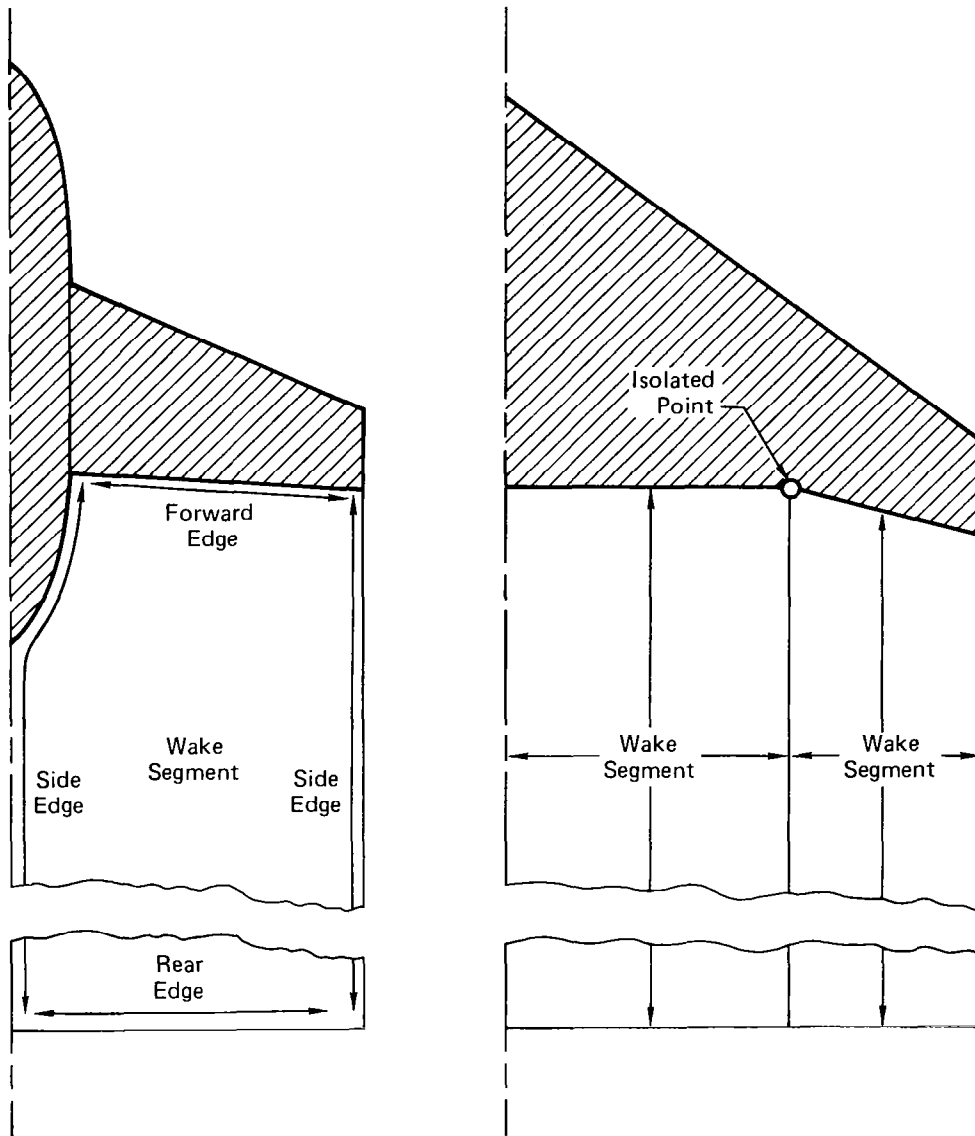


Figure 4. Illustration of Wake Segments

MATHEMATICAL FORMULATION

The MCAIR 3-D Subsonic Potential Flow Program (Version 2) is a surface panel method that is based on the combined source-doublet distribution of the classical third identity of Green (reference 10). The advantages of this combined source-doublet distribution for a surface panel method are well documented (reference 8). The mathematical formulation employs a constant source distribution and a quadratic doublet distribution on each panel, where the solution singularity strengths are determined by satisfying indirect internal perturbation potential boundary conditions (reference 4). The flow velocity on each panel is then established from local velocity-singularity relationships associated with Green's third identity, instead of the direct summation of the influences of the singularities on all the panels.

The formulation to the MCAIR 3-D Geometry Influence Coefficient Program (Version 1) is similar, with one major exception. In each step of the solution process, the derivative of each quantity with respect to geometric coordinates is established, rather than the quantity itself. This process culminates in the generation of the matrix of partial derivatives of singularity strength with respect to geometry perturbations.

The details of the mathematical formulation are presented in the following subsections. In each subsection for which mathematical formulas are presented, the first portion of the subsection presents the equations that are appropriate for the MCAIR 3-D Subsonic Potential Flow Program (Version 2), and the second portion presents the analogous differential equation for the MCAIR 3-D Geometry Influence Coefficient Program (Version 1). The third computer program [MCAIR 3-D Perturbation Analysis Program (Version 1)] is nearly identical to the first. The only significant difference is that implementation of the matrix of partial derivatives eliminates the need to calculate aerodynamic influence coefficients and to solve a large system of linear algebraic boundary condition equations.

Division of a Body Into Segments

For computational purposes, the surface of every body is considered to be divided into a set of singly-connected surfaces designated "body segments" (figure 5). Each segment is bounded by four corners and four edges. A zero length edge is permissible. However, no zero length edge can touch a ridge (except at a ridge endpoint that is also an isolated point). To be consistent with surface singularity theory, every point on the wetted surface of a body should be part of a segment.

With the exception of the following restrictions, the division of a body surface into segments is arbitrary:

- (1) Only edges (and corners) of a body segment can contact a ridge,

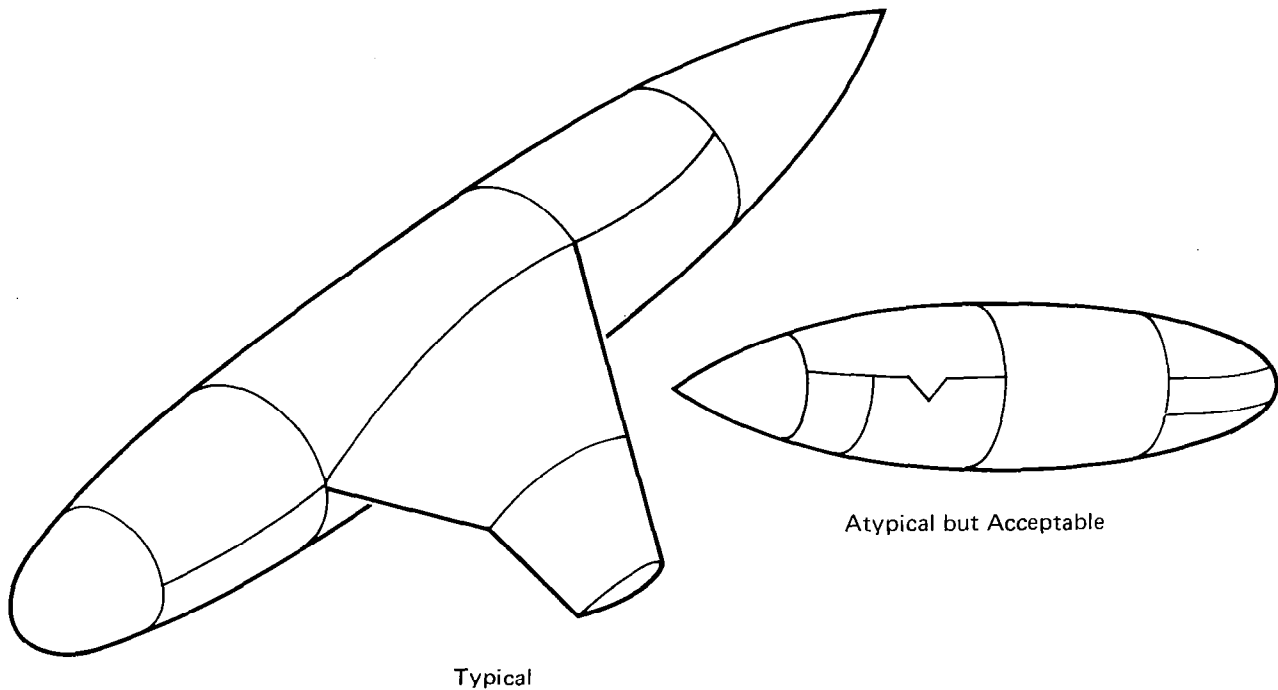


Figure 5. Division of a Body into Segments

- (2) Only corners and zero length edges of a body segment can contact an isolated point or a ridge endpoint,
- (3) Only edges (and corners) of a body segment can contact the side edge of a wake. Furthermore, such contact must occur along the full length of the body segment edge,
- (4) If a portion of a body segment edge coincides with a flow symmetry plane and the method of images is employed, then the full length of the edge must coincide with the plane.

It is permissible for two edges of one body segment to coincide. For example, a single segment could represent both the upper and lower surfaces of a wing, in which case two opposite edges of the segment would coincide at the wing trailing edge.

The total number of body and wake segments in the field is designated n_s . If the method of images is employed, the $x-z$ plane must be a flow symmetry plane and only the segments for which $y > 0$ are included in the total n_s . If the $x-y$ plane is a second flow symmetry plane, then only the segments for which both $y > 0$ and $z > 0$ are included. Each of the n_s segments is assigned an index i_s ($1 \leq i_s \leq n_s$) where the ordering is completely arbitrary. Body and wake segments are respectively identified by the nomenclature $STYPE(i_s) = 1$ and 2.

Each of the four corners and edges of a segment are identified by the indices "i_{CRN}" and "i_{EDG}" (figure 6). For a body segment, the ordering is counterclockwise with respect to an observer in the flow field looking at the surface. For both body and wake segments, the local surface normal vector is positive if it points out of the plane of the page in figure 6. For a wake segment, i_{EDG} = 1 is the forward edge, 2 and 4 are the side edges, and 3 is the rear edge. If the forward edge of two adjacent wake segments are attached to the same ridge, the adjacent side edges must be i_{EDG} = 2 of one wake segment and i_{EDG} = 4 of the other.

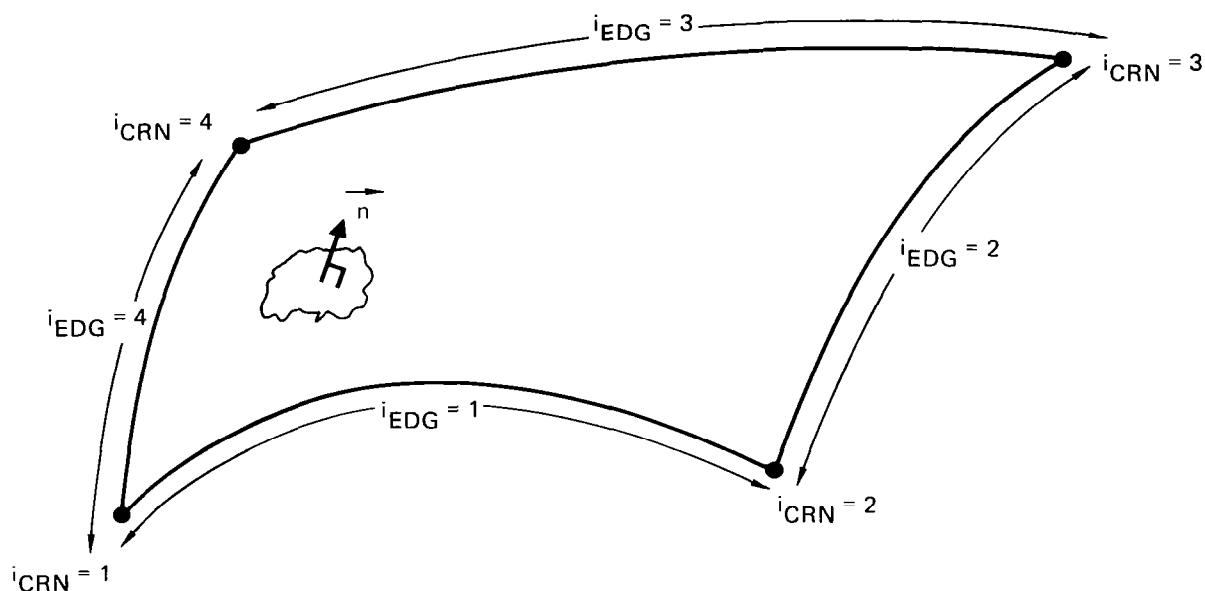


Figure 6. Ordering of Corners and Edges on a Segment

Each corner i_{CRN} of each segment i_S is categorized by CTYPE(i_{CRN}, i_S) where

CTYPE = 1 if the corner does not coincide with an isolated point,
 2 if it does.

Each edge i_{EDG} of each segment i_S is categorized by both ETYP A(i_{EDG}, i_S) and ETYP B(i_{EDG}, i_S) where

1 if the length of the edge is finite,
 ETYPA = 2 if the edge is a zero length body segment edge
 not on a ridge, and

 0 if the edge does not lie on a symmetry plane,
 ETYPB = 1 if the edge lies on the $y = 0$ symmetry plane,
 2 if the edge lies on the $z = 0$ symmetry plane.

Illustrated in figure 7 are body segments on opposite sides of a ridge. One side is selected to be designated $i_{SIDE} = 1$ and the other $i_{SIDE} = 2$. Although it is not consistent with analytical theory, it is sometimes reasonable to ignore the body on one side of a ridge. For example, the surface of a wing tip is usually not represented in practice. However, if the forward edge of a wake is attached to a ridge, then both sides of the ridge must be represented by body segments.

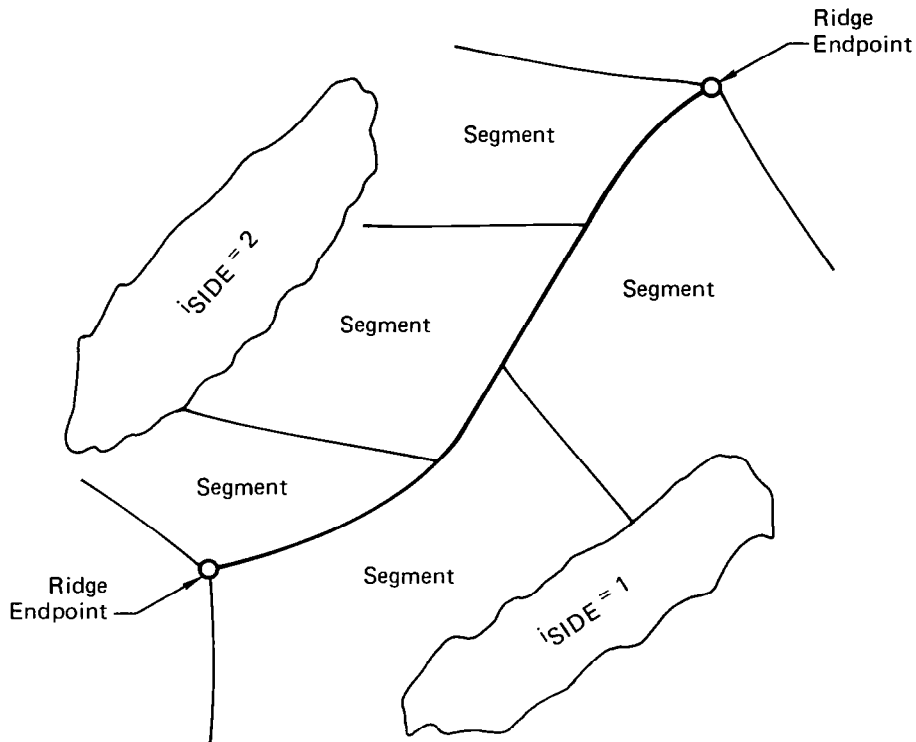


Figure 7. Body Segment Edges on a Ridge

The total number of ridges that lie along edges of the n_g body and wake segments is defined as n_R , where n_R is zero if there are no ridges. Each ridge is assigned an index i_R ($1 \leq i_R \leq n_R$). Usually, the endpoint of a ridge is an isolated point. However, if the ridge is a closed contour on which there is no isolated point, then one point on the contour must be selected as the endpoint. Furthermore, if a ridge passes through a symmetry plane and the method of images is applied, then the point on the symmetry plane is designated a ridge endpoint.

Division of a Segment Into Panels

The geometry of each segment i_g is represented by a grid of points, where the points are identified by rectangular indexing (i,j) ; see figure 8. The value of the limits m and n on the indices i and j are selected by the user and can vary from one segment to another. It is usually recommended that each point which lies on the edge of one segment should coincide with a point on the edge of an adjacent segment. However, discontinuities in point density and even geometric gaps are permitted between adjacent segment edges.

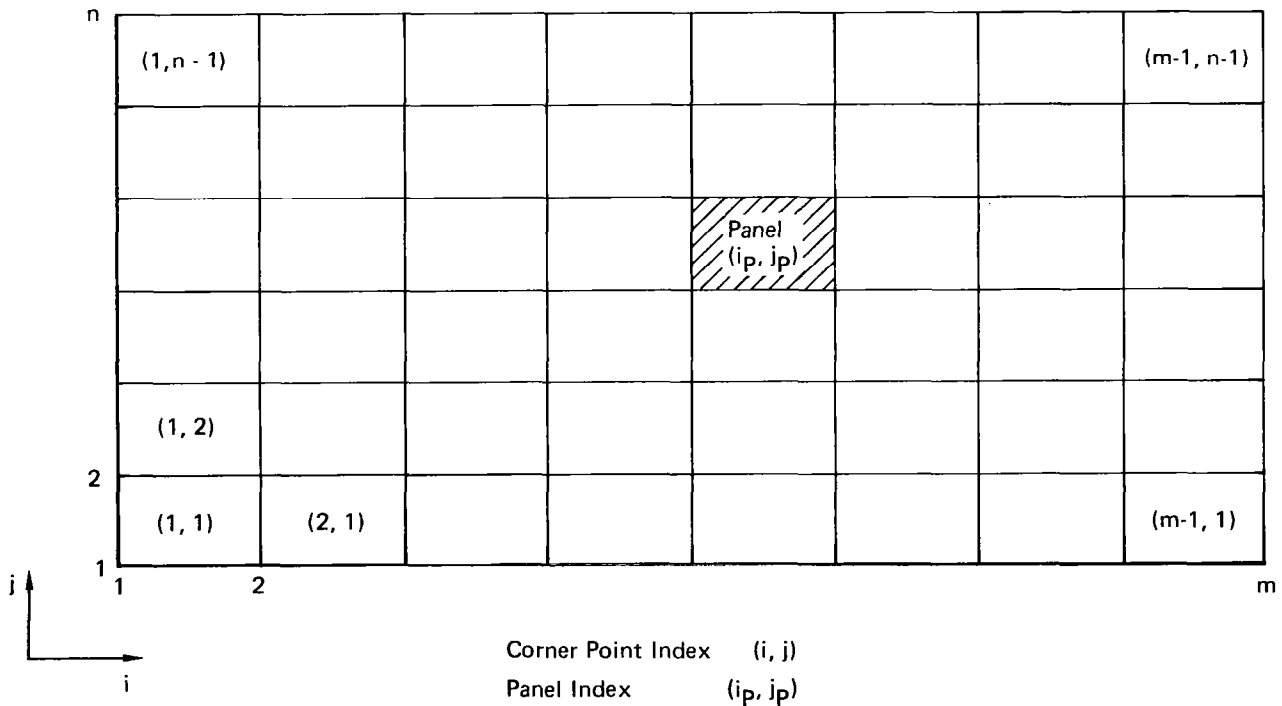


Figure 8. Schematic of a Segment Divided into Panels

For consistency with the segment corner nomenclature of figure 6, it is stipulated that the values $i_{CRN} = \{1; 2; 3; 4\}$ correspond to the points $(i,j) = \{(1,1); (m,1); (m,n); (1,n)\}$. Consequently, $i_{EDG} = \{1; 2; 3; 4\}$ corresponds to $\{j=1; i=m; j=n; i=1\}$.

The four points $\{(i,j); (i+1,j); (i+1,j+1); (i,j+1)\}$ are the four corners of a geometric panel. Each panel is identified by the pair of indices i_p and j_p . The edges of a panel are formed by the four straight line segments that connect adjacent panel corners, where the line segments are not necessarily coplanar.

A cumulative index k identifies individual points for the collective system of n_s body and wake segments. The conversion from the point indexing (i,j) of segment i_s to the cumulative index k is

$$k = k_o(i_s) + (i-1) \cdot n + j \quad (1a)$$

where

$$k_o(i_s) \equiv \left\{ \begin{array}{l} 0 \dots \dots \dots i_s = 1 \\ (i_s - 1) \\ \sum_{j_s=1} [m(j_s) \cdot n(j_s)] \quad 2 \leq i_s \leq (n_s + 1) \\ j_s = 1 \end{array} \right\} \quad (1b)$$

The geometry of the entire configuration is defined by the following array of coordinates to be specified by the user:

$$(x, y, z)_k \quad \text{where } 1 \leq k \leq k_o(n_s + 1)$$

A cumulative panel index k_p is related to the panel indexing (i_p, j_p) of segment i_s as follows:

$$k_p = k_{p_o}(i_s) + (i_p - 1) \cdot (n - 1) + j_p \quad (2a)$$

$$X_{ik} = \left. \begin{cases} \frac{1}{2}[X_{i(k-4)} + X_{i(k-3)}] & 5 \leq k \leq 7 \\ \frac{1}{2}[X_{i(k-4)} + X_{i1}] & k = 8 \\ \frac{1}{2}[X_{i5} + X_{i7}] & k = 9 \end{cases} \right\} \quad (4)$$

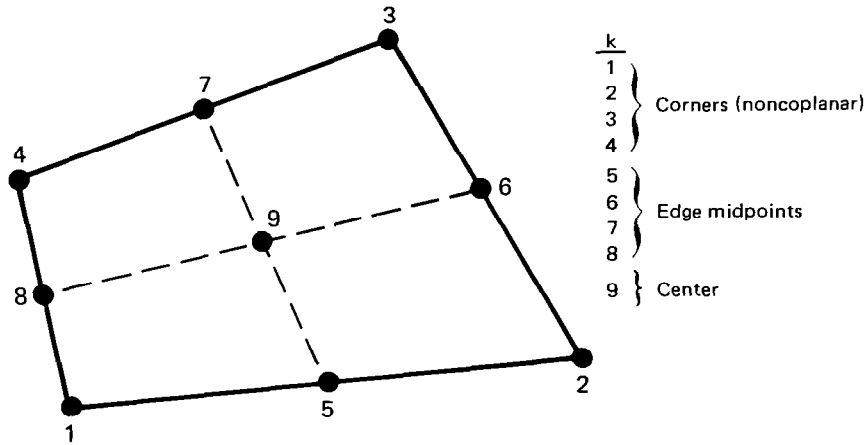


Figure 9. Definition of Point Index "k" for a Panel

The coordinates of the panel center are designated $(x, y, z)_O$.

$$(x, y, z)_O = (x_1, y_1, z_1) + (X_{19}, X_{29}, X_{39}) \quad (5)$$

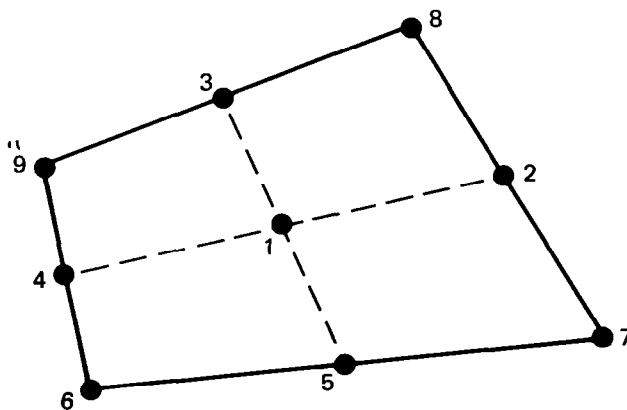
The panel area is calculated by the magnitude of a vector cross-product.

$$\text{AREA} = |(X_{i7} - X_{i5}) \times (X_{i8} - X_{i6})| \quad (6)$$

The nine points k are designated "spline control points." Suppose that an arbitrary value of doublet strength (μ_k) is assigned to each spline control point. It is desired to establish a quadratic distribution that will exactly match μ_k at the panel center and edge midpoints and approximately match μ_k at the panel corners. This is accomplished by applying the method of Appendix A, which takes advantage of the fact that points $k = 5, 7,$ and 9 are colinear and points $k = 6, 8,$ and 9 are colinear. First, it is necessary to introduce a new set of indices and a local panel coordinate system that are consistent with Appendix A.

As presented in figure 10, the index ℓ is introduced to designate the points $1 \leq k \leq 9$ in a different order. The nomenclature $\ell(k)$ and $k(\ell)$ respectively denote the conversion of k to ℓ and ℓ to k . Define the array $P_{i\ell}$ (equivalent to a vector \vec{P}_ℓ) as the coordinate displacement of each point ℓ from the panel center:

$$P_{i\ell} \equiv \vec{P}_\ell \equiv [X_{i,k(\ell)} - X_{i,k(1)}] \quad (1,1) \leq (i,\ell) \leq (3,9) \quad (7)$$



Conversion Between ℓ and k

ℓ	k
1	9
2	6
3	7
4	8
5	5
6	1
7	2
8	3
9	4

Figure 10. Definition of Point Index " ℓ " for a Panel

A local (ξ, η, ζ) Cartesian coordinate system with origin at the panel center is constructed (figure 11) such that the unit vectors $(\vec{e}_\xi, \vec{e}_\eta, \vec{e}_\zeta)$ are

$$\vec{e}_\zeta \equiv \frac{\frac{\vec{P}_2}{|\vec{P}_2|} + \frac{\vec{P}_3}{|\vec{P}_3|}}{\left| \frac{\vec{P}_2}{|\vec{P}_2|} + \frac{\vec{P}_3}{|\vec{P}_3|} \right|} \quad (8)$$

$$\vec{e}_\zeta \equiv (\vec{P}_2 \times \vec{P}_3) / |(\vec{P}_2 \times \vec{P}_3)| \quad (9)$$

$$\vec{e}_\eta \equiv (\vec{e}_\zeta \times \vec{e}_\xi) \quad (10)$$

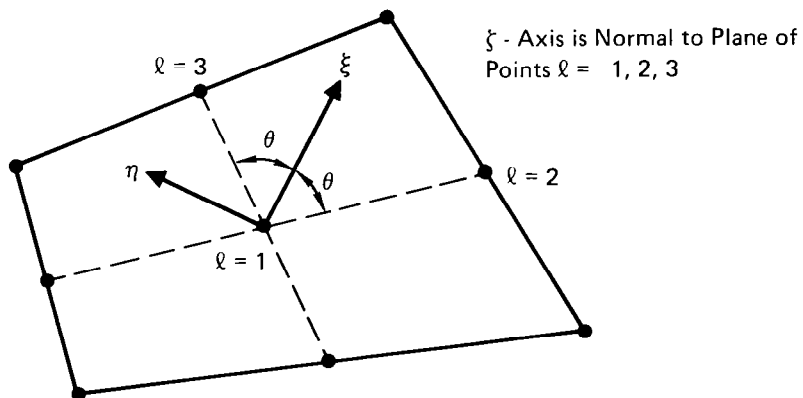


Figure 11. Local (ξ, η, ζ) - Coordinate System for a Panel

The vector \vec{e}_ζ is designated the panel unit normal vector. Equations (8) - (10) are equivalent to a rotation matrix a_{ij} , where

$$\begin{Bmatrix} \vec{e}_\xi \\ \vec{e}_\eta \\ \vec{e}_\zeta \end{Bmatrix} = [a_{ij}] \begin{Bmatrix} \vec{e}_x \\ \vec{e}_y \\ \vec{e}_z \end{Bmatrix} \quad (11)$$

The angle θ of figure 11 is

$$\theta = \frac{1}{2} \cos^{-1} [(\vec{P}_2 \cdot \vec{P}_3) / (|\vec{P}_2| \cdot |\vec{P}_3|)] \quad (12)$$

Define the distance between the panel center and point ℓ as

$$s_\ell \equiv \begin{Bmatrix} 0 & \ell = 1 \\ +|\vec{P}_\ell| & \ell = 2, 3 \\ -|\vec{P}_\ell| & \ell = 4, 5 \end{Bmatrix} \quad (13)$$

The coordinates of the panel corners in the local (ξ, η, ζ) - coordinate system are

$$\begin{Bmatrix} \xi_\ell = \vec{P}_\ell \cdot \vec{e}_\xi \\ \eta_\ell = \vec{P}_\ell \cdot \vec{e}_\eta \end{Bmatrix} \quad 6 \leq \ell \leq 9 \quad (14)$$

A coplanar adjustment is performed by setting

$$\zeta_\ell = 0 \quad (6 \leq \ell \leq 9) \quad (15)$$

With the aid of the above defined quantities, the method of Appendix A will establish the quadratic doublet distribution in the following form:

$$\begin{aligned} \mu(\xi, \eta) = & \mu_k(1) + \beta_1 \xi + \beta_2 \eta + \beta_3 \xi^2 + \beta_4 \xi \eta \\ & + \beta_5 \cdot (\eta^2 - \xi^2 \tan^2 \theta) \end{aligned} \quad (16)$$

where

$$\beta_i = \sum_{\ell=1}^5 [b_{i\ell} \cdot \mu_k(\ell)] + \delta_{i5} \cdot \sum_{\ell=6}^9 [b_{5\ell} \cdot \mu_k(\ell)] \quad (1 \leq i \leq 5) \quad (17)$$

Each quadratic coefficient β_i is a linear function of μ_k . The sensitivity matrix elements $b_{i\ell}$ [$(1,1) \leq (i, \ell) \leq (5,5)$] and $b_{5\ell}$ ($6 \leq \ell \leq 9$) are calculated independently of μ_k ; in fact, the calculations depend only on the nine quantities X_{1k}, X_{2k}, X_{3k} ($2 \leq k \leq 4$). For $k = 1$, the quantity X_{1k} is always zero and therefore does not affect the calculations.

The preceding discussion addressed the procedure for establishing the quadratic doublet distribution corresponding to known values X_{ik} and arbitrary unknown values μ_k . Now suppose that each μ_k is assigned a fixed, known value. The method for determining the first-order change in quadratic doublet distribution induced by geometry perturbations (dX_{ik}) is presented below.

Define the array "v" as follows:

$$\begin{aligned} & \{v_1, v_2, v_3, v_4, v_5, v_6, v_7, v_8, v_9\} \\ & \equiv \{X_{12}, X_{22}, X_{32}, X_{13}, X_{23}, X_{33}, X_{14}, X_{24}, X_{34}\} \end{aligned} \quad (18)$$

The purpose behind the introduction of single-subscripted array "v" is to simplify the indexing. Then dx_{ik} for $1 \leq k \leq 9$ can be expressed as

$$dx_{ik} = \sum_{j=1}^3 DXI_{kj} \cdot dv_{[i+3(j-1)]} \quad 1 \leq i \leq 3 \quad (19)$$

where

$$DXI_{kj} \equiv \left\{ \begin{array}{ll} 0 & \text{if } k = 1 \\ \delta_{k(j+1)} & \text{if } k = (2, 3, 4) \\ \frac{1}{2}[DXI_{(k-4)j} + DXI_{(k-3)j}] & \text{if } k = (5, 6, 7) \\ \frac{1}{2}[DXI_{(k-4)j} + DXI_{1j}] & \text{if } k = 8 \\ \frac{1}{2}[DXI_{5j} + DXI_{7j}] & \text{if } k = 9 \end{array} \right\} \quad (20)$$

Equations (19) and (20) give the rate of change of the 27 values X_{ik} with respect to each of the nine members of the v-array.

The derivative of $P_{i\ell}$ can be expressed as

$$dP_{i\ell} = \sum_{j=1}^3 DPI_{\ell j} \cdot dv_{[i+3(j-1)]} \quad (1,1) \leq (i,\ell) \leq (3,9) \quad (21)$$

where

$$DPI_{\ell j} \equiv [DXI_{k(\ell),j} - DXI_{k(1),j}] \quad (22)$$

By applying the calculated values DXI_{kj} and DPI_{lj} to the derivatives of equations (8) - (14), the following quantities are calculated for $1 \leq m \leq 9$:

$$\left\{ \frac{\partial a_{ij}}{\partial v_m}, \frac{\partial \theta}{\partial v_m}, \frac{\partial s_\ell}{\partial v_m} \right\} \text{ for } (1,1,2) \leq (i,j,\ell) \leq (3,3,5)$$

$$\text{and } \left\{ \frac{\partial \xi_\ell}{\partial v_m}, \frac{\partial \eta_\ell}{\partial v_m} \right\} \text{ for } 6 \leq \ell \leq 9$$

The method of Appendix A will provide calculated values for $\partial \beta_i / \partial \theta$, $\partial \beta_i / \partial s_\ell$ for $2 \leq \ell \leq 5$, and $(\partial \beta_i / \partial \xi_\ell, \partial \beta_i / \partial \eta_\ell)$ for $6 \leq \ell \leq 9$. The change in quadratic doublet coefficient ($d\beta_i$) generated by panel geometry perturbations is

$$d\beta_i = \left(\frac{\partial \beta_i}{\partial \theta} \right) d\theta + \sum_{\ell=2}^5 \left(\frac{\partial \beta_i}{\partial s_\ell} \right) ds_\ell + \sum_{\ell=6}^9 \left[\left(\frac{\partial \beta_i}{\partial \xi_\ell} \right) d\xi_\ell + \left(\frac{\partial \beta_i}{\partial \eta_\ell} \right) d\eta_\ell \right]$$

$$= \sum_{m=1}^9 \left\{ \left(\frac{\partial \beta_i}{\partial \theta} \right) \left(\frac{\partial \theta}{\partial v_m} \right) + \sum_{\ell=2}^5 \left(\frac{\partial \beta_i}{\partial s_\ell} \right) \left(\frac{\partial s_\ell}{\partial v_m} \right) \right. \quad (23)$$

$$\left. + \sum_{\ell=6}^9 \left[\left(\frac{\partial \beta_i}{\partial \xi_\ell} \right) \left(\frac{\partial \xi_\ell}{\partial v_m} \right) + \left(\frac{\partial \beta_i}{\partial \eta_\ell} \right) \left(\frac{\partial \eta_\ell}{\partial v_m} \right) \right] \right\} dv_m$$

All of the partial derivatives of equation (23) are calculated quantities. Consequently, the multiplications and summations of equation (23) can be performed to provide $\partial \beta_i / \partial v_m$ for $(1,1) \leq (i,m) \leq (5,9)$.

Now consider arbitrary simultaneous perturbations to both panel geometry (dv_m) and doublet strength at the spline control points (dv_k). Then the change in quadratic doublet coefficient ($d\beta_i$) can be predicted by the following formula.

$$\begin{aligned}
d\beta_i = & \sum_{m=1}^9 \left[\left(\frac{\partial \beta_i}{\partial v_m} \right) dv_m \right] + \sum_{\ell=1}^5 [b_{i\ell} \cdot d\mu_{k(\ell)}] \\
& + \delta_{i5} \cdot \sum_{\ell=6}^9 [b_{5\ell} \cdot d\mu_{k(\ell)}]
\end{aligned} \tag{24}$$

All the coefficients of equation (24) are known quantities, calculated by the procedure described above. In the same sense that the linear relationship between β_i and μ_k of equation (17) is appropriate for a conventional panel method, the linear relationship between $d\beta_i$ and dv_m of equation (24) is appropriate for the analysis of small geometry perturbations.

The formulation presented above in this section adjusts each noncoplanar panel in order to form a planar quadrilateral. This will typically generate small gaps between the edges of adjacent panels. Furthermore, the quadratic doublet distributions will typically be discontinuous across the edge. These small geometric and singularity discontinuities are usually insignificant, except for panels that are adjacent to a ridge. An alternate formulation that eliminates these discontinuities at the expense of increased complexity is presented in Appendix B. There each panel is divided into eight triangular subpanels. The alternate formulation is always used for each panel that is adjacent to a ridge. For the remaining panels, the formulation of this section is normally applied.

Boundary Condition Control Points

A set of control points on body and wake segments is specified as locations where flow boundary conditions are to be satisfied. The center of every panel of every body segment is always a control point. In addition, certain body segment points along ridges and certain points on the forward edge of each wake segment are boundary condition control points.

Every control point is assigned an index k_{CP} . The range of indices for body or wake segment i_S is designated

$$k_{CP_0}(i_S) + 1 \leq k_{CP} \leq k_{CP_0}(i_S+1)$$

where $k_{CP_0}(i_S)$ is the total number of control points on the segments preceding i_S .

The boundary condition control points on the panels of body segment i_S are established in the following order:

- (1) The center of each panel (i_p, j_p) is a control point, and the index is

$$k_{CP} = k_{CP_0}(i_S) + (i_p - 1) \cdot (n - 1) + j_p$$

- (2) The midpoint of each panel edge that adjoins a ridge is a control point. The control point ordering proceeds counterclockwise around the segment from $i_{EDG} = 1$ through $i_{EDG} = 4$. Exception: There is an option to be discussed later for which all the panel edge control points are eliminated on the side of the ridge designated by the user as $i_{SIDE} = 2$.
- (3) If a corner of a body segment coincides with an isolated point, there is normally a control point at the corner, and the control point indexing increases with respect to increasing corner index i_{CRN} . The control point will exist if $CTYPE(i_{CRN}, i_S) = 2$ and $ETYP(A(i_{CRN} - 1, i_S)) = 1$ [where $(i_{CRN} - 1)$ is to be replaced by 4 iff i_{CRN} is 1].

Each boundary condition control point of a body segment is located near but not on the local panel (or subpanel) surface. The location is on the interior side of the panel at a distance $\sqrt{\text{panel area}} \cdot 10^{-8}$ from the surface. The control points on panel edges and corners, (2) and (3) above, are retracted slightly in the general direction of the panel center. The approximate distance retracted is a fraction $[\epsilon(i_S)]$ of the distance to the panel center, where $\epsilon(i_S)$ is a value specified by the user [recommended value for body segments: $\epsilon(i_S) = 0.02$].

Along the forward edge of each wake segment i_S , control points are established in pairs. For each pair, one point (k_{CP}) is slightly below the local wake panel (or subpanel) and the second point ($k_{CP} + 1$) is slightly above. The line integral of velocity between the two control points ($\int \vec{V} \cdot \vec{ds}$) will be set equal to zero, thereby satisfying one Kutta condition equation for each pair of control points. For wake segment i_S , each pair of boundary condition control points is established in the following order:

- (1) There is one pair of control points centered at each panel edge midpoint along the segment forward edge ($i_{EDG} = 1$). The two control point indices are

$$k_{CP} = k_{CP_0}(i_S) + 2 \cdot (i_P - 1) + (1 \text{ or } 2)$$

- (2) There is one pair of control points centered at segment corner $i_{CRN} = 1$ if $CTYPE(1, i_S) = 2$. Furthermore, there is a pair at $i_{CRN} = 2$ if $CTYPE(2, i_S) = 2$.

Each pair of wake control points is retracted from the panel edge or corner in the same manner described above for body control points. For wake segments, however, the recommended value for the retraction factor $\epsilon(i_S)$ is generally not the value of 0.02 that is appropriate for body control points. Instead, the guidelines in the following paragraph should be employed.

Figure 12 is a cross-section view in which the forward edge of wake segment i_S is attached to a ridge of a body. Typically, the ridge will be the trailing edge of a wing. The lengths Δs_A , Δs_B , and Δs_C are the dimensions in the cross-section view of the three local panels that adjoin the ridge. The distance between the two wake control points (k_{CP} and k_{CP+1}) is approximately equal to the retraction distance from the ridge. It is recommended that the value $\epsilon(i_S)$ be specified such that

$$\epsilon(i_S) \cong 0.02 \times \left(\frac{\Delta s_A + \Delta s_B}{\Delta s_C} \right)$$

For each pair of wake control points, the unit direction vector \vec{W}_N is specified by the user. In typical practice, \vec{W}_N is normal to the local bisector of a wing trailing edge.

For each body control point and each wake control point, the calculated coordinates are designated $(x, y, z)_{k_{CP}}$. Corresponding to the discussion above, these coordinates are a function of the locations of the four corners of the local panel and, in the case of a wake control point, a function of the local vector \vec{W}_N . If the subscripts 1, 2, 3 and 4 are used to denote the four panel corners, then the first order change in control point location induced by perturbations to both the panel geometry and \vec{W}_N can be expressed as

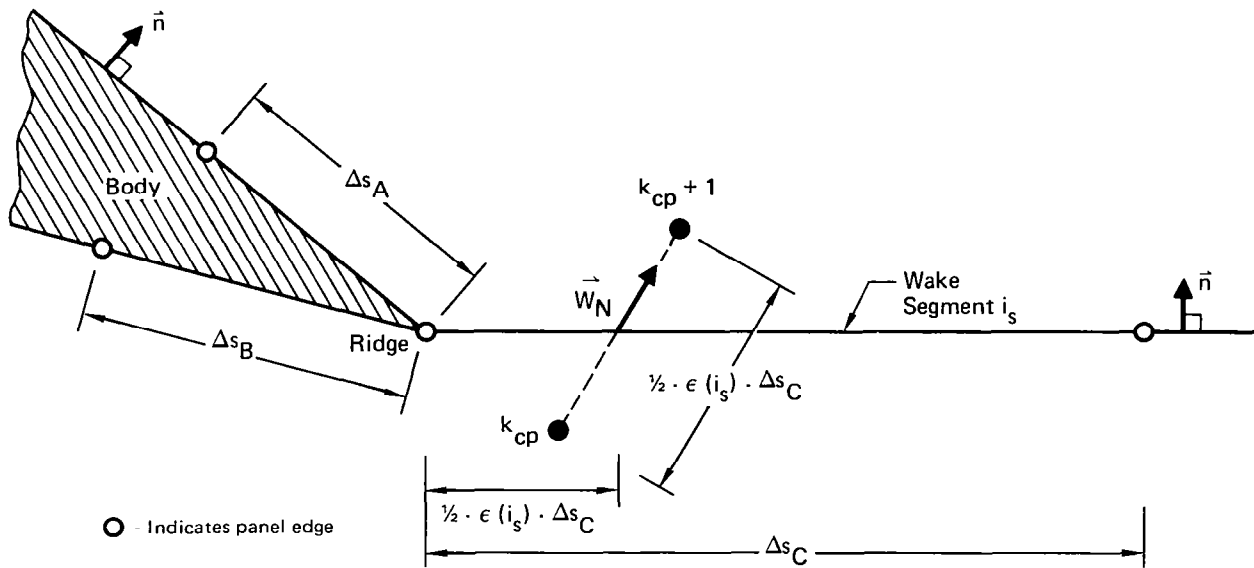


Figure 12. Pair of Wake Control Points k_{cp} and $k_{cp} + 1$

$$\begin{aligned}
 d(x,y,z)_{k_{CP}} = & +a \cdot d(x,y,z)_1 + b \cdot d(x,y,z)_2 \\
 & +c \cdot d(x,y,z)_3 + d \cdot d(x,y,z)_4 \\
 & +e \cdot d(W_{N_x}, W_{N_y}, W_{N_z})
 \end{aligned} \tag{25}$$

where the coefficients (a,b,c,d,e) are calculated quantities. For example, if the control point is at a panel center, then the coefficients a,b,c and d are each 0.25. The value of e is always zero if the control point is on a body segment. For each pair of wake control points, the effect of distance between the points is considered to be computationally insignificant, and the change in distance is therefore ignored in the perturbation analysis method.

In addition to the boundary condition control point indexing k_{cp} described above, a compressed indexing designated k'_{cp} is defined. The ordering of k'_{cp} is the same as k_{cp} , except that for each pair of wake control points k_{cp} and $k_{cp}+1$, there is only one value k'_{cp} . Therefore, the total number of indices k'_{cp} is equal to the number of body boundary condition control points plus one-half the number of wake points. For each k'_{cp} there corresponds a local unknown doublet strength that is to be determined by satisfying a local flow boundary condition.

Doublet Interpolation Between Neighboring Control Points

The section entitled "Panel Properties" described the procedure for establishing a quadratic doublet distribution for a panel on the basis of nine spline control points. For each panel on a body segment, one or more of the nine points is a boundary condition control point, and the local doublet strength is an independent unknown that is to be determined by solving a large system of linear, algebraic boundary condition equations. For the other points, however, the strength is established by interpolation between neighboring boundary condition control points. Interpolation is also performed along the forward edge of each wake segment, where there is an independent unknown doublet strength for each pair of boundary condition control points. The interpolation procedure for body and wake segments is presented in this section.

Figure 13 is a schematic of all the doublet spline control points of a segment. Each point is identified by the indices (i_μ, j_μ) . For a wake segment, the doublet strength at each point (i_μ, j_μ) is specified to be identical to the strength at the forward edge point $(i_\mu, j_\mu=1)$. This corresponds to the conventional wake condition that the streamwise doublet gradient is zero. For each wake segment, the variable index j_μ is therefore replaced by the constant $j_\mu = 1$. Cumulative indexing is defined for the doublet spline control points of all segments

$$k_\mu \equiv k_{\mu 0}(i_S) + \left\{ \begin{array}{ll} (i_\mu - 1) \cdot (2n - 1) + j_\mu & \text{if STYPE}(i_S) = 1 \\ i_\mu & \text{if STYPE}(i_S) = 2 \end{array} \right\} \quad (26)$$

where $k_{\mu 0}(i_S)$ is the total number of k_μ 's on the segments preceding i_S . If there is one or more flow planes of symmetry and the method of images is used, then the mirror image of point k_μ is assigned the same index k_μ .

The doublet strength for each k_μ is to be a weighted average of the doublet strengths at n_D neighboring k_μ 's, where each neighboring k_μ must correspond to a boundary condition control point (or to a pair of wake boundary condition control points). The neighboring locations are identified by the nomenclature $k_{\mu i}$, where $i = 1, 2, 3, \dots, n_D$. The objective is to determine the points $k_{\mu i}$ and weightings c_i such that

$$\mu(k_\mu) = \sum_{i=1}^{n_D} c_i \cdot \mu(k_{\mu i}) \quad (27)$$

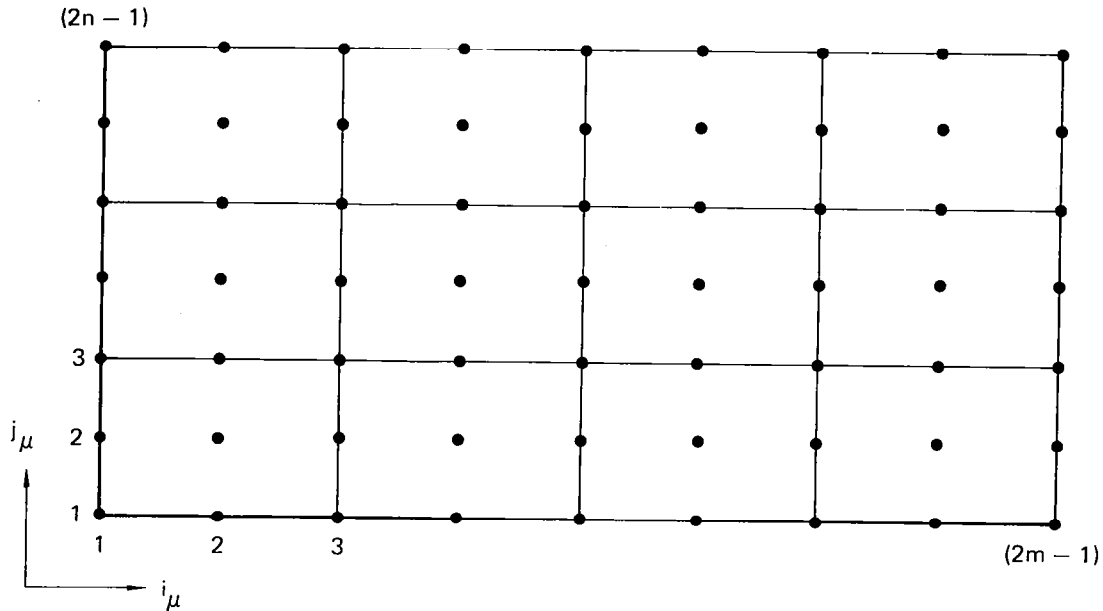


Figure 13. Doublet Spline Control Points on a Segment

If k_μ corresponds to a boundary condition control point, the weighting is trivial; i.e., $n_D = 1$, $k_{\mu i} = k_\mu$, and $c_i = 1$. In general, quadratic interpolation is required to establish the proper weighting. Surface interpolation is applied to the points on body segments. Then for body and wake points along ridges, path interpolation is applied.

Figures 14 and 15 are surface interpolation schematics of a point k_μ on a body segment and the neighboring points i ($1 \leq i \leq n_D$). Figure 14 applies if k_μ is a panel corner, i.e., if the values i_μ and j_μ are both odd. Figure 15 applies if i_μ is even and j_μ is odd. Interchanging i_μ and j_μ in figure 15 corresponds to odd i_μ and even j_μ . If the separation between k_μ and every edge of the segment on which k_μ lies is greater than one panel, then all of the n_D neighboring control points are at panel centers. Otherwise, some of the n_D points will either be on the opposite side of the segment edge or else not be panel centers. The former applies if the edge is neither part of a ridge nor a zero length edge at an isolated point, and it is the responsibility of the user to select the values on the opposite side of the edge. Otherwise, the indexing is handled automatically, and a single edge or corner control point can be identified by more than one index i .

It is noteworthy that there are unusual cases for which the eight point interpolation of Figure 15 is less accurate than twelve point interpolation. Therefore, the consistent use of

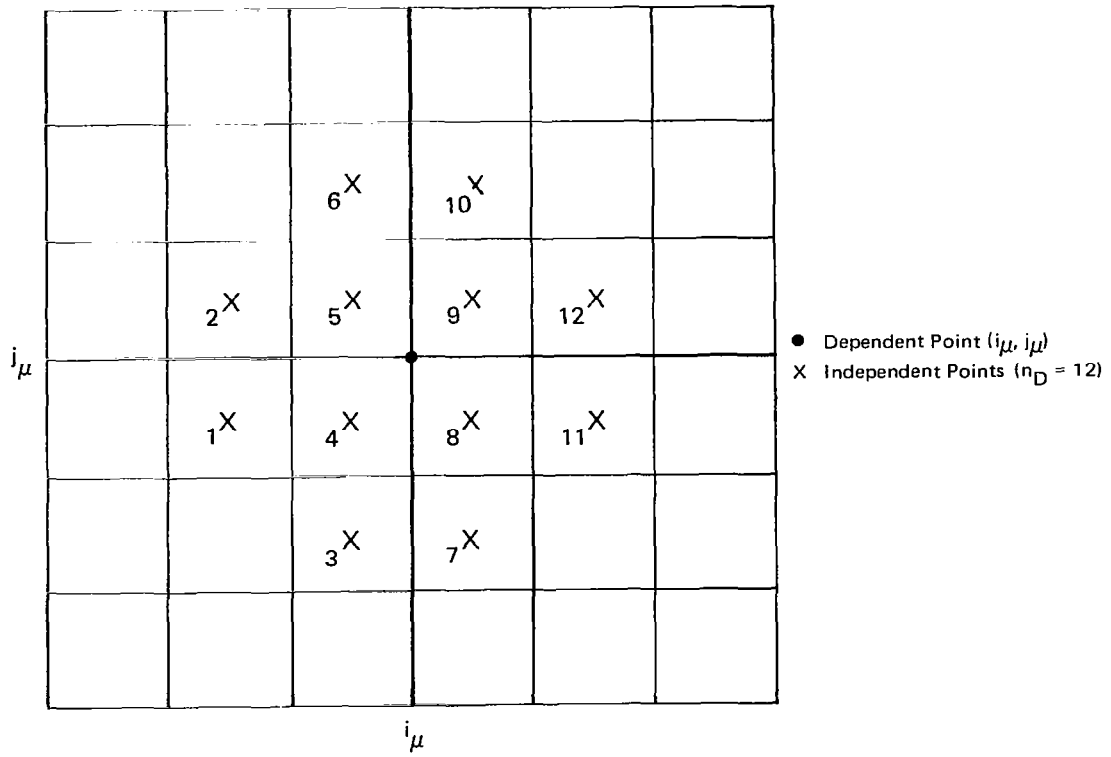


Figure 14. Local Indexing at a Panel Corner Point

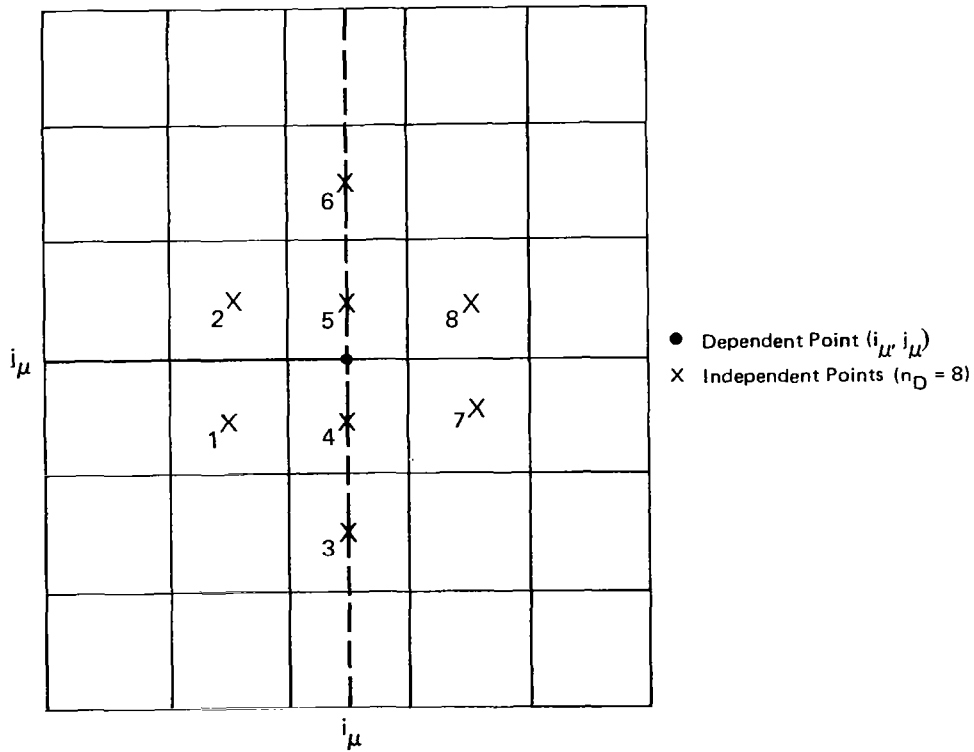


Figure 15. Local Indexing at a Panel Edge Point

twelve point interpolation in the formulation is being considered.

The quadratic surface interpolation is not applied to the conventional doublet strength μ but, rather, to a modified doublet quantity designated u . As illustrated in figure 16, this accommodates the situation in which a body segment edge that is not a ridge coincides with a side edge of a wake. In the vicinity of point k_μ , u is defined to be identical to μ . However, on the opposite side of the segment edge, u is adjusted by $\pm\Delta\mu$, where $\Delta\mu$ is the local wake doublet strength. Therefore, the quantity u corresponds to a continuous function with continuous gradient on the body surface. This makes u a suitable quantity for quadratic interpolation, whereas interpolation on μ would be inappropriate across the edge.

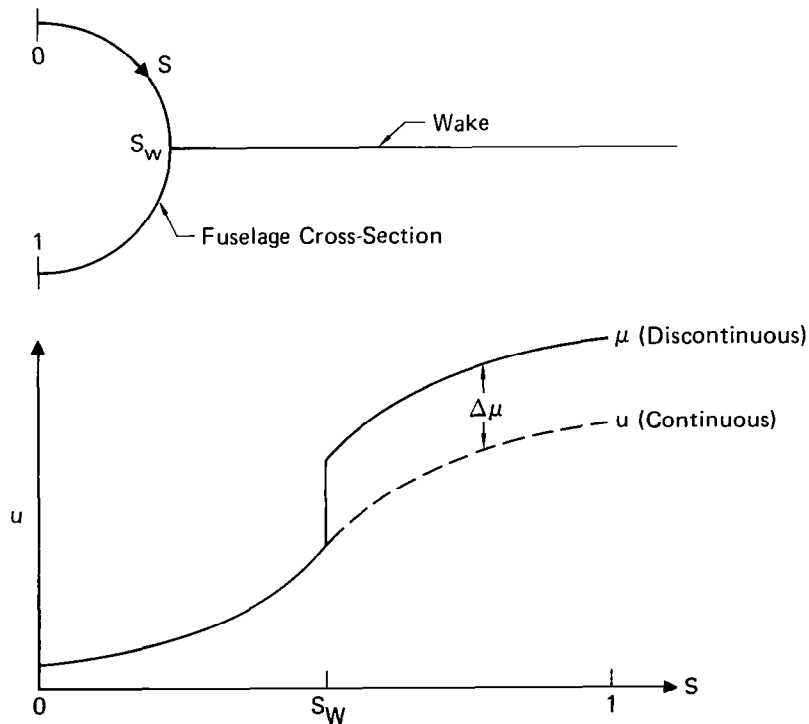


Figure 16. Doublet Discontinuity at Wake-Fuselage Intersection

Before the surface interpolation is initiated, it is necessary to establish a local (ξ, η, ζ) -coordinate system such that the origin is at k_μ and the ζ -axis is locally normal to the body surface. The vector \vec{P}_i is defined for $1 \leq i \leq n_p$.

$$\vec{P}_i = \begin{Bmatrix} P_{i1} \\ P_{i2} \\ P_{i3} \end{Bmatrix} = \begin{Bmatrix} x \\ \pm y \\ \pm z \end{Bmatrix}_{k_{\mu i}} - \begin{Bmatrix} x \\ y \\ z \end{Bmatrix}_{k_{\mu}} \quad (28)$$

where the positive sign for y and z is selected unless $k_{\mu i}$ is on the opposite side of the $y = 0$ and $z = 0$ symmetry planes, respectively. Vector \vec{P}_i is the displacement between points $k_{\mu i}$ and k_{μ} . The unit vector \vec{e}_{ζ} is a weighted average of local panel normal vectors.

$$\frac{\vec{e}_{\zeta}}{c} = \frac{n_D}{\sum_{i=1}^{n_D}} \frac{|n_x, \pm n_y, \pm n_z|_{k_P(i)}}{\sqrt{P_{i1}^2 + P_{i2}^2 + P_{i3}^2}} \quad (29)$$

where the constant c accounts for the fact that the right-hand side is not normalized, where $k_P(i)$ is the panel on which point $k_{\mu i}$ lies, where (n_x, n_y, n_z) is the unit normal vector of panel $k_P(i)$ in the (x, y, z) -coordinate system, and where the summation is to include only values i that are panel centers less than one panel distant from k_{μ} . Once again, the sign selection depends upon whether point i is on the opposite side of a symmetry plane. \vec{e}_{ξ} is defined by selecting any unit vector normal to \vec{e}_{ζ} . It follows that \vec{e}_{η} is defined as $\vec{e}_{\zeta} \times \vec{e}_{\xi}$. Each point i is then assigned coordinates in the (ξ, η, ζ) -system.

$$\begin{cases} \xi_i = \vec{P}_i \cdot \vec{e}_{\xi} \\ \eta_i = \vec{P}_i \cdot \vec{e}_{\eta} \\ \zeta_i = \vec{P}_i \cdot \vec{e}_{\zeta} \end{cases} \quad (1 \leq i \leq n_D) \quad (30)$$

In order to approximately account for surface curvature, ξ_i and η_i are both magnified by the factor

$$[(\xi_i^2 + \eta_i^2 + \zeta_i^2)/(\xi_i^2 + \eta_i^2)]^{1/2}$$

Function $u(\xi, \eta)$ is modeled as a quadratic

$$u(\xi, \eta) = \beta_1 + \beta_2 \xi + \beta_3 \eta + \beta_4 \xi^2 + \beta_5 \xi \eta + \beta_6 \eta^2 \quad (31)$$

Designating u_i as the value of u at point k_{μ_i} ($1 \leq i \leq n_D$), quadratic interpolation is performed by minimizing function E .

$$E \equiv \sum_{i=1}^{n_D} W_i^2 (\beta_1 + \beta_2 \xi_i + \beta_3 \eta_i + \beta_4 \xi_i^2 + \beta_5 \xi_i \eta_i + \beta_6 \eta_i^2 - u_i)^2 \quad (32)$$

where W_i^2 is 1.00 unless k_{μ_i} is separated from k_{μ} by less than one panel, in which case $W_i^2 = 10^8$. E is minimized with respect to the unknowns β_1, \dots, β_6 . The resulting system of linear equations is manipulated by standard matrix inversion and matrix multiplication techniques to provide the array c_i where

$$\beta_1 = \sum_{i=1}^{n_D} c_i u_i \quad (33)$$

Since the origin of the (ξ, η, ζ) -coordinate system is at point k_μ , equation (31) implies that

$$\mu(k_\mu) = \beta_1 \quad (34)$$

Combining equations (33) and (34),

$$\mu(k_\mu) = \sum_{i=1}^{n_D} c_i u_i \quad (35)$$

Equation (35) can be transformed into the desired form of equation (27) by expressing u_i as $\mu(k_{\mu_i}) \pm \Delta\mu_1 \pm \Delta\mu_2 \pm \dots$, where each $\Delta\mu_j$ corresponds to the side edge of a wake segment intersecting the body surface between points k_μ and k_{μ_i} . The value $\Delta\mu_j$ is equal to the doublet strength at a boundary condition control point on a corner of the wake segment. Therefore, equation (35) becomes

$$\mu(k_\mu) = \sum_{i=1}^{(n_D+n_W)} c_i \cdot \mu(k_{\mu_i}) \quad (36)$$

where $i > n_D$ designates the wake segment corners associated with $\Delta\mu_j$ [specifically $\Delta\mu_j \equiv \mu(k_{\mu_{n_D+j}})$]. If the limit n_D is increased to include n_W , then equation (36) is identical to equation (27).

The quadratic surface interpolation scheme described above is not applied to the points k_μ that lie on a ridge. Instead, the interpolation is based upon distance along the ridge. It is the responsibility of the user to identify the ordering of the segment index and segment edge index (i_S and i_{EDG}) along each ridge. Then the pathwise interpolation method described below is automatically employed for the points on the ridge.

Illustrated in figure 17 are four panels along a ridge. The panels can be either body panels or else be wake panels along a wake forward edge. The four panels need not belong to the same segment. The objective is to establish weightings c_i for equation (27) where point k_μ is at the panel corner depicted in figure 17, index i refers to the four panel edge midpoints, and $n_D = 4$. If the point k_μ is one panel width from a ridge

endpoint, then one of the four midpoints i either is replaced by the ridge endpoint or else is the first panel edge midpoint past the ridge endpoint. This respectively depends upon whether the endpoint is or is not an isolated point. Similarly, if k_μ is at the ridge endpoint, then either the interpolation is trivial because k_μ is also a boundary condition control point or else two of the points i are past the endpoint.

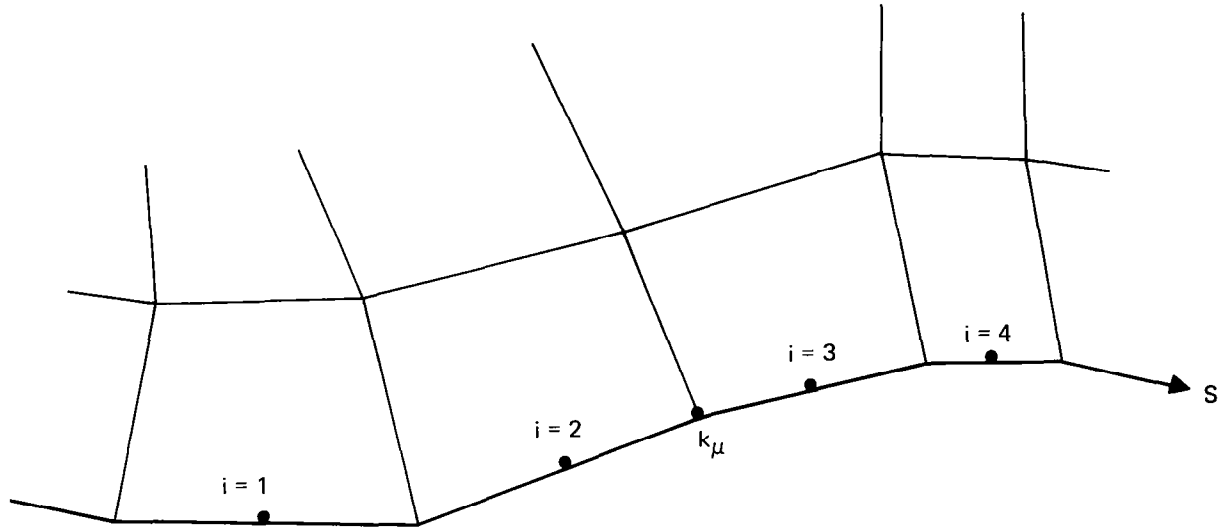


Figure 17. Four Panels Along a Ridge

The interpolation is based on the distance s in figure 17. A parabola is established that matches the doublet strength exactly at points $i = (2,3)$ and approximately at points $i = (1,4)$. Define s' such that the origin is midway between $i = 2$ and 3 .

$$s' \equiv s - \frac{1}{2}(s_2 + s_3) \quad (37)$$

Exact doublet matching at $i = 2$ and 3 implies that the quadratic $\mu(s')$ is of the form

$$\mu(s') = a \cdot \left[s'^2 - \left(\frac{s_3 - s_2}{2} \right)^2 \right] + \left(\frac{\mu_3 - \mu_2}{s_3 - s_2} \right) s' + \frac{1}{2}(\mu_2 + \mu_3) \quad (38)$$

where a is a constant. A weighted square error in matching doublet strength at $i = 1$ and 4 is defined as

$$E \equiv (s_1')^{-4} \cdot [\mu(s_1') - \mu_1]^2 + (s_4')^{-4} \cdot [\mu(s_4') - \mu_4]^2 \quad (39)$$

The constant a is evaluated by substituting equation (38) into (39) and minimizing E with respect to a . Then the value s' corresponding to point k_μ is applied to equation (38), which reduces to the desired form of equation (27).

Heretofore, it has been assumed that the points $i = 1, 2, 3, 4$ in figure 17 are boundary condition control points. However, for each ridge there is an option which eliminates the need for boundary condition control points on the side designated by the user to be "iSIDE = 2" (see figure 7). For each point k_μ on iSIDE = 2 (i.e., for each panel corner and each panel edge midpoint), the doublet strength is established directly from the theoretical condition that the net local doublet strength from iSIDE = 1 plus iSIDE = 2 plus wake (if present) must be zero. This option is usually employed because it saves computing effort.

For every spline control point k_μ , the above formulation of this section determines a set of points $k_{\mu i}$ and weightings c_i such that $\mu(k_\mu)$ is established by equation (27). Each $k_{\mu i}$ is equivalent to one boundary condition control point index k_{CP}^i . Using the nomenclature $k_{CP}^i \equiv k_{CP}^i(k_{\mu i})$ to denote the transformation from index $k_{\mu i}$ to k_{CP}^i , equation (27) is cast in the final form

$$\mu(k_\mu) = \sum_{i=1}^{n_D} c_i \cdot \mu(k_{CP}^i) \quad (40)$$

It is noteworthy that each weighting c_i is a function of the panelled geometry coordinates but not the doublet strengths. In the perturbation analysis method, the first-order change of c_i with respect to geometry perturbations could be included. However, the change is considered to be insignificant for typical applications of the perturbation analysis method and is neglected in order to reduce both formulation complexity and computing effort. Therefore, the differential form of equation (40) for the perturbation analysis method is

$$d\mu(k_\mu) = \sum_{i=1}^{n_D} c_i \cdot d\mu(k'_{CP_i}) \quad (41)$$

Singularity Distributions on a Panel

The effect of each panel on the flow is represented by a constant source distribution and a quadratic doublet distribution. Because the panel method of this report is based upon the integral surface singularity theory associated with Green's third identity (reference 10), the source strength can be determined directly from the local panel geometry, as will be described below. In order to determine the doublet distribution, it is necessary to establish and solve a system of boundary condition equations, which is the subject of a following subsection. Here it will be appropriate to establish the functional relationship between the unknown doublet strength at each control point k'_{CP} and the quadratic doublet distribution on each panel.

For each body panel, the constant source strength corresponding to Green's third identity is

$$\sigma = V_{N_P} - \vec{V}_\infty \cdot \vec{e}_\zeta \quad (42)$$

where V_{N_P} is the prescribed normal velocity boundary condition at the panel center. If the panel is divided into subpanels (Appendix B), then \vec{e}_ζ refers to the subpanel normal vector. For wake panels, the source strength σ is identically zero.

The quadratic doublet distribution on each panel is related to the doublet strength at the local spline control points by equations (16) and (17) [analogous equations (B7) and (B11) apply for subpanels]. Each of the nine spline control points in equation (17) corresponds to one value k_μ . Consequently, equation (40) can be combined with equation (17) to establish the relationship between each quadratic coefficient β_i of equation (16) and the unknown doublet strength for each point k'_{CP} . For convenience, a more conventional set of quadratic coefficients α_i ($1 \leq i \leq 6$) is defined as follows:

$$\mu(\xi, \eta) = \alpha_1 + \alpha_2 \xi + \alpha_3 \eta + \alpha_4 \xi^2 + \alpha_5 \xi \eta + \alpha_6 \eta^2 \quad (43)$$

For each panel, equations (16), (17), (40), and (43) are manipulated to establish quantities MAX, k'_{CPj} , and d_{ij} where

$$\alpha_i = \sum_{j=1}^{MAX} d_{ij} \cdot \mu(k'_{CPj}) \quad 1 \leq i \leq 6 \quad (44)$$

The calculated quantity d_{ij} depends upon the defining geometry coordinates but not upon the doublet distribution. In accordance with equation (44), each quadratic coefficient α_i varies linearly with respect to each unknown doublet strength $\mu(k'_{CP})$. If the panel is divided into subpanels, there is one set of equations (43) and (44) per subpanel.

For the perturbation analysis method, it is necessary to establish the first-order relationship between geometry perturbations and the resulting perturbations to source strength σ and quadratic coefficients α_i . The source perturbation is established from equation (42),

$$d\sigma = - \vec{V}_\infty \cdot d\vec{e}_\zeta \quad (45)$$

where the relationship between $d\vec{e}_\zeta$ and perturbations to the panel coordinates was established in the subsection entitled "Panel Properties" (or Appendix B for subpanels). For the doublet distribution, equations (24) and (41) (or analogous equations (B20) and (41) for subpanels) establish the first-order expression for perturbations to the quadratic coefficients corresponding to perturbations to both panel geometry and to the unknown doublet strength at each point k'_{CP} . Recall that the geometry of each panel is defined by the array v_j [equation (18)]. Then for each panel (or subpanel), the quantities $(\frac{\partial \sigma}{\partial v_j})$ and $(\frac{\partial \alpha_i}{\partial v_j})$ can be calculated, where

$$d\sigma = \sum_{j=1}^9 (\frac{\partial \sigma}{\partial v_j}) \cdot dv_j \quad (46)$$

$$d\alpha_i = \sum_{j=1}^9 \left(\frac{\partial \alpha_i}{\partial v_j} \right) \cdot dv_j + \sum_{j=1}^{\text{MAX}} d_{ij} \cdot d\mu(k'_{CP_j}) \quad (47)$$

and where d_{ij} is the calculated coefficient associated with equation (44).

Potential Influence Functions

Consider the planar quadrilateral panel of figure 11. With respect to the local (ξ, η, ζ) -coordinate system, the panel geometry is defined by the coordinates of the panel corners $[(\xi_k, \eta_k) \ 1 \leq k \leq 4]$. Now consider the seven following singularity distributions on the panel:

- (1) $\mu(\xi, \eta) = 1$ Constant Doublet
- (2) $\mu(\xi, \eta) = \xi$ First-Order Doublet
- (3) $\mu(\xi, \eta) = \eta$ First-Order Doublet
- (4) $\mu(\xi, \eta) = \xi^2$ Second-Order Doublet
- (5) $\mu(\xi, \eta) = \xi\eta$ Second-Order Doublet
- (6) $\mu(\xi, \eta) = \eta^2$ Second-Order Doublet
- (7) $\sigma(\xi, \eta) = 1$ Constant Source

Define ϕ_i as the potential at arbitrary field point (ξ, η, ζ) induced by the i th singularity distribution above. Mathematical formulas are available for calculating ϕ_i as a function of eleven quantities: $\{\xi_1, \eta_1, \xi_2, \eta_2, \xi_3, \eta_3, \xi_4, \eta_4, \xi, \eta, \zeta\}$ (see reference 2). The formulas are also appropriate for a triangular subpanel (figure B-2) if the subpanel is considered to be a quadrilateral for which the length of one side is zero.

Analytical differentiation of the formulas for ϕ_i establishes formulas for each of the following partial derivatives:

$$\left\{ \frac{\partial \phi_i}{\partial \xi_k}, \frac{\partial \phi_i}{\partial \eta_k}, \frac{\partial \phi_i}{\partial \xi}, \frac{\partial \phi_i}{\partial \eta}, \frac{\partial \phi_i}{\partial \zeta} \right\} \quad (1,1) \leq (i,k) \leq (7,4)$$

For application to the perturbation analysis method, the first-order change in ϕ_i induced by perturbations to both panel geometry and field point location is expressed as

$$d\phi_i = \sum_{k=1}^4 \left[\left(\frac{\partial \phi_i}{\partial \xi_k} \right) d\xi_k + \left(\frac{\partial \phi_i}{\partial \eta_k} \right) d\eta_k \right] + \left(\frac{\partial \phi_i}{\partial \xi} \right) d\xi + \left(\frac{\partial \phi_i}{\partial \eta} \right) d\eta + \left(\frac{\partial \phi_i}{\partial \zeta} \right) d\zeta \quad (48)$$

Boundary Condition Satisfaction

For each control point k'_{CP} , there is one boundary condition equation to be satisfied. On bodies, the prescribed normal velocity condition is represented by an equivalent internal condition that the net potential induced by all the singularities is zero. On wakes, the Kutta condition is satisfied by requiring that the average flow velocity component vanish between each pair of wake control points k_{CP} and $k_{CP}+1$; this is equivalent to specifying that the difference in total potential between the two points is to be equal to the local wake doublet strength.

Each boundary condition equation is established by summing the contributions from each panel (or subpanel). Using equation (43) and the definition of the influence functions ϕ_i , the potential ϕ at a boundary condition control point induced by all the singularities on one panel (or subpanel) is

$$\phi = \sigma \cdot \phi_7 + \sum_{i=1}^6 (\alpha_i \cdot \phi_i) \quad (49)$$

The substitution of equation (44) into (49) provides a linear relationship between the potential ϕ and the unknown doublet strength at control points.

The complete set of linear, algebraic boundary condition equations is set up in the following form:

$$[A_{ij}] \cdot \mu_j = RHS_i \quad (50)$$

where each index i corresponds to the boundary condition equation for one control point k'_{CP_i} , each index j corresponds to the unknown doublet strength at one control point k'_{CP_j} , and the matrix A_{ij} and vector RHS_i are arrays of calculated quantities. The solution array μ_j is determined by standard matrix algebra.

For the perturbation analysis method, it is necessary to develop a differential version of equation (50). Recall that the panelled configuration geometry is defined by a set of points $(x,y,z)_k$ (see "Division of a Segment Into Panels"). Now suppose that the geometry is distorted by a perturbation to the k th point, $(dx,dy,dz)_k$. The perturbed form of equation (50) is

$$\begin{aligned} [A_{ij}] \cdot d\mu_j + \mu_j \cdot \left[\left(\frac{\partial A_{ij}}{\partial x_k} \right) dx_k + \left(\frac{\partial A_{ij}}{\partial y_k} \right) dy_k + \left(\frac{\partial A_{ij}}{\partial z_k} \right) dz_k \right] \\ = \left(\frac{\partial RHS_i}{\partial x_k} \right) dx_k + \left(\frac{\partial RHS_i}{\partial y_k} \right) dy_k + \left(\frac{\partial RHS_i}{\partial z_k} \right) dz_k \end{aligned} \quad (51)$$

The partial derivatives of equation (51) are calculated by following the same procedure used to establish A_{ij} and RHS_i , except that each quantity encountered is replaced by its differential. For example, consider the differential form of equation (49):

$$d\phi = \sigma \cdot d\phi_7 + \phi_7 \cdot d\sigma + \sum_{i=1}^6 (\alpha_i \cdot d\phi_i + \phi_i \cdot d\alpha_i) \quad (52)$$

Each of the differentials on the right-hand side of equation (52) has previously been expressed in terms of geometry derivatives [equations (46)-(48)]. Consequently, equation (51) reduces to the form

$$[A_{ij}] \cdot d\mu_j = [B_{ik}] \cdot dx_k + [C_{ik}] \cdot dy_k + [D_{ik}] \cdot dz_k \quad (53)$$

where all the matrix coefficients are calculated quantities. By multiplying both sides of equation (53) by the matrix inverse of A_{ij} , the desired first-order relationship between geometry perturbations and singularity distribution is generated:

$$d\mu_i = \left(\frac{\partial \mu_i}{\partial x_k} \right) dx_k + \left(\frac{\partial \mu_i}{\partial y_k} \right) dy_k + \left(\frac{\partial \mu_i}{\partial z_k} \right) dz_k \quad (54)$$

where the partial derivatives in equation (54) are known, calculated values.

Velocity and Pressure Calculation

The solution array of doublet strengths is converted to surface velocity and pressure at each panel center, and then the forces and moments are integrated. For each body panel, the flow velocity in the local panel coordinate system is

$$\begin{aligned} V_\xi &= \vec{V}_\infty \cdot \vec{e}_\xi + \alpha_2 \\ V_\eta &= \vec{V}_\infty \cdot \vec{e}_\eta + \alpha_3 \\ V_\zeta &= \vec{V}_\infty \cdot \vec{e}_\zeta + \sigma = V_{N_P} \end{aligned} \quad (55)$$

where α_2 and α_3 are calculated using equation (44). Equation (55) expresses the fact that on a body surface the local source strength is equal to the perturbation velocity normal component and the local doublet strength is the local perturbation potential, corresponding to Green's third identity. For steady flow, Bernoulli's equation provides the local pressure coefficient.

$$C_p = 1 - \frac{V_\xi^2 + V_\eta^2 + V_\zeta^2}{V_{ref}^2} \quad (56)$$

Forces and moments are calculated under the approximations that the pressure is uniform on each panel and that the flat quadrilateral panel is the local geometry.

GUIDELINES FOR USING THE THREE COMPUTER PROGRAMS

For the perturbation analysis method, the operation of the three computer programs is considerably more flexible than the summary chart of figure 1 suggests. For example, it is not necessary to calculate a new partial derivative matrix for each angle of attack of interest. Furthermore, the derivative can be expressed in terms of standard aerodynamic geometry quantities such as thickness and camber distribution, in addition to the surface coordinates x , y , and z . The capabilities and operation of the three programs is described in greater detail below.

MCAIR 3-D Subsonic Potential Flow Program (Version 2)

For a panelled geometry configuration, several flow fields can be analyzed simultaneously. Each flow corresponds to a different specified free stream velocity vector $(V_{\infty x}, V_{\infty y}, V_{\infty z})$ and a different distribution of prescribed normal velocity (V_{Np}) . There is one right-hand-side vector in equation (50) for each of these flows.

MCAIR 3-D Geometry Influence Coefficient Program (Version 1)

Corresponding to any one of the flow field analysis solutions from the preceding program, this program will generate the partial derivative matrix of doublet strength with respect to geometry perturbations. Table I presents the geometric quantities that are candidates for perturbation. The user identifies which of the quantities are to be included in the differentiation; the others are ignored to save computing effort.

The structure of the partial derivative matrix is as follows. For each control point k'_{CP} , there is one row. Each column j corresponds to one independent geometry perturbation, where the total number of columns is specified by the user. If dS_j is defined as the magnitude of the j th differential geometry perturbation, then the calculated matrix element in column j and row k'_{CP} is the value of the quantity

$$\frac{\partial \mu(k'_{CP})}{\partial S_j}$$

Each independent geometry perturbation dS_j will typically represent the change to one of the quantities in Table I. However, it is the prerogative of the user to establish a more general definition for each dS_j , as follows. First, the user will designate any number of different quantities in Table I that are to be simultaneously dependent on dS_j . Second, he will prescribe a weighting for each quantity, where that weighting is to be the rate of change of the quantity with respect to dS_j . For example, suppose that the user desires the geometry perturbation dS_j to be the change in thickness at some point on a wing.

Table I. Geometric Quantities Subject to Perturbations

a. Panel Corner Points [1 ≤ k ≤ k _o (n _S + 1)]			b. Kutta Condition Direction Vectors (One Vector for Each Point k _{CP} on a Wake)		
x ₁	y ₁	z ₁	W _{Nx}	W _{Ny}	W _{Nz}
x ₂	y ₂	z ₂	↓	↓	↓
↓	↓	↓	↓	↓	↓
x _k	y _k	z _k	↓	↓	↓
↓	↓	↓	↓	↓	↓

Suppose that $z_{k_{UPR}}$ and $z_{k_{LWR}}$ from Table I are the local upper and lower surface coordinates. Then the user would specify a weighting of +1/2 for $dz_{k_{UPR}}$ and -1/2 for $dz_{k_{LWR}}$, and the desired definition of dS_j would be established:

$$\left\{ \begin{array}{l} dz_{k_{UPR}} = + 1/2 \cdot dS_j \\ dz_{k_{LWR}} = - 1/2 \cdot dS_j \end{array} \right\} \Rightarrow dS_j = (dz_{k_{UPR}} - dz_{k_{LWR}})$$

In addition to the fact that each independent perturbation dS_j can affect more than one quantity in Table I, it is permissible for any single quantity in Table I to be affected by more than one independent perturbation dS_j .

MCAIR 3-D Perturbation Analysis Program (Version 1)

Consider an arbitrary baseline configuration for which a panelled geometry representation has been established. Suppose that the two preceding computer programs have been executed for the panelled geometry at some free stream velocity ($V_{\infty x}, V_{\infty y}, V_{\infty z}$) and some prescribed normal velocity distribution (V_{Np}). Then the calculations by the two programs can be used to establish an input file for this program, the MCAIR 3-D Perturbation Analysis

Program (Version 1). For each perturbation case to be analyzed, the input to this program consists of an array of geometry perturbation values, dS_j . The program will first compute the panel corner coordinates of the perturbed geometry and then calculate the corresponding surface velocity distribution, surface pressure distribution, and forces and moments.

The only significant difference between this program and the first program [MCAIR 3-D Subsonic Potential Flow Program (Version 2)] is in the calculation of the doublet strengths $\mu(k'_{CP})$. In this (the third) program, the influence coefficient matrix A_{ij} is not calculated, and the system of linear, algebraic boundary condition equations is not solved [see equation (50)]. Instead, the following first order formula is applied:

$$\mu(k'_{CP}) = \mu_o(k'_{CP}) + \sum_j \left[\frac{\partial \mu(k'_{CP})}{\partial S_j} \right]_o \cdot dS_j \quad (57)$$

where the subscript "o" designates baseline quantities that are available in the input file. It is noteworthy that the only portion of the perturbation analysis method that is based upon first-order approximations with respect to geometry perturbations is equation (57). Velocity and pressure are not forced to vary linearly with respect to dS_j , which is expected to be significant for wing leading edge radius perturbations.

Now suppose that one or more additional input files have been generated for the baseline configuration, where each file corresponds to a different free stream velocity vector and a different prescribed normal velocity distribution (V_{NP}). Identify each file by index IFLOW ($1 \leq \text{IFLOW} \leq \text{NFLOW}$). In the third program, arbitrary linear superposition of flow solutions can be constructed from an input set of weightings W_{IFLOW} , such that the net free stream velocity and prescribed normal velocity are

$$(V_{\infty_x}, V_{\infty_y}, V_{\infty_z}) = \sum_{\text{IFLOW}=1}^{\text{NFLOW}} \left[W \cdot (V_{\infty_x}, V_{\infty_y}, V_{\infty_z}) \right]_{\text{IFLOW}} \quad (58)$$

$$V_{NP} = \sum_{\text{IFLOW}=1}^{\text{NFLOW}} \left[W \cdot V_{NP} \right]_{\text{IFLOW}} \quad (59)$$

Corresponding to each flow "IFLOW," equation (57) is used to establish $\mu(k'_{CP})$. Then the net or superimposed solution is

$$\mu(k'_{CP}) = \sum_{IFLOW=1}^{NFLOW} \left[W \cdot \mu(k'_{CP}) \right]_{IFLOW} \quad (60)$$

The linear superposition associated with the weightings W_{IFLOW} does not introduce any error to the perturbation analysis method. In other words, the only terms in equations (58) and (59) that affect the calculated solution are the net flow conditions on the left-hand side.

An illustration of the utility of equations (58)-(60) is the calculation of perturbation analysis solutions at various angles of attack from two input files. Suppose that IFLOW = 1 corresponds to $(V_{\infty x}, V_{\infty y}, V_{\infty z}) = (1, 0, 0)$ and that IFLOW = 2 corresponds to $(V_{\infty x}, V_{\infty y}, V_{\infty z}) = (0, 0, 1)$. In each case, flow tangency conditions are assumed ($V_{Np} = 0$). If the angle of attack (α) is measured with respect to the x-axis, then the weightings for an arbitrary angle of attack are $W_1 = \cos \alpha$ and $W_2 = \sin \alpha$. This procedure was employed in the example solution of the next section.

EXAMPLE SOLUTIONS

Two panelled configurations have been analyzed in order to evaluate the three computer programs of this report (figure 1). The first configuration is a simple wing-fuselage for which the sensitivity of a conventional analysis solution to small paneling gaps was tested. The second configuration is a low aspect ratio isolated wing. The perturbation analysis method was used to predict the effect of thickness, camber, and twist perturbations to the isolated wing geometry. All the calculations of this section were performed on the McDonnell Douglas CDC CYBER 750 computer.

Conventional Analysis of a Wing-Fuselage

Figure 18 is a sketch of two panelled geometry representations of a fighter-type wing mounted on an axisymmetric fuselage. In the panelling of figure 18a, there are no unpanelled gaps on the configuration surface. The panelling of figure 18b is identical, except that approximately one-half of the streamwise defining points on the fuselage were removed and the vertical plane of the wing tip was not panelled. The reduction in fuselage panel density introduced small vertical gaps between the fuselage and wing panel edges at the exposed root, where the size of the gaps is on the order of one-half of one percent of the local wing chord. The objective is to determine whether the MCAIR 3-D Subsonic Potential Flow Program (Version 2) can generate an accurate pressure distribution for the geometry with gaps in the panelling (figure 18b).

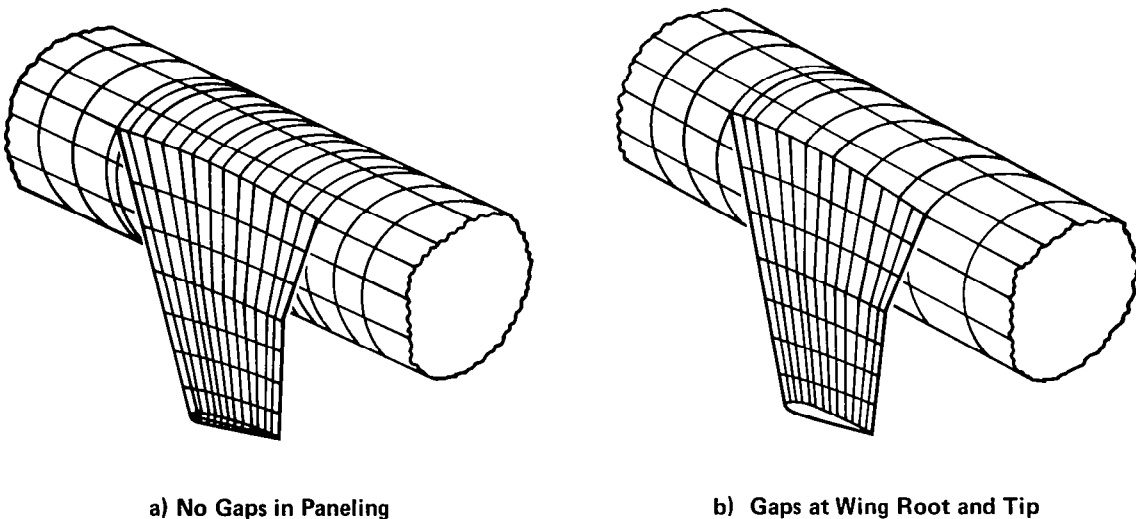


Figure 18. Two Paneled Representations of a Wing-Fuselage

As a standard of comparison, the PAN AIR pilot computer program of reference 3 was applied to the densely paneled geometry of figure 18a. The two calculated pressure distributions are nearly identical, as illustrated in the vicinity of the wing root by figure 19. It is concluded that elimination of all gaps in the panelled geometry is not necessary. The calculations for this example were performed as part of the 1980 MCAIR Independent Research and Development Program.

Perturbation Analysis Method for an Isolated Wing

The wing panelling of figure 20 was selected as the baseline geometry for demonstrating the perturbation analysis method. At each span station, the wing section is an untwisted NACA 0012 airfoil (12% thickness ratio). Each of the five perturbed wing geometries of figure 21 was analyzed by both the conventional panel method [MCAIR 3-D Subsonic Potential Flow Program (Version 2)] and the perturbation analysis method. A comparison of the calculations will establish an indication of the accuracy of the perturbation analysis method.

Each of the perturbed wing geometries was generated by coordinate displacements normal to the baseline wing chord plane (Δz). No perturbations in the x or y-directions were considered. Ruled surfaces were used to define the panelling between the root and tip sections, with one exception. For Wing B, the twist distribution was specified to vary linearly across the span. All of the wings (except E) were analyzed at two angles of attack, 0° and 5°. Here, angle of attack is measured with respect to the baseline wing chord plane.

The conventional panel method solution for the baseline wing is presented in figures 22-25. For verification, a solution by the PAN AIR pilot computer program is also presented. For PAN AIR only, additional panels were distributed across the open wing tip of the baseline geometry to eliminate unpanelled gaps. The section properties c_l , c_d , c_m of figures 23 and 25 are based upon the local chord, and the moment reference point for c_m is the quarter chord of the local wing section. It is noteworthy that at zero incidence the inboard and outboard section drag coefficients are approximately +100 and -100 counts, respectively (figure 23). However, the total wing drag coefficient is less than one count for both panel methods, which is consistent with the potential flow law that nonlifting bodies have zero drag.

Perturbation analysis solutions for wings A through E at 0° and 5° angle of attack are presented in figures 26-43. The legend "exact solution" in the figures designates the conventional panel method solution for the perturbed wing geometry. It is apparent that the perturbation analysis method is quite accurate for a variety of large geometry perturbations.

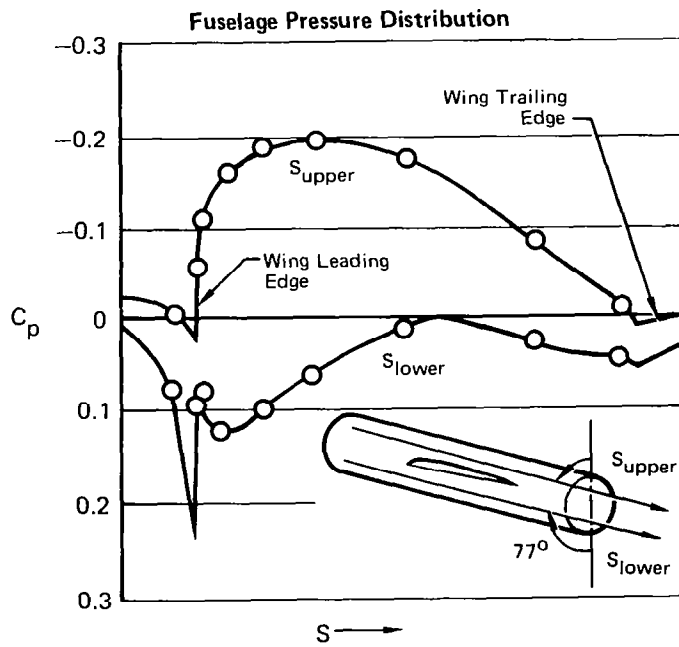
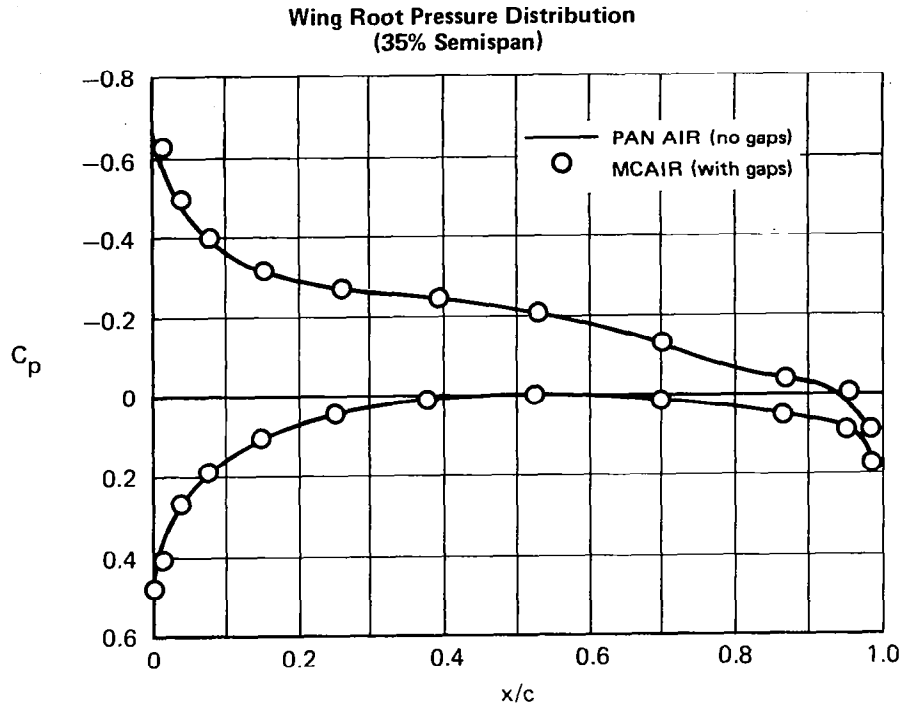


**Figure 19. Calculated Pressures Near Wing Root
4° Angle-of-Attack**

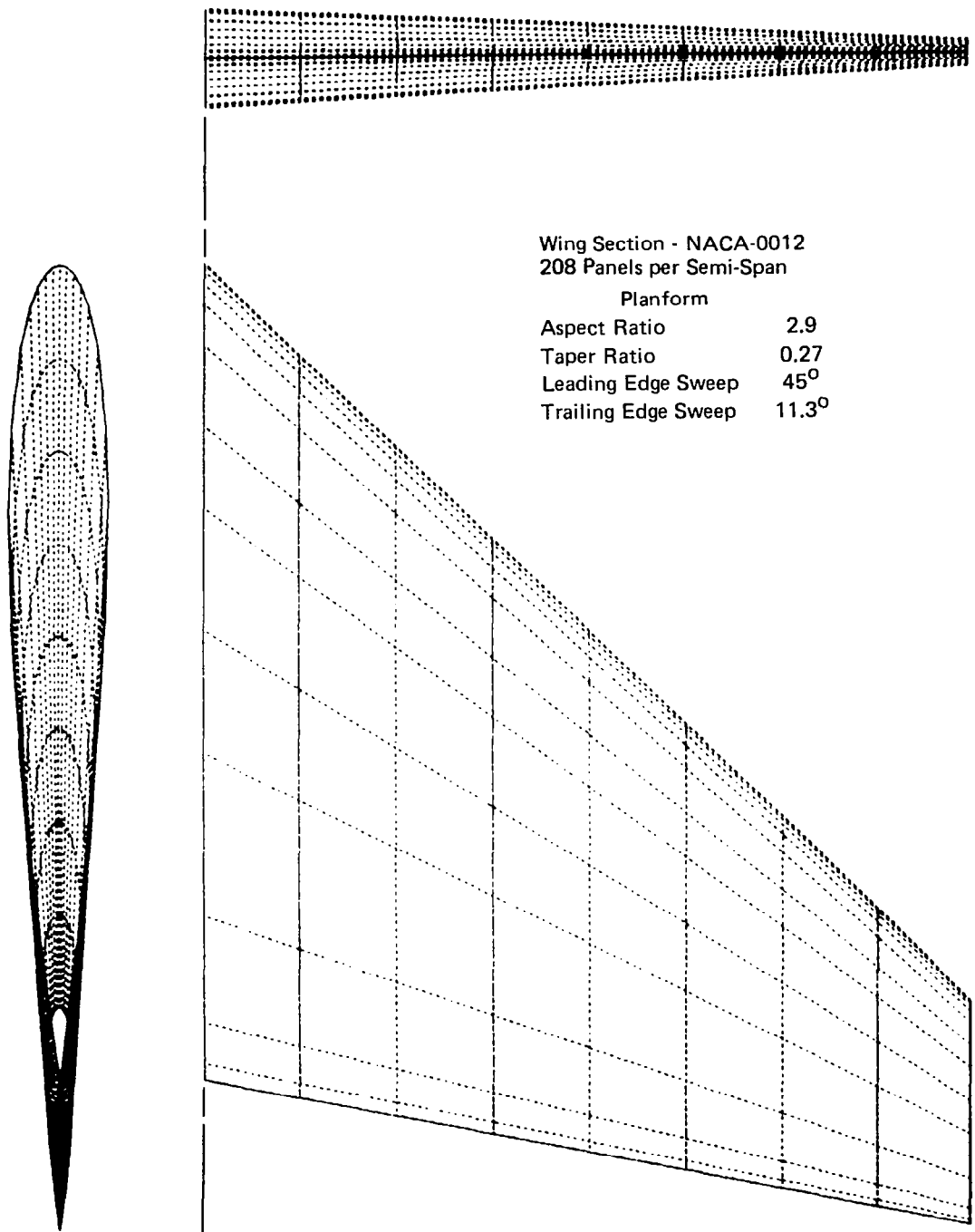


Figure 20. Baseline Wing Paneling for Demonstration of Perturbation Analysis Method

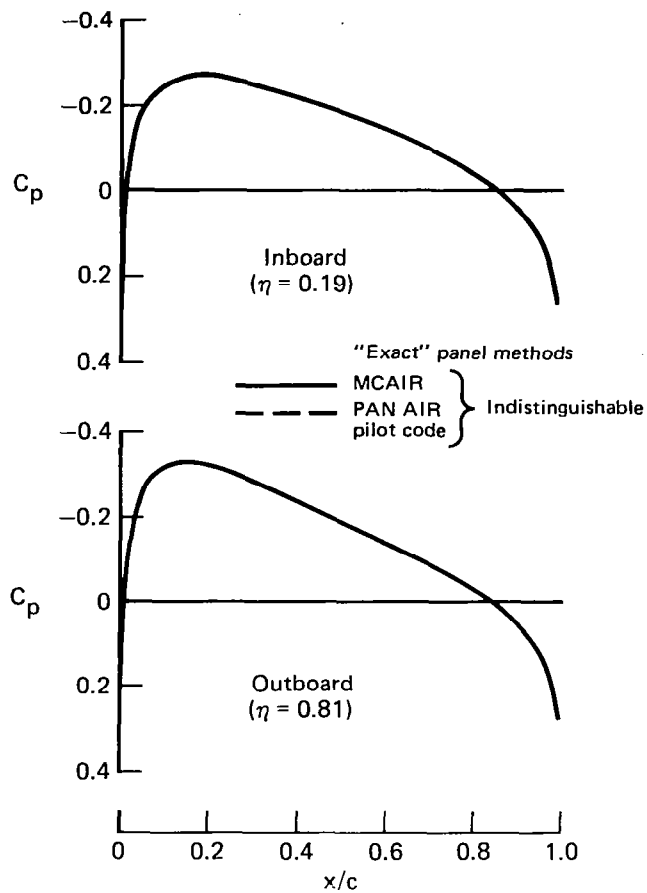
	Root Section	Tip Section
Baseline Wing (NACA 0012)		
Wing A (NACA 0006)		
Wing B. (10° Twist)		
Wing C (Supercritical)		
Wing D (Fighter)		
Wing E (20° Flaps)		

Figure 21. Test Cases for the Perturbation Analysis Method

Unlike the existing small disturbance (linearized) methods, the accuracy does not diminish substantially in the leading edge region, even if the radius of curvature is changed.

The only appreciable difference between the perturbation and exact solutions is the pressure distribution on the lower surface of the wing with deflected flaps and the aft lower surface of the supercritical wing. The explanation for this difference is apparent upon examining figures 22 and 42. The 20° flap deflection changes the level of lower surface pressure coefficient from the baseline level $c_p \sim 0$ to $c_p \sim 1/2$. This represents one-half of the theoretical maximum perturbation (to stagnation). The perturbation analysis method does not account for the fact that the lower surface velocity cannot decrease indefinitely with respect to increasing flap deflection; therefore, the perturbation analysis method slightly overestimates the magnitude of the local pressure coefficient.

Based on figures 26-43, it is concluded that for section geometry perturbations representative of preliminary aerodynamic design of clean wings, the accuracy of the perturbation analysis method is competitive with conventional panel methods. The advantage of the perturbation analysis method is the small computing effort required for each additional perturbation case. In the present example, each perturbation case required only 7 seconds computing time versus 245 seconds for the conventional analysis solution. The generation of the partial derivative matrix by the MCAIR 3-D Geometry Influence Coefficient Program (Version 1) required 925 seconds each for 0° and 90° angle of attack. In the present example, it is cost efficient to employ the perturbation analysis method if nine or more cases are to be analyzed.



**Figure 22. Baseline Pressure Distribution at 0° Angle-of-Attack
NACA 0012**

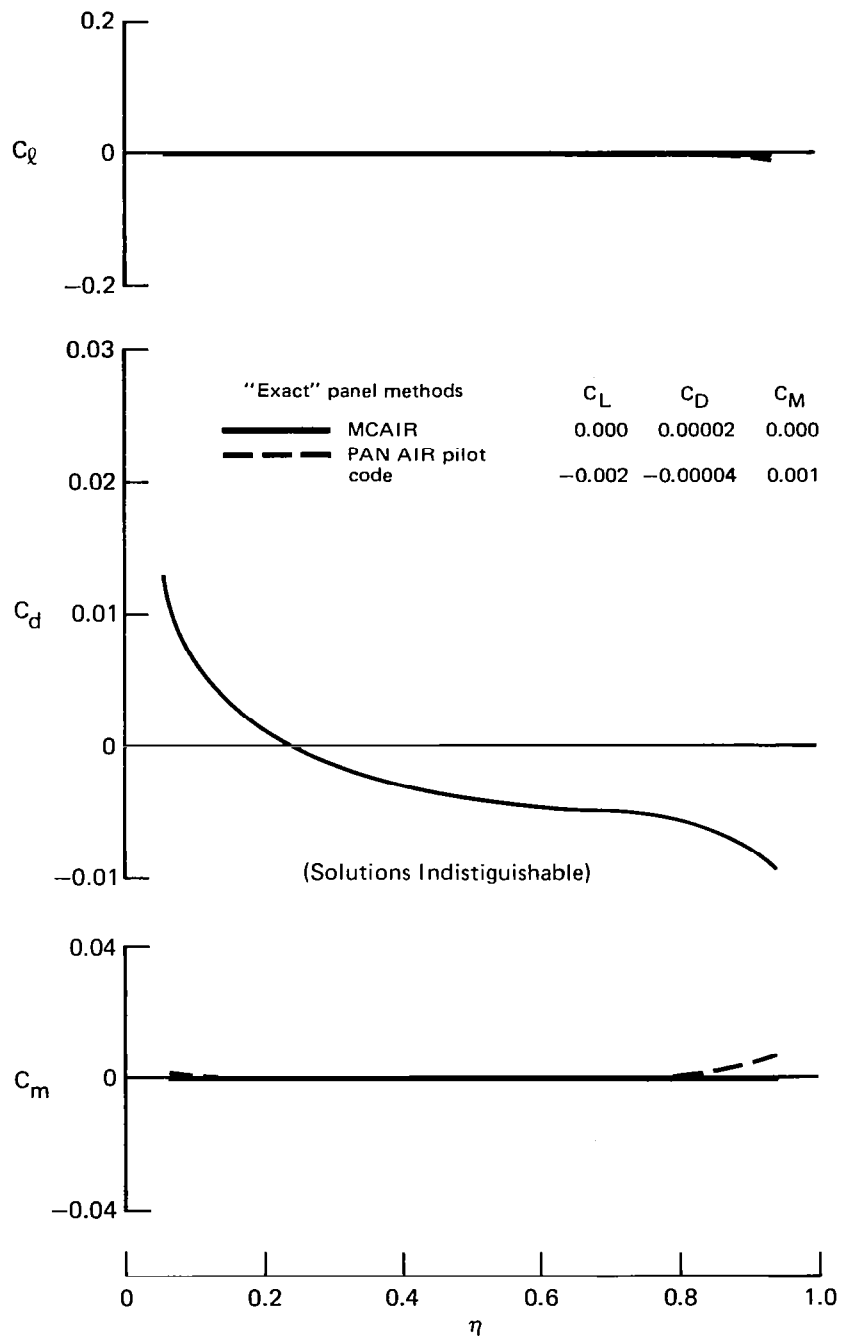


**Figure 23. Baseline Force and Moment Distribution at 0° Angle-of-Attack
NACA 0012**

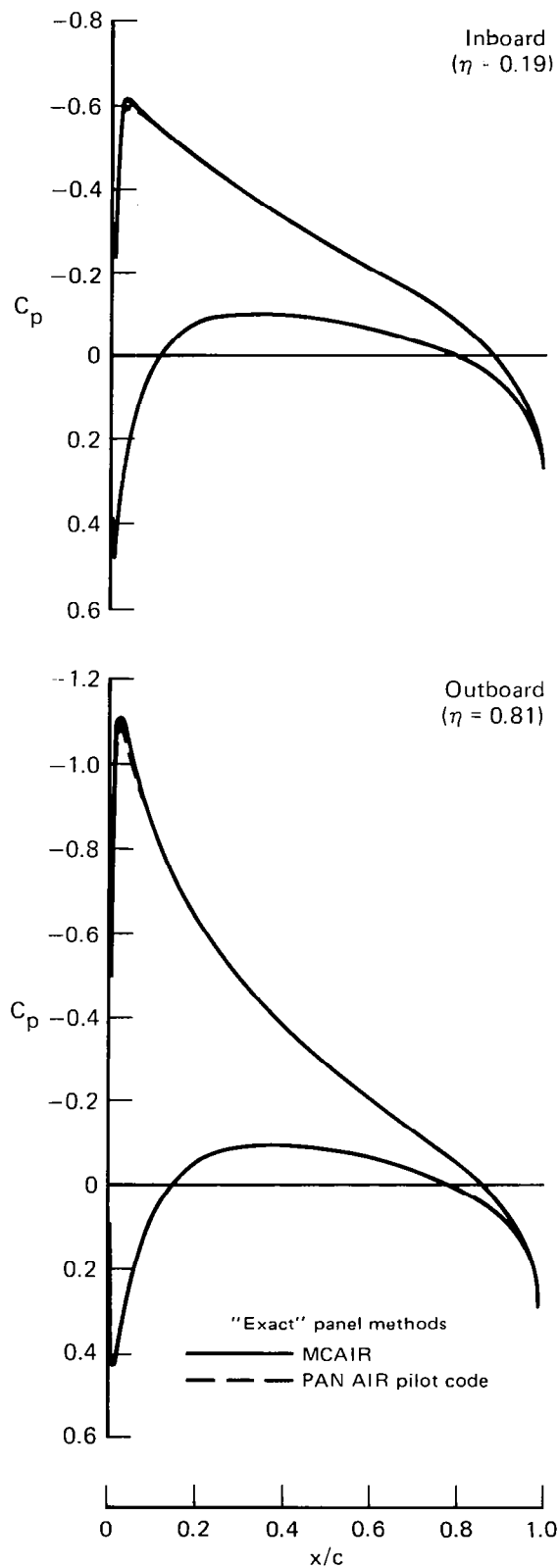


Figure 24. Baseline Pressure Distribution at 5° Angle-of-Attack NACA 0012

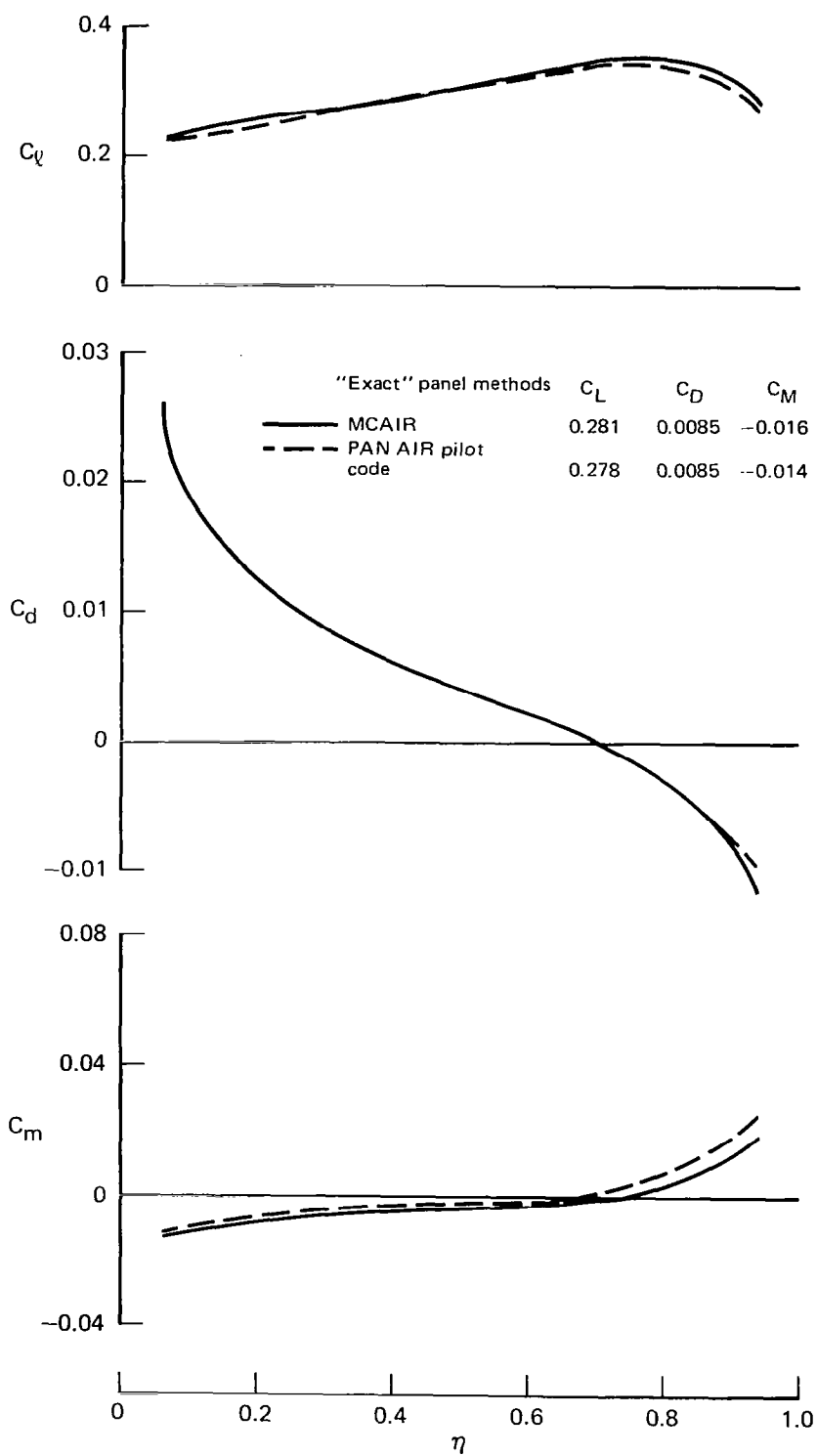
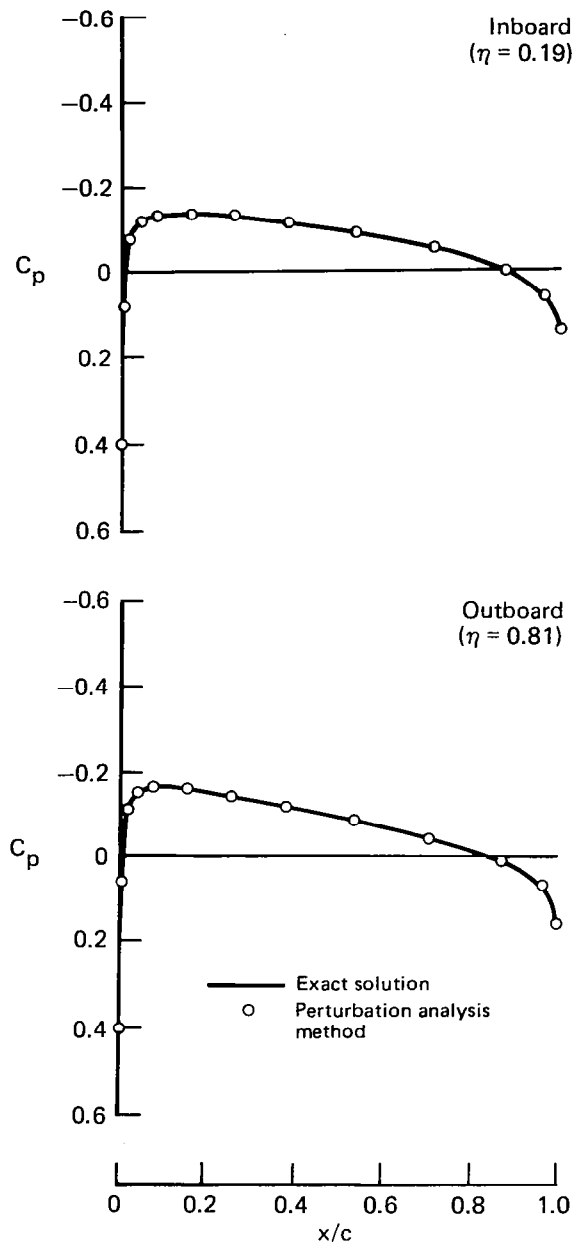
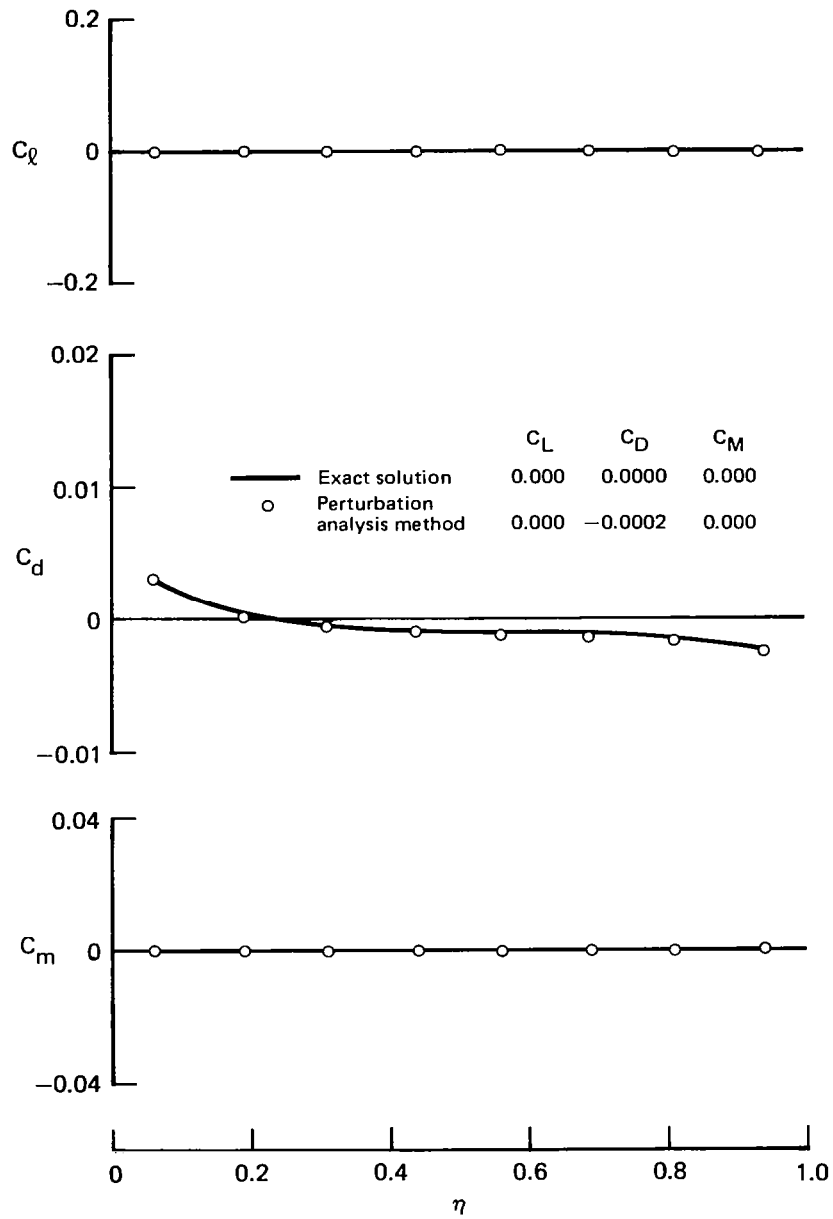


Figure 25. Baseline Force and Moment Distribution at 5° Angle-of-Attack
NACA 0012



**Figure 26. Pressure Distribution of Wing A
at 0° Angle-of-Attack
NACA 0006**



**Figure 27. Force and Moment Distribution of Wing A at 0° Angle-of-Attack
NACA 0006**

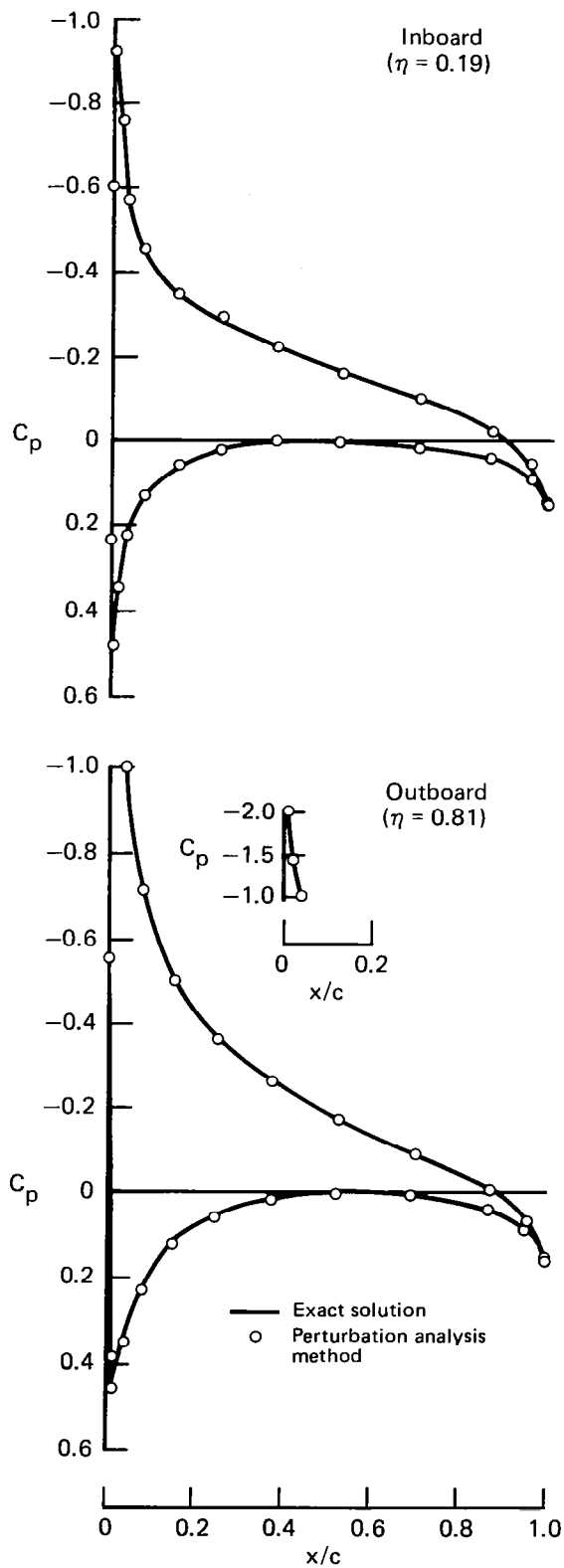


**Figure 28. Pressure Distribution of Wing A at 5° Angle-of-Attack
NACA 0006**

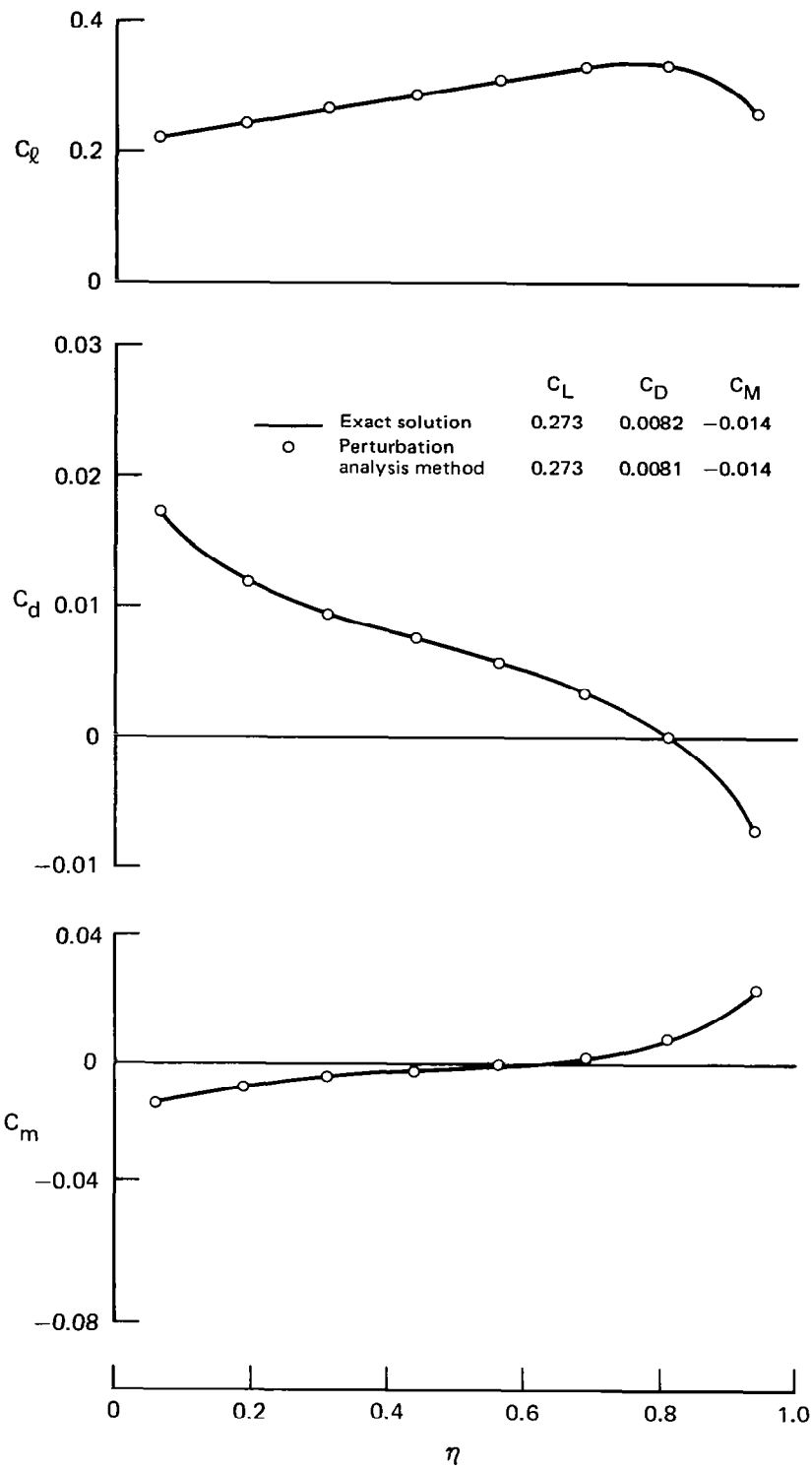


**Figure 29. Force and Moment Distribution of Wing A at 5° Angle-of-Attack
NACA 0006**

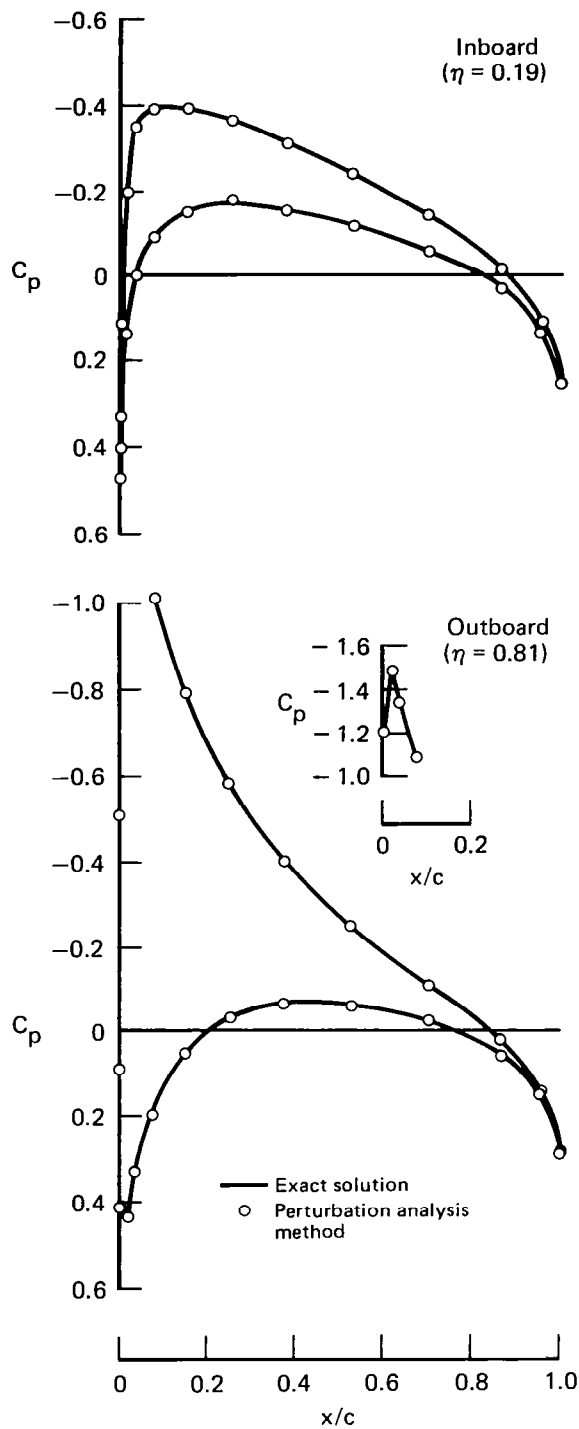


**Figure 30. Pressure Distribution of Wing B at 0° Angle-of-Attack
10° Twist**

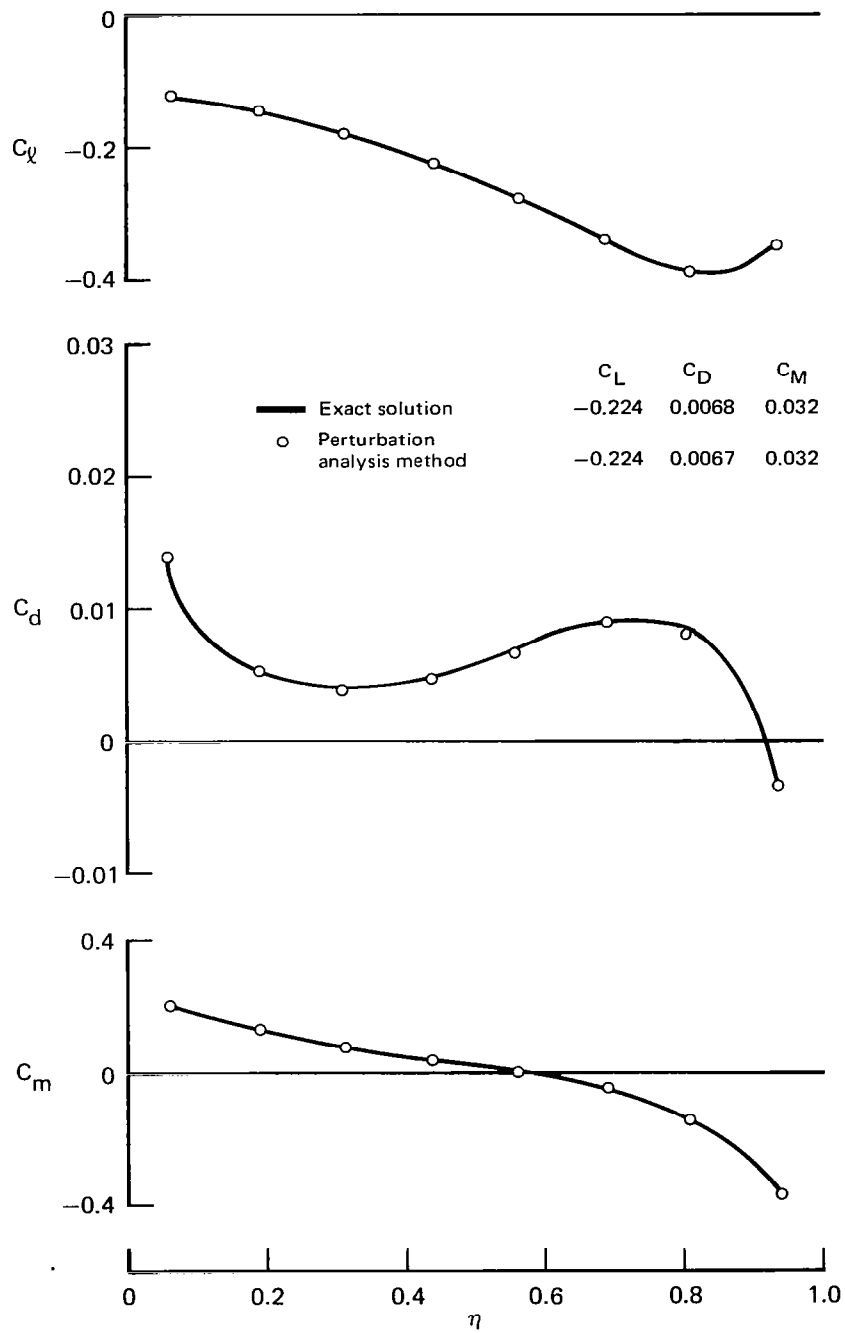
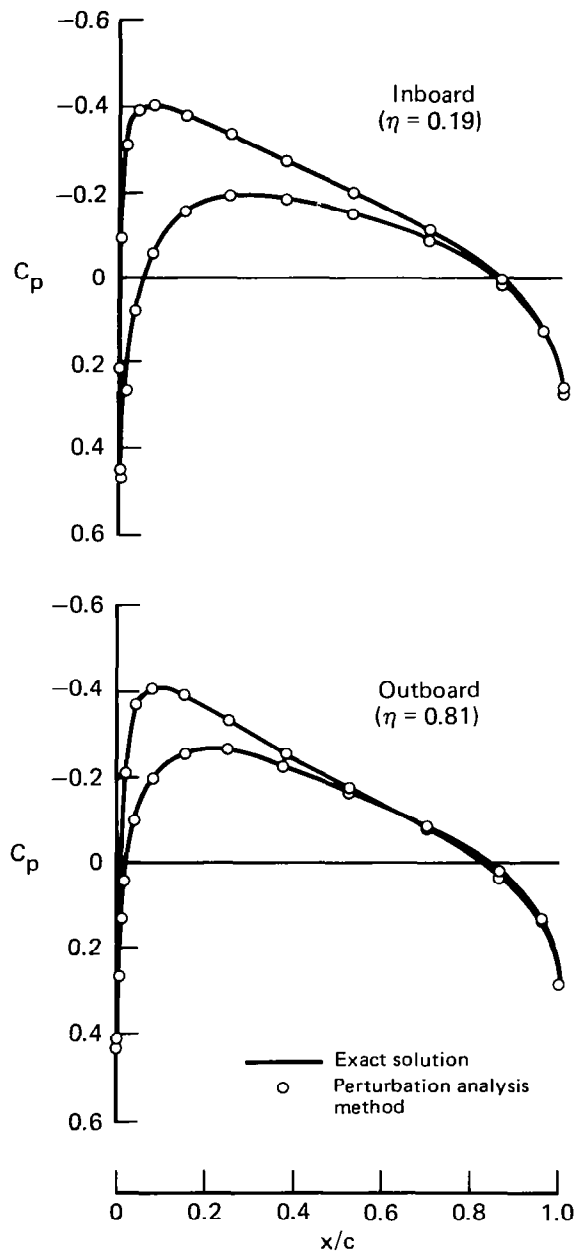
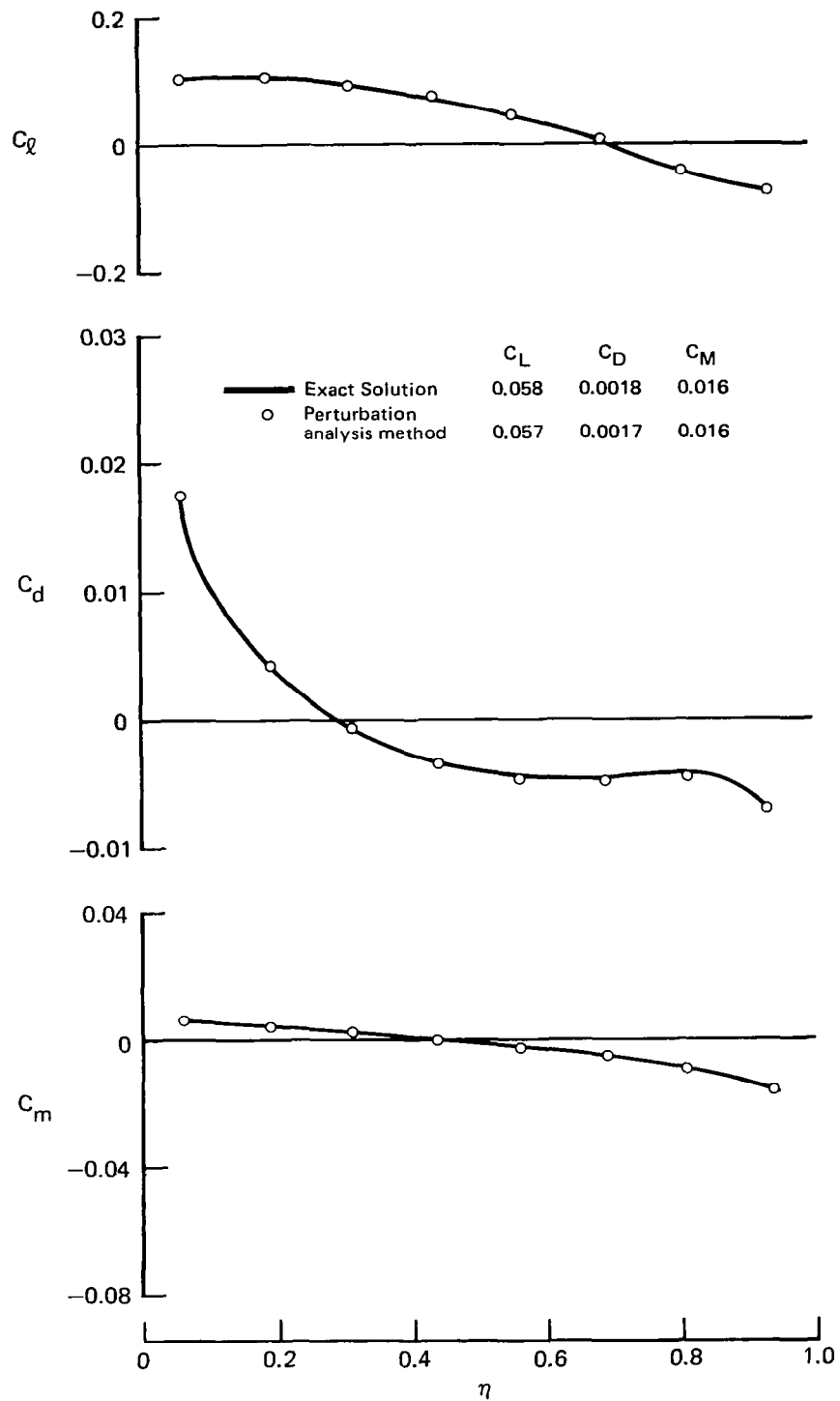


Figure 31. Force and Moment Distribution of Wing B at 0° Angle-of-Attack 10° Twist



**Figure 32. Pressure Distribution of Wing B at 5° Angle-of-Attack
10° Twist**



**Figure 33. Force and Moment Distribution of Wing B at 5° Angle-of-Attack
10° Twist**

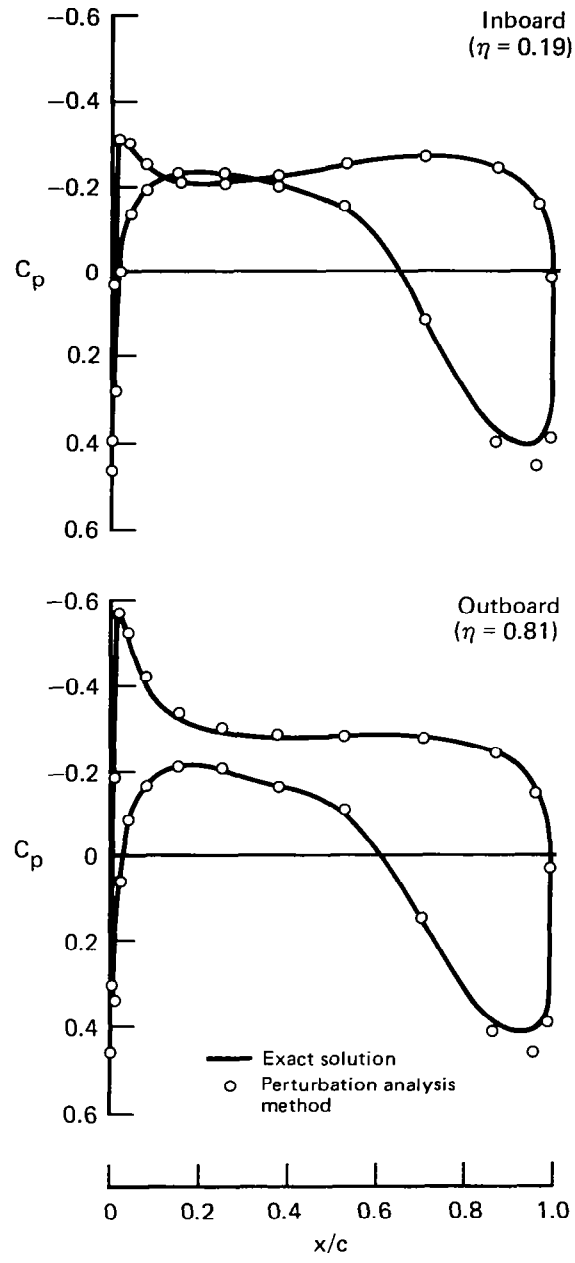


Figure 34. Pressure Distribution of Wing C at 0° Angle-of-Attack Supercritical

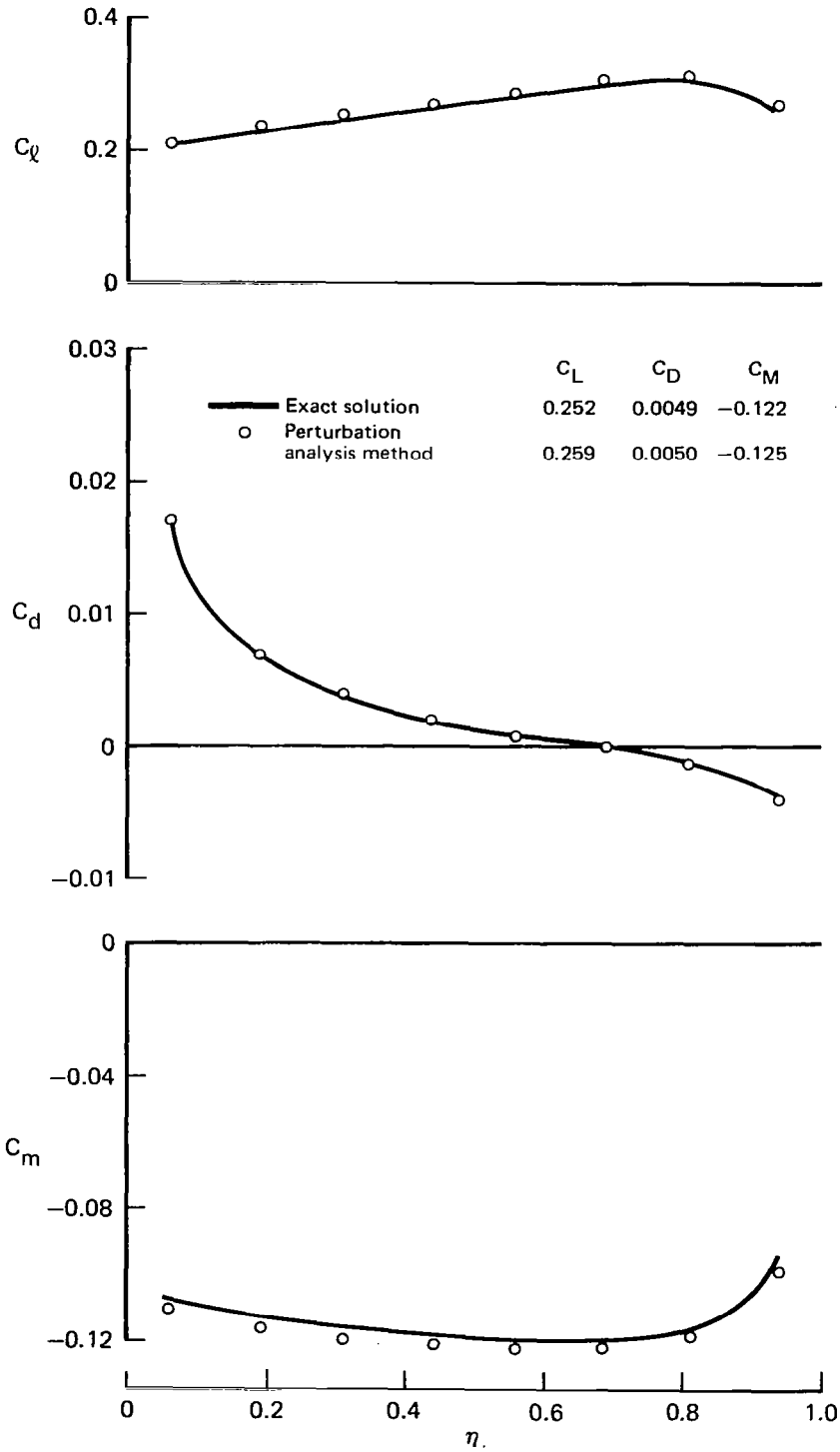


Figure 35. Force and Moment Distribution of Wing C at 0° Angle-of-Attack Supercritical

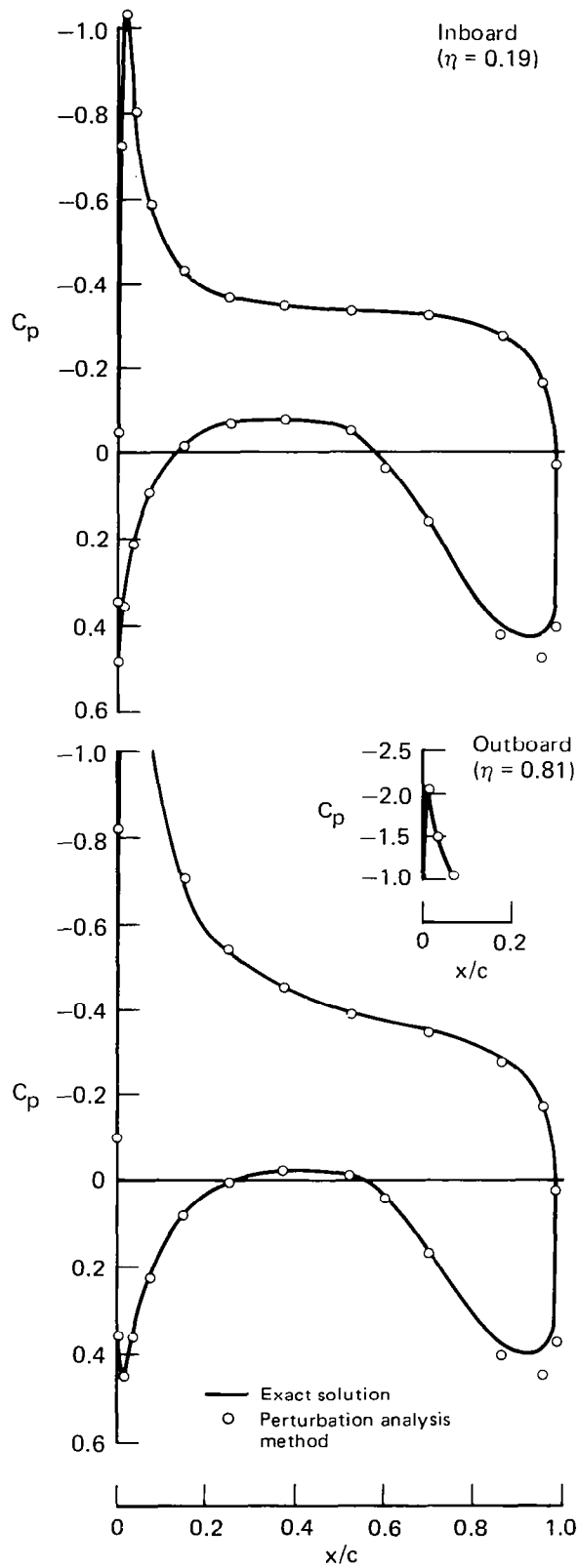


Figure 36. Pressure Distribution of Wing C at 5° Angle-of-Attack Supercritical

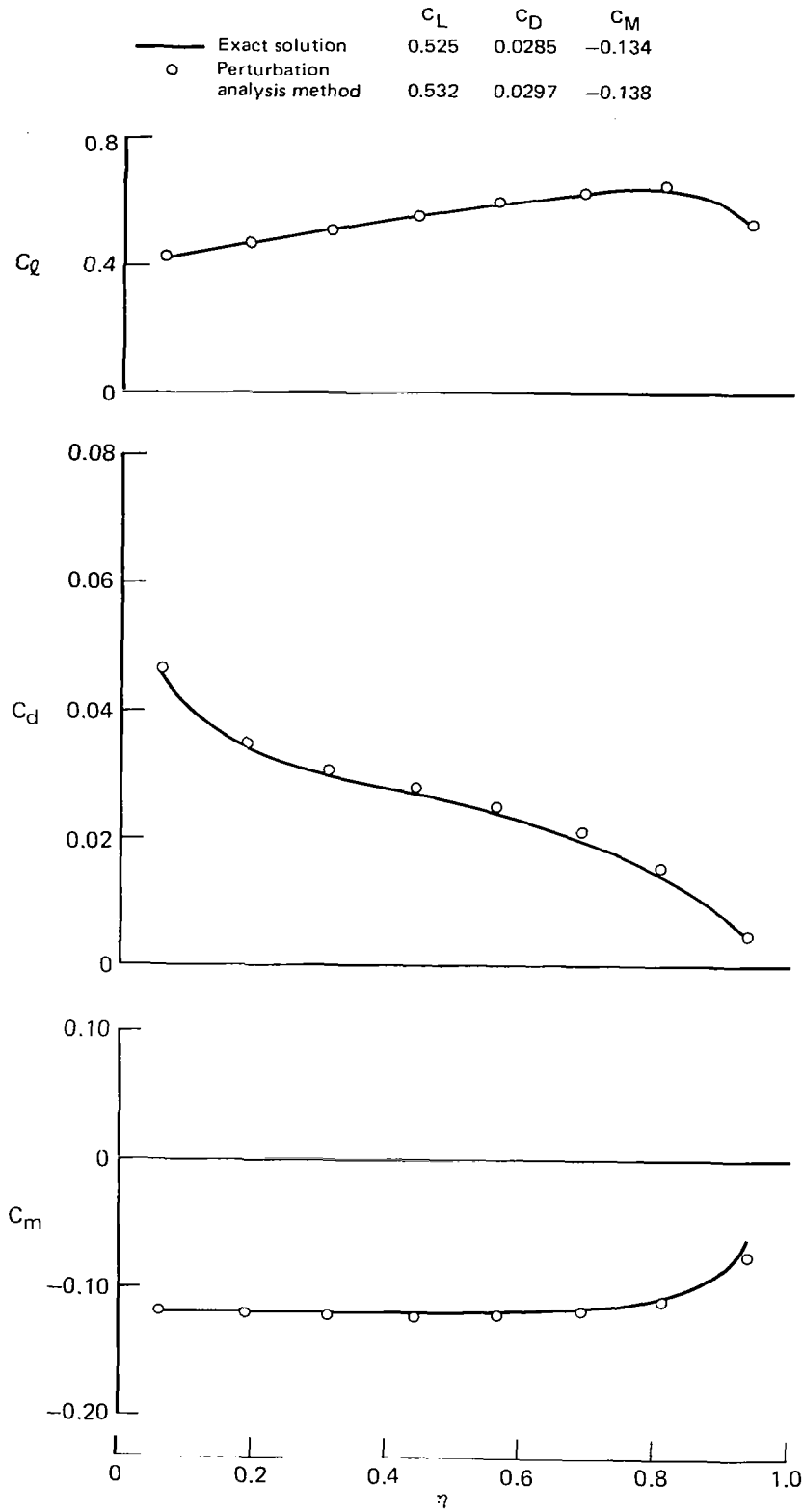


Figure 37. Force and Moment Distribution of Wing C at 5° Angle-of-Attack Supercritical

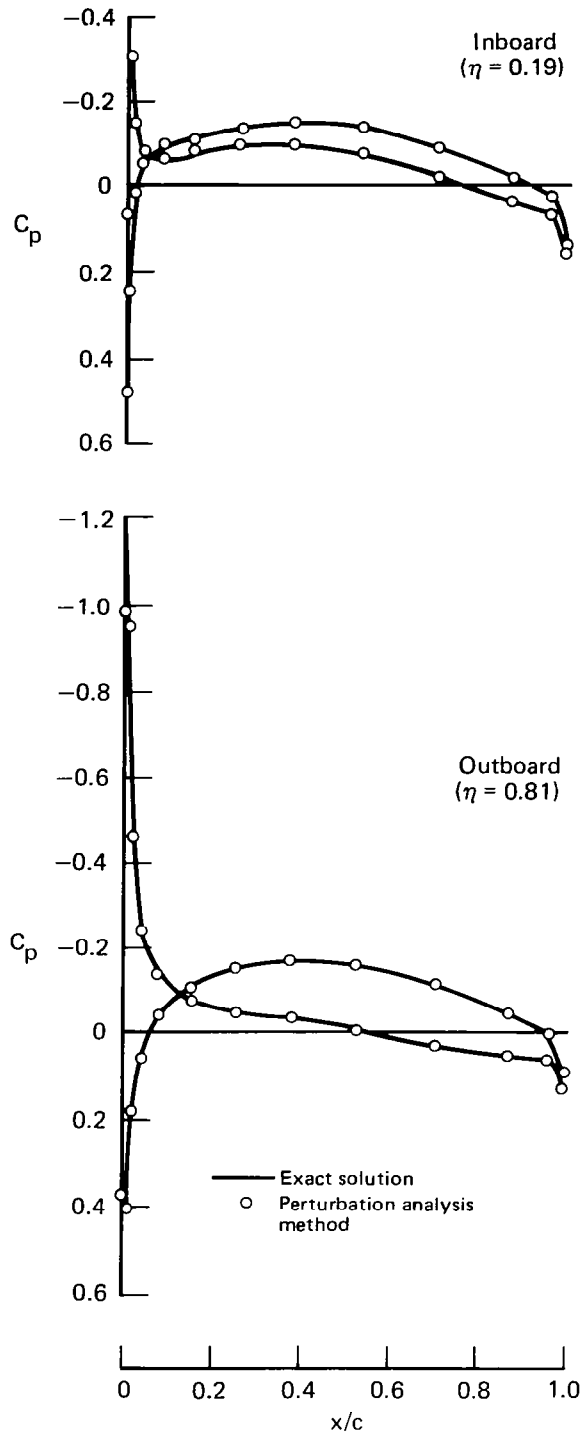


Figure 38. Pressure Distribution of Wing D at 0° Angle-of-Attack Fighter

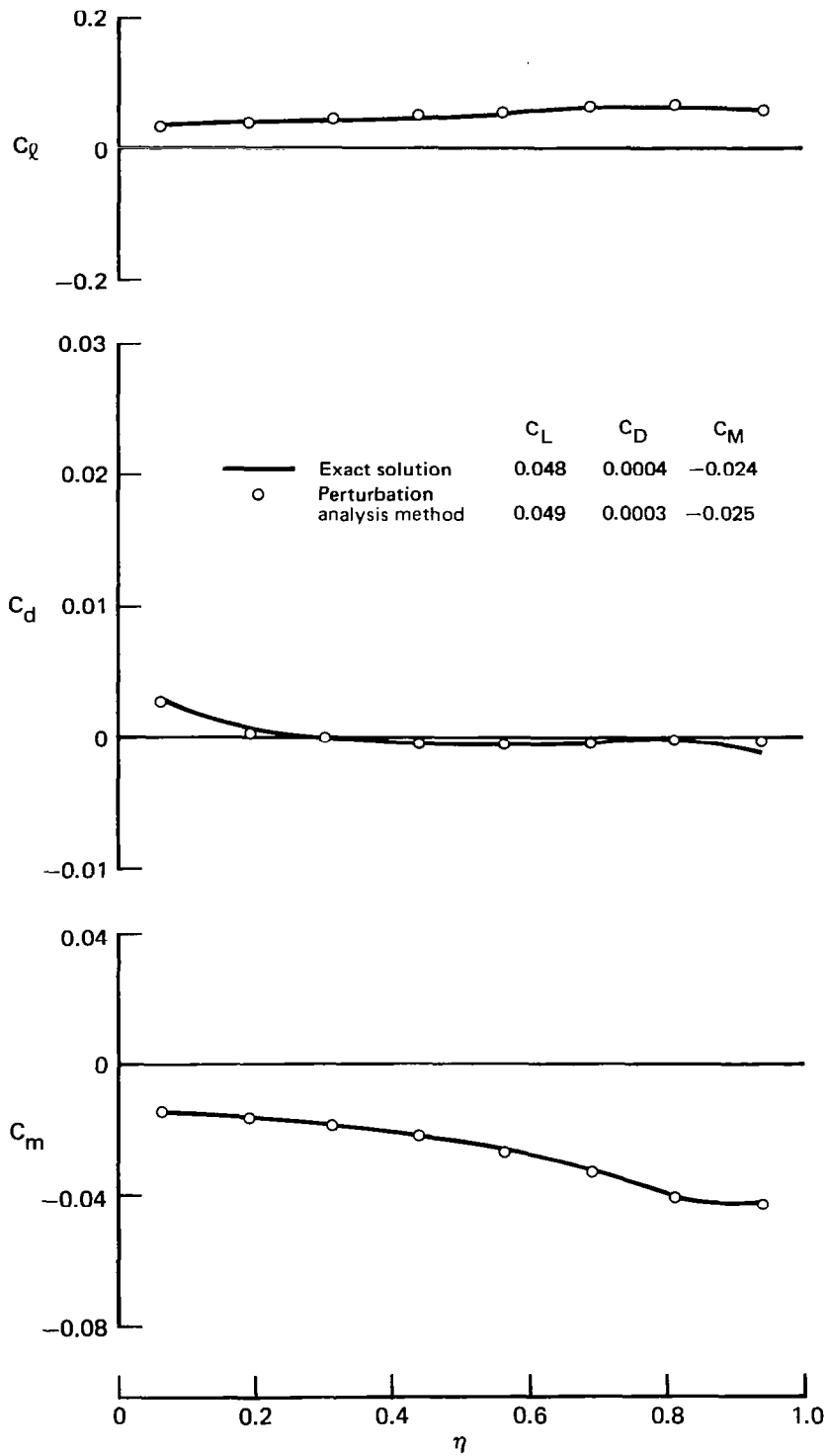


Figure 39. Force and Moment Distribution of Wing D at 0° Angle-of-Attack Fighter

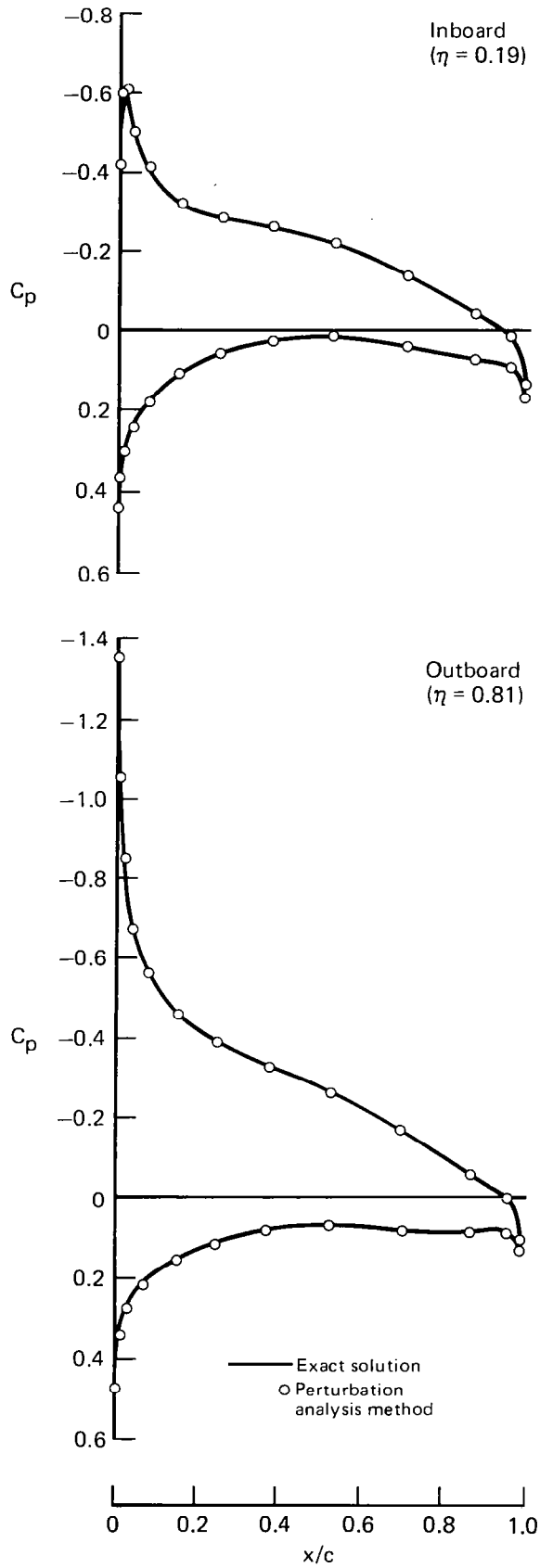


Figure 40. Pressure Distribution of Wing D at 5° Angle-of-Attack Fighter

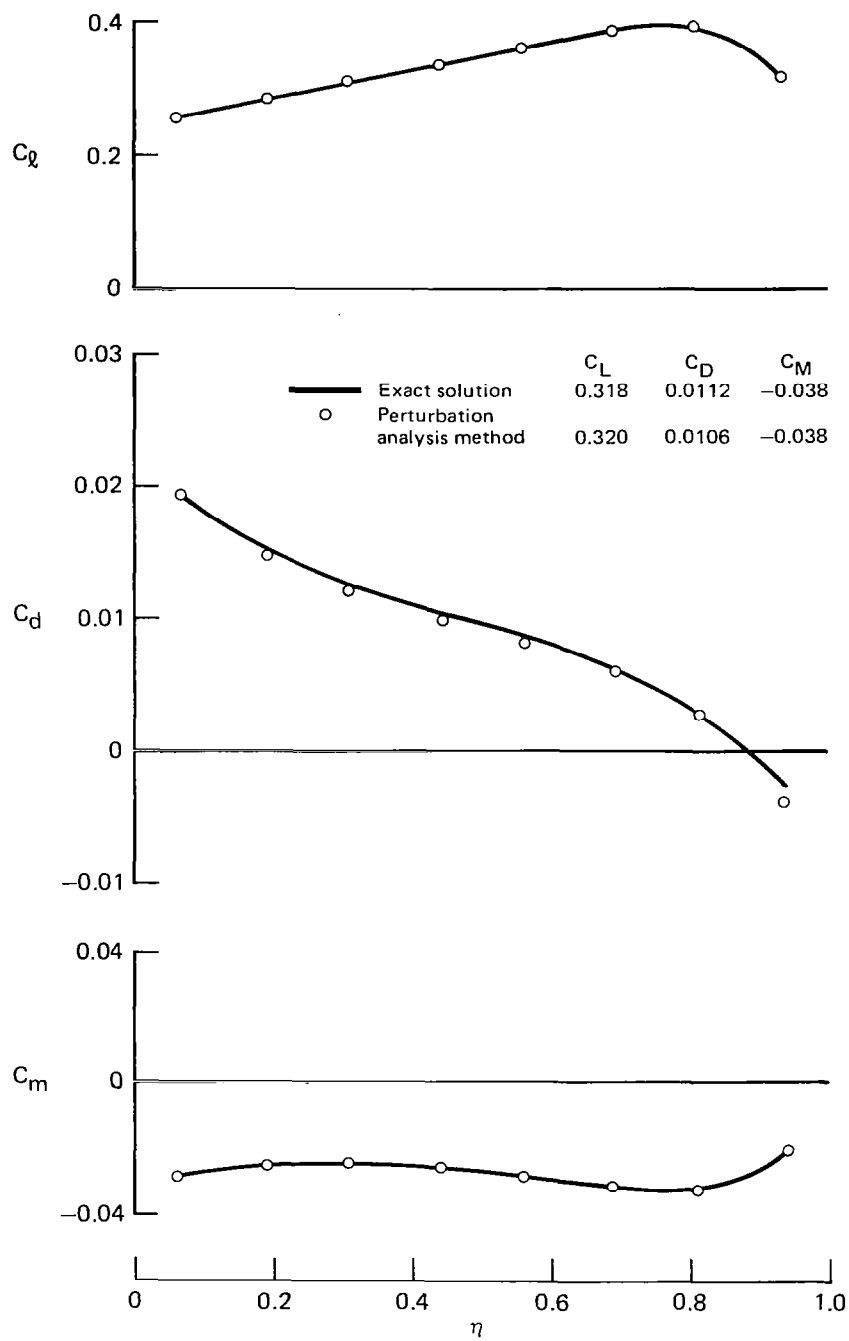
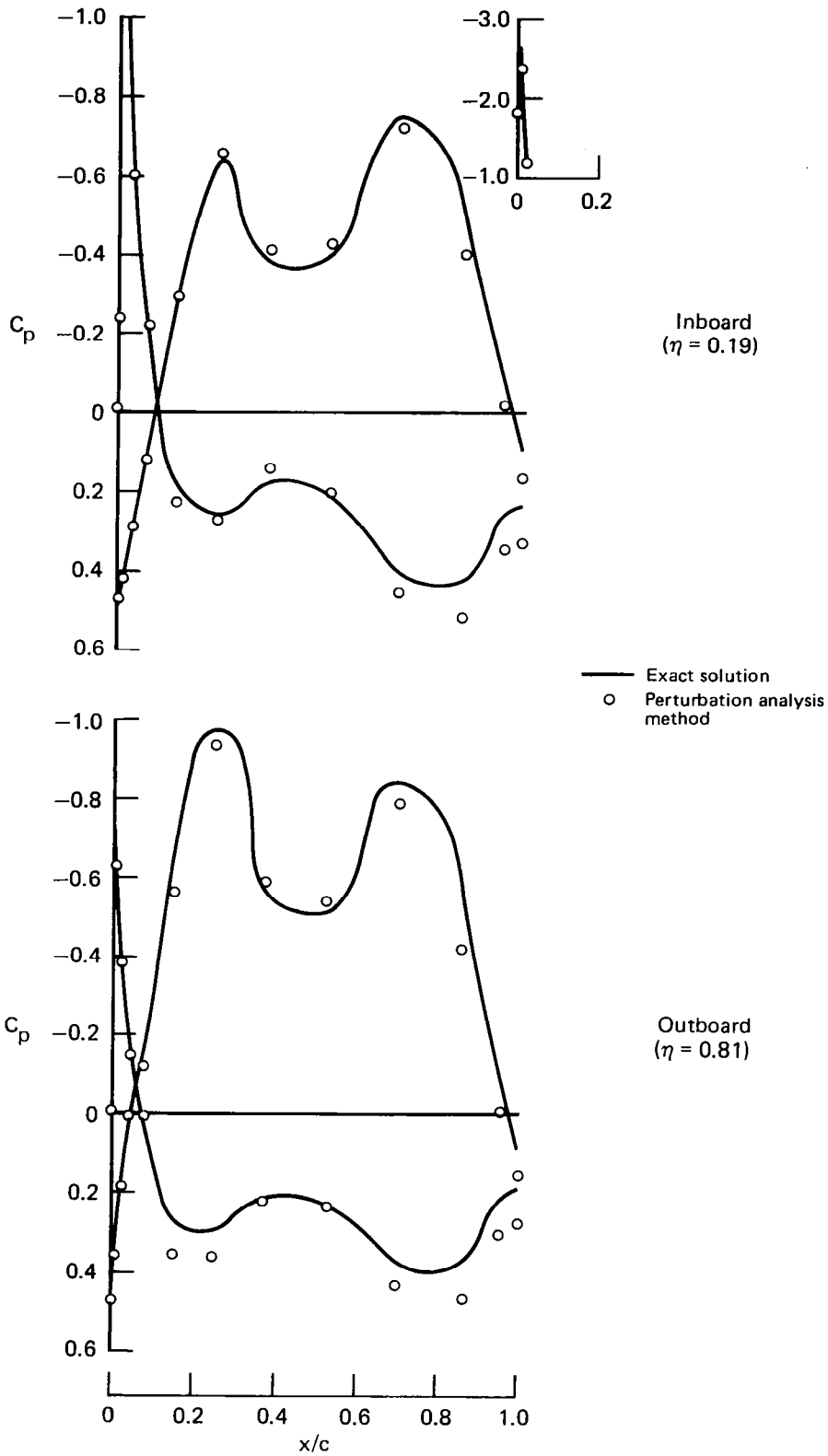
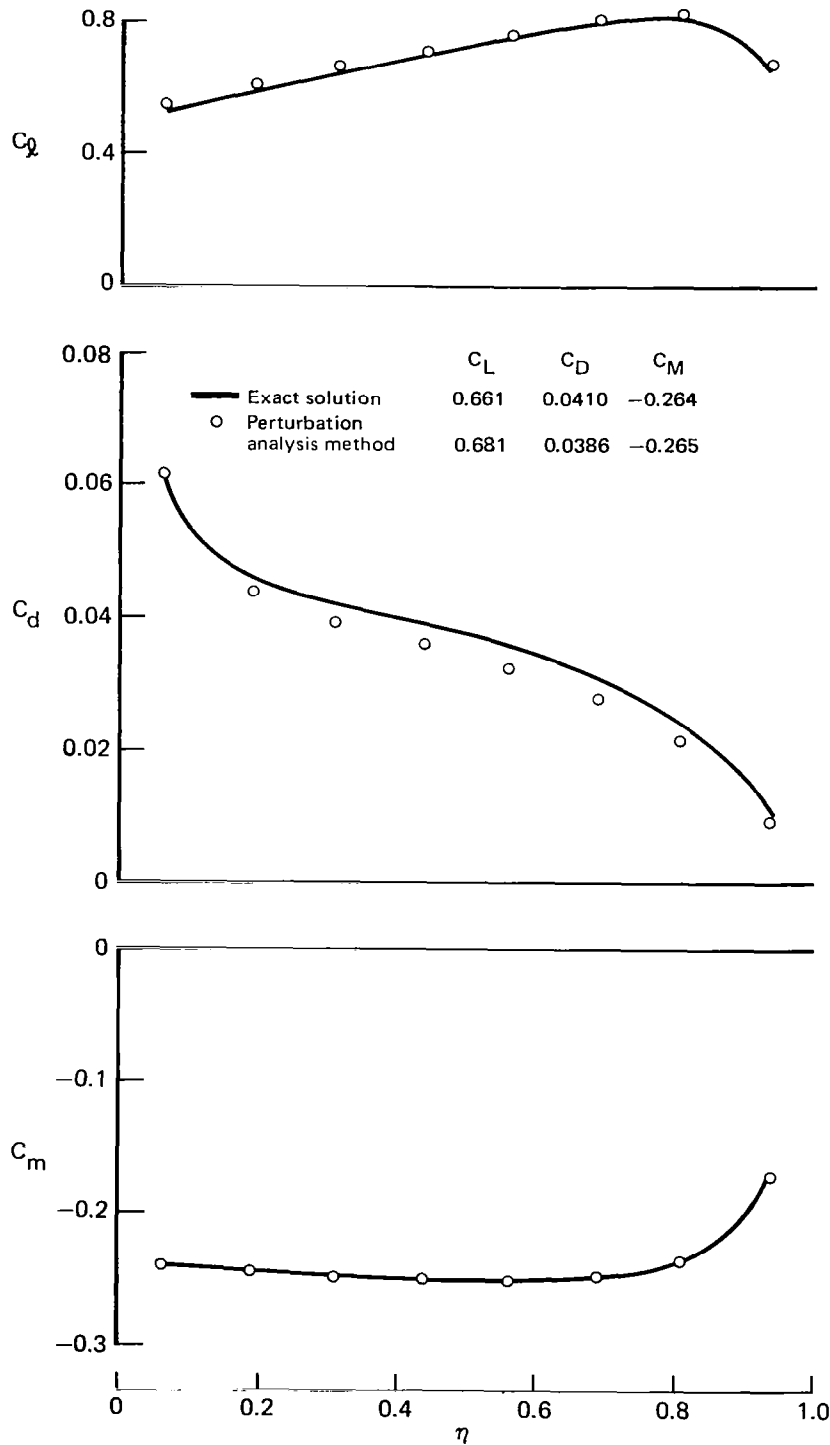


Figure 41. Force and Moment Distribution of Wing D at 5° Angle-of-Attack Fighter



**Figure 42. Pressure Distribution of Wing E at 0° Angle-of-Attack
20° Flaps**



**Figure 43. Force and Moment Distribution of Wing E at 0° Angle-of-Attack
20° Flaps**

CONCLUSIONS

The perturbation analysis method is similar to classical small disturbance methods in the sense that linearized boundary conditions are employed. However, the perturbation analysis method is significantly more accurate for two reasons. First, the linearization is performed on an arbitrary baseline geometry, not a flat plate. Second, only the doublet strengths at discrete points are linearized, not surface velocity and pressure.

After the partial derivative matrix has been established for a baseline configuration, each perturbation analysis is more than an order of magnitude more efficient than a conventional panel method solution. The reason is that there is no aerodynamic influence coefficient matrix to calculate nor is there a large system of linear, algebraic boundary condition equations to solve. It has been demonstrated that the accuracy of the perturbation analysis method is competitive with conventional surface panel methods for analyzing the effect of large changes in wing section geometry.

The utility of the perturbation analysis method for preliminary design is obvious. There are two additional applications for which the method is expected to be equally useful. The first is in iterative solutions to prescribed pressure design problems, where the cost of analyzing the updated geometry of each iteration cycle would no longer be a deterrent. The second application is the prediction of strong viscous-inviscid interactions by iteration between viscous and inviscid flow analyses. The number of iteration cycles and/or angles of attack would not be limited by the high cost of conventional inviscid flow analysis.

APPENDIX A

QUADRATIC SURFACE FIT THROUGH
TWO SETS OF THREE COLINEAR POINTS

Consider the points ℓ ($1 < \ell < \text{MAX}$) in figure A-1, where MAX is either 6, 7, 8 or 9. The set of points [1,2,4] is colinear, and the set of points [1,3,5] is colinear. The objective is to establish a quadratic function $\mu(\xi, \eta)$ that will match arbitrary values μ_ℓ exactly at points $1 < \ell < 5$ and approximately at points $6 \leq \ell \leq \text{MAX}$. The given (known) quantities are θ , s_ℓ for $2 \leq \ell \leq 5$, MAX, and $(\xi, \eta)_\ell$ for $6 \leq \ell \leq \text{MAX}$. Any or all of the values s_ℓ ($2 \leq \ell \leq 5$) can be negative or positive. Assume that the function $\mu(\xi, \eta)$ is expressed in the form

$$\mu(\xi, \eta) = \mu_1 + \beta_1 \xi + \beta_2 \eta + \beta_3 \xi^2 + \beta_4 \xi \eta + \beta_5 (\eta^2 - \xi^2 \tan^2 \theta) \quad (\text{A1})$$

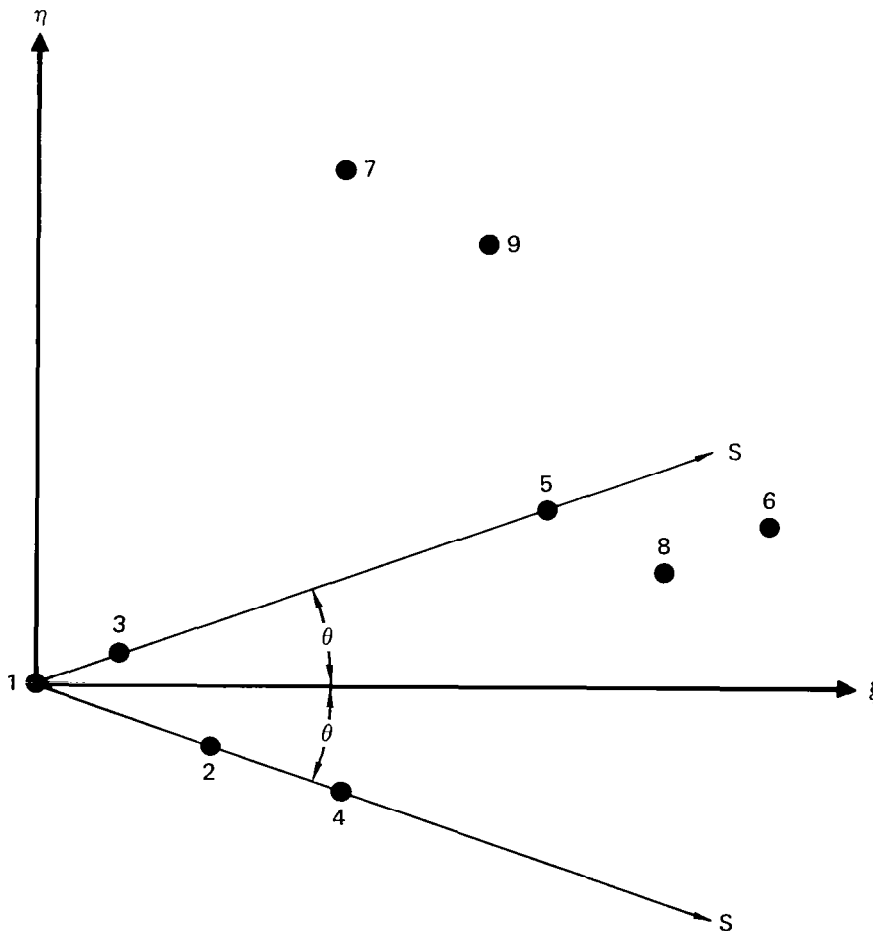


Figure A-1. Nomenclature for Two Sets of Three Colinear Points

Then the coefficients β_i can be readily established from the following formulas:

$$\beta_1 \cdot 2\cos\theta = \left\{ \frac{s_5^2(\mu_3 - \mu_1) - s_3^2(\mu_5 - \mu_1)}{s_3 s_5 (s_5 - s_3)} \right\} + \left\{ \frac{s_4^2(\mu_2 - \mu_1) - s_2^2(\mu_4 - \mu_1)}{s_2 s_4 (s_4 - s_2)} \right\} \quad (\text{A2})$$

$$\beta_2 \cdot 2\sin\theta = \left\{ \frac{s_5^2(\mu_3 - \mu_1) - s_3^2(\mu_5 - \mu_1)}{s_3 s_5 (s_5 - s_3)} \right\} - \left\{ \frac{s_4^2(\mu_2 - \mu_1) - s_2^2(\mu_4 - \mu_1)}{s_2 s_4 (s_4 - s_2)} \right\} \quad (\text{A3})$$

$$\beta_3 \cdot 2\cos^2\theta = \left\{ \frac{s_3(\mu_5 - \mu_1) - s_5(\mu_3 - \mu_1)}{s_3 s_5 (s_5 - s_3)} \right\} + \left\{ \frac{s_2(\mu_4 - \mu_1) - s_4(\mu_2 - \mu_1)}{s_2 s_4 (s_4 - s_2)} \right\} \quad (\text{A4})$$

$$\beta_4 \cdot 2\cos\theta \sin\theta = \left\{ \frac{s_3(\mu_5 - \mu_1) - s_5(\mu_3 - \mu_1)}{s_3 s_5 (s_5 - s_3)} \right\} - \left\{ \frac{s_2(\mu_4 - \mu_1) - s_4(\mu_2 - \mu_1)}{s_2 s_4 (s_4 - s_2)} \right\} \quad (\text{A5})$$

$$\beta_5 = \frac{\sum_{\ell=6}^{\text{MAX}} \text{SGN}_{\ell} \left\{ \mu_{\ell} - \mu_1 - \beta_1 \epsilon_{\ell} - \beta_2 \eta_{\ell} - \beta_3 \epsilon_{\ell}^2 - \beta_4 \epsilon_{\ell} \eta_{\ell} \right\}}{\sum_{\ell=6}^{\text{MAX}} |\eta_{\ell}^2 - \epsilon_{\ell}^2 \cdot \tan^2\theta|} \quad (\text{A6})$$

where

$$\text{SGN}_{\ell} \equiv \begin{cases} -1 & \text{if } \ell = 6 \text{ or } 8 \\ +1 & \text{if } \ell = 7 \text{ or } 9 \end{cases}$$

The above definition of term SGN_ℓ is based on the assumption that the quantity $(\eta_\ell^2 - \xi_\ell^2 \tan^2 \theta)$ is ≤ 0 if ℓ is 6 or 8 and ≥ 0 if ℓ is 7 or 9. This assumption is always valid for the panel method formulation of this report.

The orientation of the (ξ, η) -coordinate system of figure A-1 and the functional form of equation (A1) were selected to simplify the determination of equations (A2) through (A6). The derivation is straightforward but will not be presented here because a simple substitution into equation (A1) validates the formulas for β_i .

It is noteworthy that each β_i is linear with respect to μ_ℓ . Specifically, equations (A2) through (A6) are in the form

$$\beta_i = \sum_{\ell=1}^5 (b_{i\ell} \cdot \mu_\ell) + \delta_{i5} \sum_{\ell=6}^{\text{MAX}} (b_{5\ell} \cdot \mu_\ell) \quad (1 \leq i \leq 5) \quad (\text{A7})$$

where $\delta_{i5} \equiv (0,1)$ if i is $(\neq 5, =5)$, and where the coefficients $b_{i\ell}$ are explicit functions of the given quantities defined earlier.

Now suppose that the given quantities include known values for μ_ℓ ($1 \leq \ell < \text{MAX}$) and that it is desired to determine $\partial \beta_i / \partial \theta$, $\partial \beta_i / \partial s_\ell$ for $2 \leq \ell < 5$, and $(\partial \beta_i / \partial \xi_\ell, \partial \beta_i / \partial \eta_\ell)$ for $6 \leq \ell < \text{MAX}$. This is accomplished by differentiating equations (A2) through (A6). First, it is convenient to introduce twelve quantities defined by equations (A8) and (A9).

$$\begin{aligned} A_N &\equiv s_5^2 (\mu_3 - \mu_1) - s_3^2 (\mu_5 - \mu_1) & A_D &\equiv s_3 s_5 (s_5 - s_3) \\ B_N &\equiv s_4^2 (\mu_2 - \mu_1) - s_2^2 (\mu_4 - \mu_1) & B_D &\equiv s_2 s_4 (s_4 - s_2) \\ C_N &\equiv s_3 (\mu_5 - \mu_1) - s_5 (\mu_3 - \mu_1) & C_D &\equiv s_3 s_5 (s_5 - s_3) \\ D_N &\equiv s_2 (\mu_4 - \mu_1) - s_4 (\mu_2 - \mu_1) & D_D &\equiv s_2 s_4 (s_4 - s_2) \end{aligned} \quad (\text{A8})$$

$$\begin{aligned}
F_A &\equiv (A_N/A_D) & F_B &\equiv (B_N/B_D) \\
F_C &\equiv (C_N/C_D) & F_D &\equiv (D_N/D_D)
\end{aligned}
\tag{A9}$$

The partial derivatives of F_A , F_B , F_C , and F_D follow.

$$\begin{aligned}
\frac{\partial F_A}{\partial s_3} &= \{-A_D 2s_3(\mu_5 - \mu_1) - A_N s_5(s_5 - 2s_3)\}/A_D^2 \\
\frac{\partial F_A}{\partial s_5} &= \{+A_D 2s_5(\mu_3 - \mu_1) + A_N s_3(s_3 - 2s_5)\}/A_D^2 \\
\frac{\partial F_B}{\partial s_2} &= \{-B_D 2s_2(\mu_4 - \mu_1) - B_N s_4(s_4 - 2s_2)\}/B_D^2 \\
\frac{\partial F_B}{\partial s_4} &= \{+B_D 2s_4(\mu_2 - \mu_1) + B_N s_2(s_2 - 2s_4)\}/B_D^2 \\
\frac{\partial F_C}{\partial s_3} &= \{+C_D(\mu_5 - \mu_1) - C_N s_5(s_5 - 2s_3)\}/C_D^2 \\
\frac{\partial F_C}{\partial s_5} &= \{-C_D(\mu_3 - \mu_1) + C_N s_3(s_3 - 2s_5)\}/C_D^2 \\
\frac{\partial F_D}{\partial s_2} &= \{+D_D(\mu_4 - \mu_1) - D_N s_4(s_4 - 2s_2)\}/D_D^2 \\
\frac{\partial F_D}{\partial s_4} &= \{-D_D(\mu_2 - \mu_1) + D_N s_2(s_2 - 2s_4)\}/D_D^2
\end{aligned}
\tag{A10}$$

With the aid of the preceding quantities, equations (A2) through (A6) are differentiated to establish equations (A11) through (A16).

$$\begin{aligned}
 2\cos\theta d\beta_1 = 2\beta_1\sin\theta d\theta + \left(\frac{\partial F_B}{\partial s_2}\right) ds_2 + \left(\frac{\partial F_A}{\partial s_3}\right) ds_3 \\
 + \left(\frac{\partial F_B}{\partial s_4}\right) ds_4 + \left(\frac{\partial F_A}{\partial s_5}\right) ds_5
 \end{aligned} \tag{A11}$$

$$\begin{aligned}
 2\sin\theta d\beta_2 = -2\beta_2\cos\theta d\theta - \left(\frac{\partial F_B}{\partial s_2}\right) ds_2 + \left(\frac{\partial F_A}{\partial s_3}\right) ds_3 \\
 - \left(\frac{\partial F_B}{\partial s_4}\right) ds_4 + \left(\frac{\partial F_A}{\partial s_5}\right) ds_5
 \end{aligned} \tag{A12}$$

$$\begin{aligned}
 2\cos^2\theta d\beta_3 = 4\beta_3\cos\theta\sin\theta d\theta + \left(\frac{\partial F_D}{\partial s_2}\right) ds_2 + \left(\frac{\partial F_C}{\partial s_3}\right) ds_3 \\
 + \left(\frac{\partial F_D}{\partial s_4}\right) ds_4 + \left(\frac{\partial F_C}{\partial s_5}\right) ds_5
 \end{aligned} \tag{A13}$$

$$\begin{aligned}
 2\cos\theta\sin\theta d\beta_4 = -2\beta_4\cos(2\theta) d\theta - \left(\frac{\partial F_D}{\partial s_2}\right) ds_2 + \left(\frac{\partial F_C}{\partial s_3}\right) ds_3 \\
 - \left(\frac{\partial F_D}{\partial s_4}\right) ds_4 + \left(\frac{\partial F_C}{\partial s_5}\right) ds_5
 \end{aligned} \tag{A14}$$

$$\begin{aligned}
d\beta_5 = & \left(\frac{1}{\text{TDEN}} \right) \sum_{\ell=6}^{\text{MAX}} \text{SGN}_{\ell} \cdot \left\{ \begin{aligned} & - \xi_{\ell} d\beta_1 - \eta_{\ell} d\beta_2 - \xi_{\ell}^2 d\beta_3 - \xi_{\ell} \eta_{\ell} d\beta_4 \\ & + (-\beta_1 - 2\xi_{\ell} \beta_3 - \eta_{\ell} \beta_4) d\xi_{\ell} \\ & + (-\beta_2 - \xi_{\ell} \beta_4) d\eta_{\ell} \end{aligned} \right\} \\
& + \left(\frac{\text{TNUM}}{\text{TDEN}^2} \right) \sum_{\ell=6}^{\text{MAX}} (2 \cdot \text{SGN}_{\ell}) \cdot \left\{ \xi_{\ell} \tan^2 \theta d\xi_{\ell} - \eta_{\ell} d\eta_{\ell} + \left(\frac{\xi_{\ell}^2 \sin \theta}{\cos^3 \theta} \right) d\theta \right\}
\end{aligned} \tag{A15}$$

where

$$\begin{aligned}
\text{TNUM} & \equiv \sum_{\ell=6}^{\text{MAX}} \text{SGN}_{\ell} \left\{ \mu_{\ell} - \mu_1 - \beta_1 \xi_{\ell} - \beta_2 \eta_{\ell} - \beta_3 \xi_{\ell}^2 - \beta_4 \xi_{\ell} \eta_{\ell} \right\} \\
\text{TDEN} & \equiv \sum_{\ell=6}^{\text{MAX}} | \eta_{\ell}^2 - \xi_{\ell}^2 \cdot \tan^2 \theta |
\end{aligned} \tag{A16}$$

The desired partial derivatives of β_i are expressed implicitly by the coefficients of the differentials in equations (A11) through (A15).

APPENDIX B

DIVISION OF A PANEL INTO SUBPANELS

The division of an arbitrary noncoplanar quadrilateral panel into eight triangular subpanels is based upon the approach of reference 3. For each subpanel, a quadratic doublet distribution is established by a fit to the doublet strength at several spline control points on the panel. A sensitivity matrix is generated for which each matrix element is the contribution of a unit strength doublet density at one spline control point to one of the six coefficients of the quadratic distribution. The present approach differs from that of reference 3 in the sense that the sensitivity matrix is generated from simple, explicit mathematical functions and no matrix inversion is required. The mathematical formulation is presented in this Appendix. Also presented is the procedure for generating a second sensitivity matrix, one that relates the quadratic doublet coefficients to panel geometry perturbations.

The division of a noncoplanar panel into eight triangular subpanels is illustrated in figure B-1. The subpanel vertices of figure B-1 are the same nine points $1 < k < 9$ that were depicted in figure 9. Similarly, the coordinate displacement arrays X_{ik} defined by equations (3) and (4) also apply to this Appendix. It is easily proved that the four interior subpanels ($5 < i_{sp} < 8$) are coplanar, regardless of whether the four corner points ($k = 1, 2, 3, 4$) are coplanar.

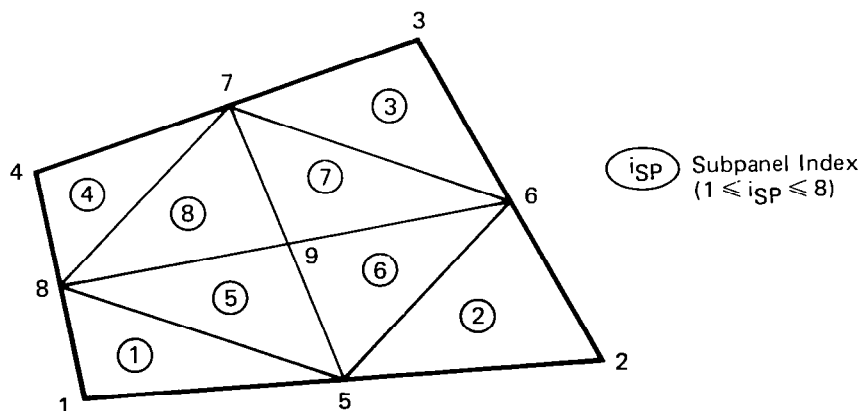


Figure B-1. Division of a Panel Into Subpanels

The nine points k are the spline control points. Suppose that an arbitrary value of doublet strength (μ_k) is assigned to each spline control point. For each subpanel, it is desired to establish the quadratic doublet distribution that will satisfy the following conditions:

- (i) Consider the three spline control points at the subpanel vertices and the two spline control points that lie on extensions of the subpanel edges. At each of these five points k , the quadratic distribution is to match μ_k .
- (ii) Consider the subpanel edge that separates interior from exterior subpanels. At the midpoint of this edge, both the doublet strength and the derivative of the doublet distribution in the direction normal to the edge are to match the corresponding values for the adjacent subpanel. This will generate continuity and slope continuity at the edge midpoint.

The above two conditions imply that for each pair of adjacent subpanels, the quadratic doublet distributions will match at three points along the common edge (or an extension of that edge). This matching is (usually) enforced even if the adjacent subpanels are not part of the same full panel. Along an edge, the quadratic surface distribution is a parabola. Since there is only one parabola that can pass through a set of three points, the doublet distribution will be continuous across the entire common edge of each pair of adjacent subpanels.

Figure B-2 illustrates a local coordinate system (ξ, η, ζ) that is defined for each subpanel i_{sp} . The ζ -axis is perpendicular to the subpanel, and the origin is at the one subpanel vertex that is not coincident with an edge midpoint of the full panel. The index ℓ denotes the spline control points in an order different from index k (see Table B-I). The ordering of ℓ was selected to be consistent with the method of Appendix A, which will be employed in establishing the quadratic doublet distribution. For each subpanel i_{sp} , the nomenclature $k(\ell)$ and $\ell(k)$ refers to the conversion between ℓ and k that is provided by Table B-I.

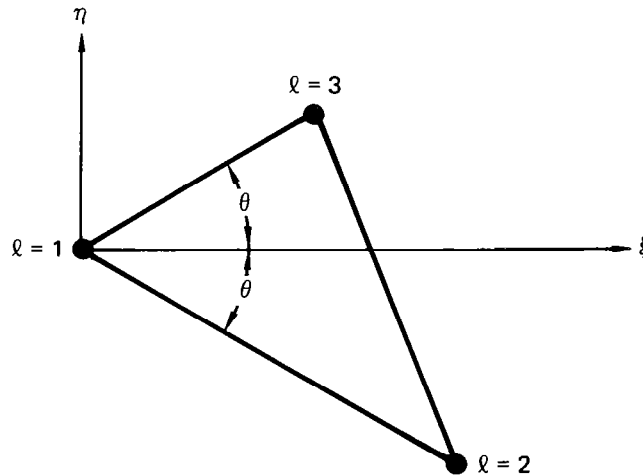


Figure B-2. Local Coordinate System for a Subpanel

Table B-1. Conversion Between Index k and Indices (l , i_{SP})

ℓ	k (for $1 \leq i_{SP} \leq 4$)	k (for $5 \leq i_{SP} \leq 8$)
1	i _{SP}	9
2	(i _{SP} + 4)	(i _{SP} - 1) if i _{SP} ≠ 5 8 if i _{SP} = 5
3	(i _{SP} + 3) if i _{SP} ≠ 1 8 if i _{SP} = 1	i _{SP}
4	(i _{SP} + 1) if i _{SP} ≠ 4 1 if i _{SP} = 4	(i _{SP} + 1) if i _{SP} ≠ 8 5 if i _{SP} = 8
5	(i _{SP} - 1) if i _{SP} ≠ 1 4 if i _{SP} = 1	(i _{SP} + 2) if i _{SP} ≤ 6 (i _{SP} - 2) if i _{SP} > 6
6	9	(i _{SP} - 4)
7	(i _{SP} + 5) if i _{SP} ≠ 4 5 if i _{SP} = 4	(i _{SP} - 3) if i _{SP} ≠ 8 1 if i _{SP} = 8
8	(i _{SP} + 6) if i _{SP} ≤ 2 (i _{SP} + 2) if i _{SP} > 2	(i _{SP} - 5) if i _{SP} ≠ 5 4 if i _{SP} = 5
9	(i _{SP} + 2) if i _{SP} ≤ 2 (i _{SP} - 2) if i _{SP} > 2	(i _{SP} - 2) if i _{SP} ≤ 6 (i _{SP} - 6) if i _{SP} > 6

Quantities designated $\{P_{i\ell}, \theta, s_\ell, a_{ij}, \xi_2, \eta_2, \xi_3, \eta_3, \xi_M, \eta_M\}$ are to be calculated for each subpanel i_{SP}. The formulas are provided below:

$$P_{i\ell} \equiv \vec{P}_\ell \equiv X_{i,k(\ell)} - X_{i,k(1)} \quad (1,1) \leq (i,\ell) \leq (3,5) \quad (B1)$$

$$\theta = \frac{1}{2} \text{Cos}^{-1} [(\vec{P}_2 \cdot \vec{P}_3) / (|\vec{P}_2| \cdot |\vec{P}_3|)] \quad (B2)$$

$$s_\ell = c \cdot |\vec{P}_\ell| \quad 1 \leq \ell \leq 5 \quad (\text{B3})$$

where

$$c = \left\{ \begin{array}{l} -1 \quad \text{if } i_{SP} \geq 5 \text{ and } \ell \geq 4 \\ 0 \quad \text{if } \ell = 1 \\ +1 \quad \text{otherwise} \end{array} \right\}$$

$$\begin{Bmatrix} \vec{e}_\zeta \\ \vec{e}_\eta \\ \vec{e}_\xi \end{Bmatrix} = [a_{ij}] \begin{Bmatrix} \vec{e}_x \\ \vec{e}_y \\ \vec{e}_z \end{Bmatrix} \quad (\text{B4})$$

where

$$\vec{e}_\zeta = \frac{\frac{P_{j2}}{|\vec{P}_2|} + \frac{P_{j3}}{|\vec{P}_3|}}{\left| \frac{P_{j2}}{|\vec{P}_2|} + \frac{P_{j3}}{|\vec{P}_3|} \right|}}$$

$$\vec{e}_\xi = \frac{(\vec{P}_2 \times \vec{P}_3)}{|\vec{P}_2 \times \vec{P}_3|} \quad \vec{e}_\eta = (\vec{e}_\zeta \times \vec{e}_\xi)$$

$$\left\{ \begin{array}{l} \xi_2 = s_2 \cos\theta \\ \eta_2 = -s_2 \sin\theta \\ \xi_3 = s_3 \cos\theta \\ \eta_3 = s_3 \sin\theta \end{array} \right\} \quad (B5)$$

$$\left\{ \begin{array}{l} \xi_M = \frac{1}{2}(\xi_2 + \xi_3) \\ \eta_M = \frac{1}{2}(\eta_2 + \eta_3) \end{array} \right\} \quad (B6)$$

The method of Appendix A is to be employed in order to establish the quadratic function that will exactly match $\mu_{k(\ell)}$ for $1 < \ell < 5$ and also match some dummy value μ_M at the point (ξ_M, η_M) , where subscript "M" designates the midpoint between sub-panel vertices 2 and 3. The required given values for Appendix A are θ from equation (B2), s_ℓ from equation (B3), "MAX" which is 6, and the coordinates (ξ_M, η_M) from equation (B6). It is noteworthy that the coordinates designated (ξ_M, η_M) here correspond to (ξ_6, η_6) in Appendix A. From these given values, the method of Appendix A will provide an array of coefficients $b_{i\ell}$ [$(1,1) \leq (i,\ell) \leq (5,5)$] and a single coefficient b_{5M} such that

$$\mu(\xi, \eta) = \mu_{k(1)} + \beta_1 \xi + \beta_2 \eta + \beta_3 \xi^2 + \beta_4 \xi \eta + \beta_5 (\eta^2 - \xi^2 \tan^2 \theta) \quad (B7)$$

where

$$\beta_i = \sum_{\ell=1}^5 b_{i\ell} \cdot \mu_{k(\ell)} + \delta_{i5} b_{5M} \cdot \mu_M \quad (B8)$$

Regardless of the value for μ_M , equations (B7) and (B8) satisfy condition (i). It remains to determine μ_M such that condition (ii) is satisfied. For doublet continuity, the value of μ_M for each exterior subpanel i_{SP} must be equal to the value of μ_M for the adjacent interior subpanel ($i_{SP}+4$). For slope continuity,

$$\begin{aligned} & \left\{ \vec{\nabla} \mu(\xi_M, \eta_M) \cdot [+(\eta_3 - \eta_2) \vec{e}_\xi - (\xi_3 - \xi_2) \vec{e}_\eta] \right\}_{i_{SP}} \\ &= \left\{ \vec{\nabla} \mu(\xi_M, \eta_M) \cdot [-(\eta_3 - \eta_2) \vec{e}_\xi + (\xi_3 - \xi_2) \vec{e}_\eta] \right\}_{(i_{SP}+4)} \end{aligned} \quad (B9)$$

With the aid of equations (B7) and (B8), equation (B9) can be expressed in the following form:

$$\mu_M = \sum_{\ell=1}^5 \left\{ c_\ell \cdot [\mu_k(\ell)]_{i_{SP}} + d_\ell \cdot [\mu_k(\ell)]_{(i_{SP}+4)} \right\} \quad (B10)$$

where c_ℓ and d_ℓ are calculated coefficients that are independent of μ_k .

By substituting equation (B10) into (B8) and then redefining the coefficients $b_{i\ell}$ to include the contributions of c_ℓ and d_ℓ , equation (B8) becomes

$$\beta_i = \sum_{\ell=1}^5 \{ b_{i\ell} \cdot \mu_k(\ell) \} + \delta_{i5} \sum_{\ell=6}^8 \{ b_{5\ell} \cdot \mu_k(\ell) \} \quad (B11)$$

For each subpanel i_{SP} ($1 \leq i_{SP} \leq 8$), equations (B7) and (B11) provide the desired quadratic doublet distribution. Each coefficient β_i ($1 \leq i \leq 5$) is a linear function of μ_k ($1 \leq k \leq 9$). The sensitivity matrix elements $b_{i\ell}$ [$(1,1) \leq (i,\ell) \leq (5,5)$] and $b_{5\ell}$ ($6 \leq \ell \leq 8$) are calculated independently of μ_k by applying the formulation described above to the nine given quantities X_{1k} , X_{2k} , X_{3k} ($2 \leq k \leq 4$); recall that $X_{11} \equiv X_{21} \equiv X_{31} \equiv 0$. If one of the edges of the full panel is zero length, the above formulation requires only two slight modifications. First, the two exterior subpanels that lie on the zero length edge collapse to zero area and are ignored. Second, for each of the two interior subpanels that touch the zero length panel edge, the linear relationship

between μ_M and μ_k is established by passing a parabola through μ_k at the three spline control points on the panel edge that touches the subpanel point (ξ_M, η_M) .

The preceding portion of this Appendix described the procedure for establishing the quadratic doublet distribution corresponding to known values X_{ik} and arbitrary unknown values μ_k . Now suppose that each μ_k is assigned a fixed, known value. The method for determining the first-order change in quadratic doublet distribution induced by geometry perturbations (dX_{ik}) is presented below.

Define the array v_m ($1 \leq m \leq 9$) by equation (18). Then dX_{ik} for $1 \leq k \leq 9$ can be expressed by equations (19) and (20). For each subpanel isp , the derivative of equation (B1) provides the formula for $dP_{i\ell}$:

$$dP_{i\ell} = \sum_{j=1}^3 \left\{ DPI_{\ell j} \cdot dv_{[i+3(j-1)]} \right\} \quad (1,1) \leq (i,\ell) \leq (3,5) \quad (B12)$$

where $DPI_{\ell j} \equiv \{DXI_{k(\ell),j} - DXI_{k(1),j}\} \quad (B13)$

By applying the calculated values DXI_{kj} and $DPI_{\ell j}$ to the derivatives of equations (B2)-(B6), the following quantities are calculated for each subpanel isp :

$$\left\{ \frac{\partial \theta}{\partial v_m}, \frac{\partial s_\ell}{\partial v_m}, \frac{\partial a_{ij}}{\partial v_m}, \frac{\partial \xi_2}{\partial v_m}, \frac{\partial \eta_2}{\partial v_m}, \frac{\partial \xi_3}{\partial v_m}, \frac{\partial \eta_3}{\partial v_m}, \frac{\partial \xi_M}{\partial v_m}, \frac{\partial \eta_M}{\partial v_m} \right\}$$

$$(1,1,1,1) \leq (i,j,\ell,m) \leq (3,3,5,9)$$

Calculated values for $\partial\beta_i/\partial\theta$, $\partial\beta_i/\partial s_\ell$, $\partial\beta_i/\partial\xi_M$, and $\partial\beta_i/\partial\eta_M$ are generated by applying the procedure of Appendix A to the following known values for each subpanel i_{SP} :

$$\{\theta, s_\ell, \xi_M, \eta_M, \mu_{K(\ell)}, \mu_M\} \quad (1 \leq \ell \leq 5).$$

The value $\mu_M \equiv \mu(\xi_M, \eta_M)$ is obtained from equations (B7) and (B11). Again, "MAX" is 6 and the index $\ell=6$ of Appendix A corresponds to the midpoint "M" here. The formulation of Appendix A is based on the presumption that μ_M is a fixed quantity ($d\mu_M = 0$). Here, however, μ_M is dependent upon geometry perturbations ($d\mu_M \neq 0$), and the differential expression for $d\beta_i$ is written in the form

$$d\beta_i = \frac{\partial\beta_i}{\partial\theta} d\theta + \sum_{\ell=2}^5 \left(\frac{\partial\beta_i}{\partial s_\ell} \right) ds_\ell + \frac{\partial\beta_i}{\partial\xi_M} d\xi_M + \frac{\partial\beta_i}{\partial\eta_M} d\eta_M + \delta_{i5} b_{5M} \cdot d\mu_M \quad (B14)$$

All the coefficients of equation (B14) are known quantities, including b_{5M} which appeared earlier in equation (B8). It remains to establish formulas for $\partial\beta_i/\partial v_m$.

$$d\beta_i = \left\{ \sum_{m=1}^9 \left[\frac{\partial\beta_i}{\partial\theta} \cdot \frac{\partial\theta}{\partial v_m} + \sum_{\ell=2}^5 \left(\frac{\partial\beta_i}{\partial s_\ell} \cdot \frac{\partial s_\ell}{\partial v_m} \right) + \frac{\partial\beta_i}{\partial\xi_M} \cdot \frac{\partial\xi_M}{\partial v_m} + \frac{\partial\beta_i}{\partial\eta_M} \cdot \frac{\partial\eta_M}{\partial v_m} \right] \cdot dv_m \right\} + \delta_{i5} \cdot b_{5M} \cdot d\mu_M \quad (B15)$$

$$\equiv \sum_{m=1}^9 (DB_{im} \cdot dv_m) + \delta_{i5} \cdot b_{5M} \cdot d\mu_M$$

In order to determine the relationship between $d\mu_M$ and dv_m , equation (B9) is written in the following form:

$$\left\{ \sum_{i=1}^5 (g_i \beta_i) \right\}_{i_{SP}} + \left\{ \sum_{i=1}^5 (g_i \beta_i) \right\}_{(i_{SP}+4)} = 0 \quad (B16)$$

where

$$\begin{aligned}
 g_1 &= n_3^{-n_2} \\
 g_2 &= \xi_2^{-\xi_3} \\
 g_3 &= 2\xi_M \cdot (n_3^{-n_2}) \\
 g_4 &= [\eta_M(n_3^{-n_2}) + \xi_M(\xi_2^{-\xi_3})] \\
 g_5 &= 2[\eta_M(\xi_2^{-\xi_3}) - \tan^2\theta \cdot \xi_M(n_3^{-n_2})]
 \end{aligned} \tag{B17}$$

The substitution of equation (B15) into the differential form of equation (B16) results in the following equation:

$$\begin{aligned}
 &\left\{ (g_5 \cdot b_{5M}) d\mu_M + \sum_{m=1}^9 \left[\sum_{i=1}^5 \left(g_i \cdot DB_{im} + \beta_i \frac{\partial g_i}{\partial v_m} \right) \right] dv_m \right\}_{i_{SP}} \\
 &+ \left\{ (g_5 \cdot b_{5M}) d\mu_M + \sum_{m=1}^9 \left[\sum_{i=1}^5 \left(g_i \cdot DB_{im} + \beta_i \frac{\partial g_i}{\partial v_m} \right) \right] dv_m \right\}_{(i_{SP}+4)} = 0
 \end{aligned} \tag{B18}$$

Equation (B18) can be written as

$$d\mu_M = \sum_{m=1}^9 (DC_m \cdot dv_m) \tag{B19}$$

where DC_m is calculated by consolidating the coefficients of equation (B18). Finally, when equation (B19) is substituted into equation (B15), the accumulated coefficients of dv_m are the desired values $\partial\beta_i/\partial v_m$ $[(1,1) \leq (i,m) \leq (5,9)]$. If one of the edges of the full panel is zero length, the procedure for calculating $\partial\beta_i/\partial v_m$ requires two modifications that correspond to

those described earlier. First, the two exterior subpanels that lie on the zero length edge are ignored. Second, for each of the two interior subpanels that touch the zero length panel edge, $d\mu_M = 0$.

Now consider arbitrary simultaneous perturbations to both panel geometry (dv_m) and doublet strength at the spline control points ($d\mu_k$); see equation (B11). For each subpanel i_{sp} , the change in quadratic doublet coefficient ($d\beta_i$) can be predicted by the following formula:

$$d\beta_i = \sum_{m=1}^9 \left(\frac{\partial \beta_i}{\partial v_m} \right) dv_m + \sum_{\ell=1}^5 b_{i\ell} \cdot d\mu_{k(\ell)} + \delta_{i5} \sum_{\ell=6}^8 b_{5\ell} \cdot d\mu_{k(\ell)}$$

(B20)

All the coefficients of equation (B20) are known quantities, calculated by the procedures presented above in this Appendix. In the same sense that the linear relationship between β_i and μ_k of equation (B11) is appropriate for a conventional panel method, the linear relationship between $d\beta_i$ and dv_m of equation (B20) is appropriate for the analysis of small geometry perturbations.

REFERENCES

1. Hess, J.L.: Calculation of Potential Flow About Arbitrary Three-Dimensional Lifting Bodies. MDC J5679-01, McDonnell Douglas, October 1972.
2. Johnson, F. T.: A General Panel Method for the Analysis and Design of Arbitrary Configurations in Incompressible Flows. NASA CR-3079, May 1980.
3. Moran, J.; Tinoco, E.N.; and Johnson, F.T.: User's Manual, Subsonic/Supersonic Advanced Panel Pilot Code. NASA CR-152047, February 1978.
4. Morino, Luigi; and Kuo, Ching-Chiang: Subsonic Potential Aerodynamics for Complex Configurations: A General Theory. AIAA J., Vol. 12, No. 2, February 1974, pp. 191-197.
5. Woodward, F.A.: An Improved Method for the Aerodynamic Analysis of Wing-Body-Tail Configurations in Subsonic and Supersonic Flow. Part I - Theory and Application. NASA CR-2228, 1973.
6. Tulinius, J.R.: Theoretical Prediction of Thick Wing and Pylon-Fuselage-Fanpod-Nacelle Aerodynamic Characteristics at Subcritical Speeds. NASA CR-137578, July 1974.
7. Hunt, B.: The Panel Method for Subsonic Flows: A Survey of Mathematical Formulations and an Outline of the New British Aerospace Scheme. VKI Lecture Series 4, 1978.
8. Bristow, D.R.; and Grose, G.G.: Modification of the Douglas Neumann Program to Improve the Efficiency of Predicting Component Interference and High Lift Characteristics. NASA CR-3020, August 1978.
9. Bristow, D.R.: Development of Panel Methods for Subsonic Analysis and Design. NASA CR-3234, February 1980.
10. Kellogg, O.D.: Foundations of Potential Theory. Dover Publications, Inc., 1953.

1. Report No. NASA CR-3528	2. Government Accession No.	3. Recipient's Catalog No.	
4. Title and Subtitle SUBSONIC PANEL METHOD FOR THE EFFICIENT ANALYSIS OF MULTIPLE GEOMETRY PERTURBATIONS		5. Report Date March 1982	
		6. Performing Organization Code	
7. Author(s) D. R. Bristow and J. D. Hawk		8. Performing Organization Report No.	
		10. Work Unit No.	
9. Performing Organization Name and Address McDonnell Aircraft Company McDonnell Douglas Corporation P.O. Box 516 St. Louis, MO 63166		11. Contract or Grant No. NAS1-16156	
		13. Type of Report and Period Covered Contractor Report	
12. Sponsoring Agency Name and Address National Aeronautics and Space Administration Washington, D. C. 20546		14. Sponsoring Agency Code	
		15. Supplementary Notes Langley Technical Monitor: James L. Thomas Topical Report	
16. Abstract An accurate and efficient method has been developed for the aerodynamic analysis of a series of arbitrary small geometry perturbations to a given baseline configuration. The method is appropriate for wing-fuselage configurations in incompressible, potential flow. Mathematical formulations are presented for three computer programs that are employed. The first program is a conventional surface panel method for calculating the baseline singularity distribution. The second program calculates a partial derivative matrix. Each element of the matrix is the rate of change of singularity strength at one point with respect to a surface coordinate of a different point. For each baseline configuration, the calculated quantities from the first two programs establish an input file for the third. The purpose of the third program is to calculate the surface pressure distribution and forces and moments for a series of geometry perturbations. The procedure is similar to a conventional panel method, except that no aerodynamic influence coefficients are calculated and no large system of linear, algebraic equations is solved. Instead, the solution singularity strengths are generated at no appreciable computing expense by linear extrapolation using the partial derivative matrix. Example calculations are presented to demonstrate the accuracy and efficiency of the perturbation analysis method.			
17. Key Words (Suggested by Author(s)) Low Speed Flow Potential Flow Panel Method Wing-Fuselage		18. Distribution Statement Unclassified - Unlimited Subject Category 02	
19. Security Classif (of this report) Unclassified	20. Security Classif (of this page) Unclassified	21. No. of Pages 100	22. Price A05